ELECTROCHEMICAL PURIFICATION OF HAZARDOUS ORGANIC COMPOUNDS FROM WASTEWATER BY MEANS OF NOVEL ELECTRODE MATERIALS AND A SOLID-POLYMER-ELECTROLYTE-REACTOR SYSTEM

by
Jürgen Grimm

Dissertation presented for the degree of

Doctor of Philosophy (Polymer Science)

at the

University of Stellenbosch

Promotor
Prof. Dr. R.D. Sanderson

Stellenbosch
December 1999

Declaration

I, the undersigned hereby declare that the work contained in this thesis is my own original work and has not previously in its entirety or in part been submitted at any university for a degree.

List of Contents

Abstract

A novel sol-gel $Ti/SnO_2/Sb_2O_5$ electrode material for the electrocatalytic oxidation (combustion) of hazardous organic compounds in water has been designed and characterised.

Kinetic studies revealed the mechanism of the combustion reaction.

Two reactor systems supporting this catalytic material can be conceived of for application supporting the novel electrode material for water purification, namely:

- a Solid Polymer Electrolyte (SPE) sandwich reactor and

- a fluidised bed reactor, hosting the electro-catalyst as a powder.

An SPE-reactor system has been designed and evaaluated for its performance.

As the electrode material seemed to be promising for perchlorate production as well, the oxidation of chlorate to perchlorate was investigated.

Opsomming

'n Nuwe sol-gel $Ti/SnO_2/Sb_2O_5$ elektrode materiaal vir die elektrokatalitiesie oksidasie (verbranding) van risiko organiese stowwe in water is ontwerp en gekarakteriseer.

Kinetiese studies het die meganisme van die verbrandingreaksie getoon.

Twee reaktorsisteme vir watersuiwering wat die katalitiese materiaal en die nuwe elektrode ondersteun kan voorgstel word, naamlik:

- 'n Soliede Polimeer Elektroliet (SPE) toebroodjiereaktor en

- 'n sweefbedreaktor wat die elektro-katalisator as 'n poeier bevat.

'n SPE-reaktorsisteem is ontwerp en nagegaan vir doeltreffendheid.

Angesien die elektrode materiaal ook belowend vir perchloraat produksie geblyk het, is die oksidasie van chloraat na perchloraat ook ondersoek.

Extended abstract

A novel electrode material for the oxidation of hazardous organic compounds in water was designed. Titanium foil was chosen as the support for the electrocatalytic coating. An antimony-doped SnO_2 film was deposited on the titanium by a sol-gel dip-coating method. Two different sol-gel routes were used:

- an inorganic route with $SnCl_2$ and $SbCl_3$ dissolved in ethanol as precursors and

- an organic route using Sn (II) 2-ethylhexanoate and Antimony(III) butoxide with buthanol and triethanolamine as a solvent.

A PbO_2 based electrode material on Ebonex was prepared, by coating plates of Ebonex anodically for 30 min with PbO_2 in an acidic solution of $Pb(NO_3)$. Additional PbO_2 electrodes on steel supportss were obtained from a plasma injection technique, as delivered from the Deutsche Forschungsanstalt für Luft- und Raumfahrt e.V. (DLR).

Experimental techniques used for the electrode characterisation included:

- Conductivity measurements of the films,

- X-ray Photoelectron Spectroscopy (XPS) and microprobe,

- Cyclic voltammetry,

- Electrochemical impedance measurements,

- Fibre-optics UV/VIS spectroscopy for phenol detection,

- Fibre-optics UV/VIS spectroscopy for kinetic measurements.

Kinetic measurements proved the existence of •OH-radicals as intermediates and driving force for the oxidation (combustion) of the organics. N,N-dimethyl-p-nitrosoaniline (RNO) was used as a spin trap for the specific detection of the •OH-radicals.

Phenol was chosen as a standard contaminant during the electrolysis, because of its toxicity, high stability (caused by the aromatic ring structure) and the wide range of references to it in the literature.

This study was also directed at the development of a reactor system for efficient application of the electrode material. Two different approaches can be visualised:

• A Solid Polymer Electrolyte (SPE) reactor, comprising a perfluorinated Nafion-like cation-exchange membrane in H^+-ionic form, sandwiched by the porous working- and counter-electrode.

• A fluidised bed reactor system, consisting of Sb-doped SnO_2 particles filling up an anodic compartment with the anode attached to the particles.

An SPE-reactor system has been designed and evaluated for its performance in water purification.

The properties of the $Ti/SnO_2/Sb_2O_5$-electrode included a very high electrochemical overpotential for the oxygen-evolution reaction. Other chemical conversions running at a high anodic potential such as the perchlorate production, thus, seem to be promising applications as well and were surveyed in this study.

Acknowledgements

Chapter 1

Introduction and objectives

Along with electricity, water is one of the basic commodities which will be needed in ever increasing quantities as the industrialisation and urbanisation of our world progresses. The rising demand can only be met if we learn to apply suitable scientific and technical resources available to us in stepping up the productivity of process technologies for turning low grade water into pure water.

Water treatment in its broadest context can be defined as the subjection of water to an agent or process with the objective of transforming the source quality to meet application-specific criteria or standards. Water treatment has been a concern for all human settlements since earliest times. Prior to the industrial revolution, water treatment was evolved based on empirical observations without a scientifically based understanding of the underlying mechanism of treatment processes. In the public sector, the major objective of water treatment up to the 20th century, was providing a desirable aesthetic quality while at the same time protecting consumers from water-borne diseases. In the industrial sector, during this time, the primary concern was obtaining water in sufficient quantity and quality to permit expansion of the growing industrial centres.

In comparison to the predominance of empirical developments, the post-19th century era of water treatment has seen a rapid application of the principles of chemistry, materials science, microbiology and engineering science towards improvements in process efficiencies, optimisation of existing processes, and the development of new processes for the removal of contaminants from water. In the industrialised nations, these applications have led to a near eradication of acute health hazards caused by water-borne diseases. At the same time,

advances in analytical chemistry and toxicological science have raised new concerns regarding potential chronic health hazards from drinking water containing trace (less than 0.1 mg/l) levels of organic chemicals, not of natural origin.

Modern state of the art technologies for water purification include among others the following:

• Separation by

Pressurised Membrane Systems, including reverse osmosis, nanofiltration, ultrafiltration and microfiltration, and by

Electrodialysis membrane separation,

• Disinfection with UV-radiation, ozone, ozone/H_2O_2, including still newer technologies which are:

Electrochemical ozone generation and

Electrochemical anodic combustion.

In this study the complete electrochemical oxidation (combustion) of phenol, which is often found in the literature as a standard contaminant for hazardous organic compounds in water, has been investigated.

The key factor leading to complete anodic oxidation is the choice and design of a suitable electrode material.

The first high performing electrode material investigated for the oxidation of hazardous organic compounds in water was PbO_2 and a number of successful approaches were achieved with that material [Kirk, 1984; Wabner, 1985]. Lead dioxide is of great practical importance, firstly as the positive plate in the lead-acid battery [Randle, 1979] and, secondly, as an inert electrode for different anodic processes, because noble metal electrodes, e.g. platinum electrodes, used for anodic electro-synthesis, are expensive, inherently only slightly stable, and chemically as well as electrochemically less noble than is generally assumed. PbO_2 electrodes are relatively stable from the mechanical, chemical and electrochemical point of

view, and they are comparatively cheap. These electrodes have still another very interesting advantage: the anodic oxygen evolution at the PbO_2 takes place at an essentially more positive potential, compared with, for instance, the platinum electrode [Wabner, 1985].

For the coating, PbO_2 was preferably deposited galvanostatically on a suitable substrate [Wabner, 1974; Fleischmann, 1958]. In this work PbO_2 coated Ebonex was used as reference material for comparison. Ebonex, as Magneli phase titanium suboxides which are blue-black in colour and electrically conductive, are known as an excellent support for any kind of electrocatalytic coating [Park, 1995]. The remarkable combination of its electrical conductivity and very high corrosion resistance makes this material most suitable for use in electrochemical cells with particularly corrosive electrolytes [Graves, 1992]. Additionally, the ceramic-rutile based structure of Ebonex makes it very compatible with rutile-structured surface coatings such as iridium dioxide, ruthenium dioxide and lead dioxide.

The Ebonex/PbO_2 electrodes were used for comparison with the novel Ti/SnO_2 based electrodes prepared by a sol-gel method with respect to their oxidation behaviour.

Comninellis et al. [Comninellis, 1993] discovered that hydroxyl radicals ($\bullet$OH radicals), as intermediates on the electrode's surface, are the driving force for the complete oxidation (combustion) of even very stable organic compounds in water, such as phenol. As a detection method for the $\bullet$OH radicals, Comninellis used a method well established in biology and biochemistry, i.e. spin-trapping with p-nitrosodimethylaniline (RNO) [Bors, 1978]. SnO_2 proved to be an excellent material with high stability and radical output. SnO_2 is intrinsically a large band-gap (3.7 eV) semiconductor whose resistance may be decreased enormously by doping. Thus, Comninellis improved the conductivity and the electrocatalytic properties of those electrodes by the introduction of traces of Sb_2O_5 to the SnO_2 films as a dopant. Its incorporation in the SnO_2 matrix, by isomorphis of Sn atoms, is rather easy and leads to a low lattice-parameter modification [Boudeulle, 1983].

As a substrate for the electrocatalytic SnO_2 films the preferred material in the literature is titanium.

There are a variety of methods available for coating the catalyst support to obtain dimensionally stable anodes.

Methods of film preparation include:

- Chemical vapour deposition [Kadam, 1990; Popova, 1990],

- Reactive sputtering [Czapla, 1989],

- Sol-gel dip coating [Arfsten, 1984],

- Spray-pyrolysis [Popova, 1990; Chaudhuri, 1990; Karlsson, 1992; Comninellis, 1993].

In this work we have chosen the dip-coating sol-gel method for the preparation of SnO_2-films on Ti substrates. Interest in the sol-gel processing of inorganic ceramic and glass materials began as early as the mid-1800s with Ebelman and Graham's studies on silica gels. These early investigations observed that the hydrolysis of tetraethyl orthosilicate (TEOS), $Si(OC_2H_5)_4$, under acidic conditions, yielded SiO_2 in the form of glass-like material [Ebelmen, 1846; Ebelmen, 1847; Graham, 1864]. However, extremely long drying times of 1 year or more were necessary to prevent the silica gels from fracturing into a fine powder and, consequently, there was little technological interest. For a period from the late 1800s through the 1920s gels became of considerable interest to chemists, stimulated by the phenomenon of Liesegang Rings [Liesegang, 1896; Heinisch, 1970] formed from gels. A huge volume of descriptive literature resulted from these studies [Lloyd, 1926; Holmes, 1926; Stern, 1967], but a relatively sparse understanding of the physical-chemical principles remained.

Roy and co-workers [Roy, 1954; Roy, 1956; Roy, 1969; McCarthy, 1971] recognised the potential for achieving very high levels of chemical homogeneity in colloidal gels and used the sol-gel method in the 1950s and 1960s to synthesise a large number of novel ceramic oxide compositions, involving Al, Si, Ti, Zr, etc., that could not be made using traditional ceramic powder methods. The motivation for sol-gel processing is primarily the potentially

oxide compositions, involving Al, Si, Ti, Zr, etc., that could not be made using traditional ceramic powder methods. The motivation for sol-gel processing is primarily the potentially higher purity and improved homogeneity and the lower processing temperatures associated with sol-gel compared with traditional glass melting or ceramic powder methods. During the last decade there has been an enormous growth in the interest in the sol-gel process. This growth has been stimulated by several factors. On the basis of Kistler's early work [Kistler, 1931], several teams have produced very low density silica monoliths, called aerogels, by hypercritical point drying [Fricke, 1986].

It has been shown that the dip-coating method is well-suited for the preparation of defect free films [Maier, 1993]. In the past this procedure has been used for the preparation of catalytically active membrane films [Maier, 1995; Lange, in print]. The method has major advantages [Chaleton, 1994]: starting materials of high purity, ease of coating of large and complex-shaped substrates and low cost. The sol-gel dipping technique leads to very high-quality SnO_2 layers with respect to structure and morphology. Chemical modifications, achieved readily by the addition of selected dopants, like antimony alkoxides, antimony chlorides, $K_2[PtCl_6]$ or fluoride to the sol, should reduce the band gap between the valence- and conducting bands as an n-donor in the oxide and thus increase conductivity.

As already mentioned above, a special feature of the SnO_2-based electrode material is the high anodic overpotential for the oxygen evolution reaction. Consequently, the material should also be feasible for other electrochemical reactions, running at high anodic potentials, such as the perchlorate production. The common industrial method of producing perchlorate is the electrochemical oxidation of aqueous chlorate solutions [Ibl, 1981]. The anode material is crucial to obtain a high current efficiency for the perchlorate formation. So far only two materials, viz. smooth platinum and lead dioxide are used industrially [Ibl, 1981]. Munichandraiah et al. suggested that a one-electron-transfer step to give an adsorbed hydroxyl radical as the rate-determining step for the overall reaction [Munichandraiah, 1987]. Tin

Ion exchange membranes can function as Solid Polymer Electrolytes (SPE) in non-conductive liquids and, therefore, electro-organic synthesis as well as the electrochemical combustion of organic compounds in water are feasible without supporting electrolytes. The SPE process was primarily developed by industry for electrolysis of pure water and for fuel cells (now usally called Proton Exchange Membrane PEM fuel cells). The first application of the SPE process for electro-organic synthesis were published by Ogumi et al. in Japan and by Tallec et al. in France and Grinberg et al. in Russia [Ogumi, 1981; Sarrazin, 1982; Grinberg, 1983]. Further investigations were published in recent years by Liu and Fedkiw and by Chen and Chou [Liu, 1992; Chen, 1993].

A different approach to a reactor system is the principle of fluidised bed electrolysis designed by Goodridge and Fleischmann [Backhurst, 1969]. The electrolyte flows from bottom to top through a loose bed of particles thus fluidising it. The fluidised particles are charged via a feeder electrode. This provides a large surface area for the reaction zone, described as a three-dimensional electrode.

The objectives of the dissertation were:

- Overall, the design of novel electrode material for optimising OH radical production electrochemically.

- The development of sol-gel techniques to create catsalytic surfacs on the electrode.

- The characterisation of the electrode material by:

Conductivity measurements of the films

Cyclic voltammetry

Impedance Spectroscopy

X-ray Photo-Spectroscopy (XPS) surface analysis

Microprobe surface analysis.

- Study of the electrochemical performance of the electrode by:

  Fibre-optics UV/VIS for the determination of hydroxyl radicals

  UV/VIS for the analysis of the phenol concentration.

- The design of a Solid Polymer Electrolyte reactor and its characterisation.

- Examine the reactor system for the production of perchlorate.

Chapter 2

Electro-assisted methods for water purification

Abstract

Many different methods for improving the hygienic quality of waste, industrial and drinking water are already established. These include pressure-driven membrane-based methods such as reverse osmosis, ultrafiltration and microfiltration, biological treatment, treatment of water by means of various chemicals such as ozone or chlorine, and treatment with UV radiation. This review deals with electro-assisted methods for water purification which stand apart from the well-established technologies. Although electrodialysis is a competitive electro-assisted method for water treatment, electrochemical systems for water treatment have, in general, not yet attracted adequate attention. Electrochemistry, a link between physical chemistry and electronic science, has proved to be a clean, versatile and powerful tool for the development of new advanced methods for water purification. The freedom of choice in adjusting the electrode potential and electrode material, to meet almost any demand, makes electrochemistry extremely selective and flexible. This survey covers both established and recent developments in the field of electrochemical technologies for waste water and drinking water treatment.

2.1 Introduction

Water and electricity are both basic commodities which will be needed in ever-increasing quantities with continued industrialisation and urbanisation in the world. Water treatment in its broadest context, entails the subjection of the water to an agent or process with

17

the objective of improving its source quality, to meet application-specific criteria or standards. The challenge of the rising demand for quality water can only be met if we apply all available, suitable scientific techniques to increase the productivity of process technology for converting low-grade water into pure water. Electrochemistry must therefore be taken into consideration. The adequate supply of quality water is of major concern to South Africa and many other arid areas of the world as the main source of life and an important factor for industrialisation. The treatment of waste water and delivery of high quality water is a wide field for research.

The supply of water to rural communities is of major concern, especially as groundwater, which plays a key role in supplying rural communities with water, can often not be consumed without pretreatment. The advantages of using electrochemical units for water purification are the ease of handling and application in the field.

The post-19th century era of water treatment has seen a rigid application of the principles of chemistry and materials science, with improvements in processes such as ozone generation [Bhattacharyya, 1995], microfiltration, ultrafiltration and reverse osmosis.

As electricity is available at low cost in South Africa, research should be focused on electrochemical methods for water treatment.

The purpose of this chapter is firstly, to define the problems arising from certain contaminants in water in various regions of South Africa and secondly, to review the electro-assisted methods which could be used to solve these particular problems. Emphasis will be placed on novel techniques rather than on well-established systems, which have already been described elsewhere [Kreysa and Heitz, 1986].

2.2. Contaminants and their risks

In the industrialised countries improvements in water treatment have led to a near eradication of acute health hazards caused by water-borne diseases. At the same time, however, the situation in the less-developed countries has become more serious and advances in analytical chemistry and toxicological science have revealed a situation that gives cause for new concern regarding potential chronic health hazards from drinking water containing trace (less than 0.1 mg/l) levels of organic chemicals not of natural origin.

Drinking-water quality criteria, with special reference to the South African situation, and their impact on water-borne diseases have already been extensively studied [Pieterse, 1989].

A brief description of the major types of water pollutants is given below.

2.2.1. Biological assessment

Despite the fact that bacteriological contamination of water no longer plays a major role in the industrialised countries, it remains of concern in rural and developing communities where the levels of sanitation, standards of living and education can be correlated with the occurrence of infections. Because of the long incubation periods of pathogens and problems of diagnosis, the paths of infection are often difficult to detect. In addition, the absence of an infrastructure for the detection and recording of such infections results in little available information on water-borne diseases in South Africa. The pathogens involved include a wide variety of viruses, bacteria and protozoan parasites, which usually belong to the group of organisms basically transmitted by the oral-faecal route.

Examples of common diseases related to pathogens in water are gastroenteritis and hepatitis. Methods for monitoring pathogens in water have been reported by Grabow

[Grabow, 1996]. As various water-borne pathogens are able to change their prevalence, electrochemical decomposition of all organics rather than chemical treatment and disinfection might be an effective method for their removal.

2.2.2. Contamination by heavy metals

Waste water containing toxic metal ions is produced in many industrial processes, such as electroplating, cellulose acetate production, photographic development and the production of printed circuits and batteries. Because of intensive gold-mining activities on the Witwatersrand in Gauteng, RSA, the water there is, in places, severely polluted. The removal of metal ions is of major concern, because the contaminants may accumulate in the human body and their presence manifests itself in long-term effects and diseases. As the problem has already been extensively described elsewhere [Galvin, 1996], this article will only refer to the main contaminants which have major effects on human health.

Cadmium and associated contaminants

Cadmium is considered to be highly toxic [Friberg, 1974; Turner, 1957] and therefore its permitted concentration in water is limited to 5-10 ppb. In recent years cadmium has become of major environmental concern due to its introduction to natural water reservoirs. The main sources of cadmium contamination are: 1) Ni/Cd battery production which may deliver both cadmium and nickel to groundwater in untreated aqueous wastes, or because of uncontrolled disposal of used batteries; 2) cadmium plating, which also introduces cyanide which is used as a strong complexing agent; and 3) cadmium-rich phosphate fertilisers which introduce cadmium directly to the ground and into the water resources in cultivated areas. The latter has been reported to interfere with the metabolism by plants of some mineral

substances, mainly calcium [Verbost, 1989], magnesium [Lundberg, 1987] and phosphorus [Wesenberg, 1982]. Symptoms such as osteoporosis, hypercalcuria and altered protein synthesis strongly suggest that cadmium disturbs calcium-dependent processes [Vallee, 1972; Yoshiki, 1975].

The main electrochemical approach used for cadmium removal has been cathodic reduction [Oren, 1983].

The metal can be deposited on the electrode matrix according to the equation:

$$Cd^{2+} + 2e^- \rightarrow Cd \tag{1}$$

At sufficiently high cathodic potentials alkaline local pH values can be generated at the solution-electrode interface due to water and oxygen reduction:

$$2H_2O + 2e^- \rightarrow 2OH^- + 2H_2 \tag{2}$$

$$2H_2O + O_2 + 4e^- \rightarrow 4OH^- \tag{3}$$

Under such conditions $Cd(OH)_2$ is formed and can be removed from the solution by adsorption to the electrode as a charged colloidal particle.

However, the most commonly used procedure is the precipitation of $Cd(OH)_2$ by the addition of alkali. Both methods may also be used for the removal of nickel, if it is present in the solution. With cyanide as an associated contaminant, electrochemical treatment by radicals can be used.

Mercury

Mercury levels in waters are generally very low and do not exceed more than $1\mu g/l$ [USEPA, 1977]. Higher concentrations, however, occur in waste water discharged by certain industries. Strict attention must be paid to the control of Hg levels in water, because of the high toxicity of the metal. Mercury exhibits bioaccumulation and accumulates in fatty tissues, brain, renal systems, muscles, bones and nervous system, with a tendency to cause muscular paralysis, visual disruption and brain damage. The extent of Hg contamination, and its becoming part of the trophic chain, is described in a study of Minimata, a town in Japan [WHO, 1986].

Lead

Lead is an important material with widespread industrial applications, as in accumulators and as an additive in fuels, paints, pesticides etc. As lead has been used in piping, high concentrations of the metal (up to 2 mg/l) may occur in the water in numerous households, where lead pipes have not yet been replaced. Its toxic characteristics and its tendency to accumulate in the body, makes analysis of the water and, if required, treatment of the water necessary. Electrochemistry may be used for the removal of lead by cathodic deposition.

2.2.3. Organic wastes

Apart from inorganic pollutants, industrial waste water also contains organic pollutants which have to be treated before the water can be discharged. Because of expansion of the chemical industry, it is not only the quantities of chemicals, but also the variety of organic

pollutants released to waste water which is constantly increasing. The numerous new organic compounds entering the industrial sphere make their toxic classification increasingly difficult and, what is even more serious, these substances may be stable and the traditional methods of biological treatment may not be effective. Chemical oxidation processes are effective but can generally not be carried out on halogenated organic compounds because of the stability of carbon-halogen bonds.

The electrochemical combustion of organic compound offers considerable advantages. Firstly, it can be carried out at moderate temperatures and under clean conditions. Secondly, electrochemistry provides a means for the total destruction of the pollutants, promoting their oxidation all the way down to CO_2, and no by-products are left in the effluent. The electrochemical oxidation methods comprise direct and indirect oxidation, the latter oxidising the organics by an intermediate formed at the anode.

2.2.4. Fluorides and Nitrates

Fluorides are usually not regarded as having a great effect on the quality of groundwater, because their concentration is usually far below all international and national drinking-water standards. However, in the Western Bushveld area of South Africa, and in some of the western and northern areas in China [Sun Li-Cheng, 1985], fluorine contamination of the groundwater results in endemic dental and, in fewer cases, skeletal fluorosis [McCaffrey et al., 1995]. The enrichment of fluoride in the ground water takes place primarily as a result of dissolution of fluorite and the chemical weathering of F-containing minerals. Concentrations of fluorine in drinking water should not exceed 5 mg/l, although a recommended limit is 1 mg/l. In the area of Sun City, South Africa, Archean granite causes a concentration of fluorine exceeding 5 ppm in the groundwater. Electrochemical treatment of

the fluorides is possible only by electrodialysis, since oxidation in aqueous medium is impossible because of the high electronegativity of fluorine.

Nitrate removal also plays an important role in improving the quality of drinking water. Intensive farming and the application of agricultural fertilisers and inadequate control of human and animal excreta can result in high nitrate concentrations, unfavourable to human health. It is recommended that the concentration of nitrates in drinking water should be less than 10 mg/l. Electrochemical treatment methods range from electrodialysis to direct electrochemical reduction.

2.3. Why Electrochemistry?

Electrochemistry, as a branch of physical chemistry, plays an important role in most areas of science and technology. Furthermore, it is increasingly acknowledged as a significant means for handling environmental and energy problems facing us today and in the near future. Briefly, electrochemistry deals with the charge transfer at the interface between an electrically conductive (or semi-conductive) material and an ionic conductor (e.g. liquids, melts or solid electrolytes) as well as with the reactions within the electrolytes and the resulting equilibrium. Electrochemical waste destruction shows several benefits in terms of costs and safety. The process runs at very high electrochemical efficiency and operates essentially under the same conditions for a wide variety of wastes. Operation at room temperature and atmospheric pressure reduces the possibility of volatilisation and the discharge of unreacted waste. The waste treatment can be terminated within seconds by simply cutting off power to the electrodes.

The removal of undesired components from aqueous phases is based on the choice of the appropriate electrode material and potential, or by assisting membrane systems to drive the electrode processes selectively. In addition to the low cost of electricity in South Africa, it

has the advantage of being applicable to a wide range of waste-water purification process. Furthermore, electrochemical combustion offers a means of oxidising the pollutants to water and CO_2 so that a simple shift of the problem, by moving the contaminants from one phase to the other, is avoided. Electrochemical combustion is therefore presented as a clean and versatile method.

The following electrochemical approaches may be distinguished:

- indirect electrochemical oxidation of inorganic or organic contaminants;

- direct electrochemical oxidation of the contaminants;

- cathodic removal of metal-cations (mostly heavy metals);

- separation through membranes using an electric field.

The choice of electrode material must focus on high activation energies for undesired side-reactions. If side-reactions are to be reduced cathode materials should have high over-voltages for hydrogen-evolution, such as Pb or Cd. The anodes should preferably show high over-voltages [Bard and Faulkner, 1980] for the evolution of oxygen.

For a better understanding of the principles of electrochemical design, a description of the main purposes of reactor design is given in section 2.4.

2.4. Electrochemical reactor design

Thinking of three-dimensional electrode-structures one would first consider porous electrodes where reactions would then occur inside the pores of a porous bulk. Unfortunately such configurations are of little use for water treatment because the mass transport of the contaminants to the inside of the pores is slow. This can be improved by arranging thin, porous layers of electrodes, as in fuel cells.

Another possibility is the use of particle-electrodes. These electrodes have already been extensively studied for their use in the deposition of heavy metals from waste waters [Kreysa and Heitz, 1986].

The two different types of construction are

-       an electrochemical packed-bed reactor,

and

-       an electrochemical fluidised-bed reactor.

For the evaluation of the economic efficiency of an electrochemical cell, the Space-Time-Gain is a useful tool. The Space-Time-Gain (ρ) is described as the product gain per cell-volume and operating hour. The unit is kg l^{-1} h^{-1} and is calculated by:

$$\rho = \frac{M}{nF} \cdot a \cdot j \cdot A_V \,, \tag{4}$$

where a is the gain-factor and A_V the proportion of electrode-surface to the volume of the cell (cm^{-1}). M stands for the molecular mass and j for the current density. Desirable high Space-Time-Gains are thus related to high current-densities and/or high A_V values. Three-dimensional electrodes guarantee a high value for A_V.

The electrochemical packed-bed reactor is shown schematically in Fig. 1. A bed of conductive and non-conductive spherical particles, such as graphite and synthetics, is situated between two electrodes and the contaminated water flows through it. If the conductivity of the solution

26
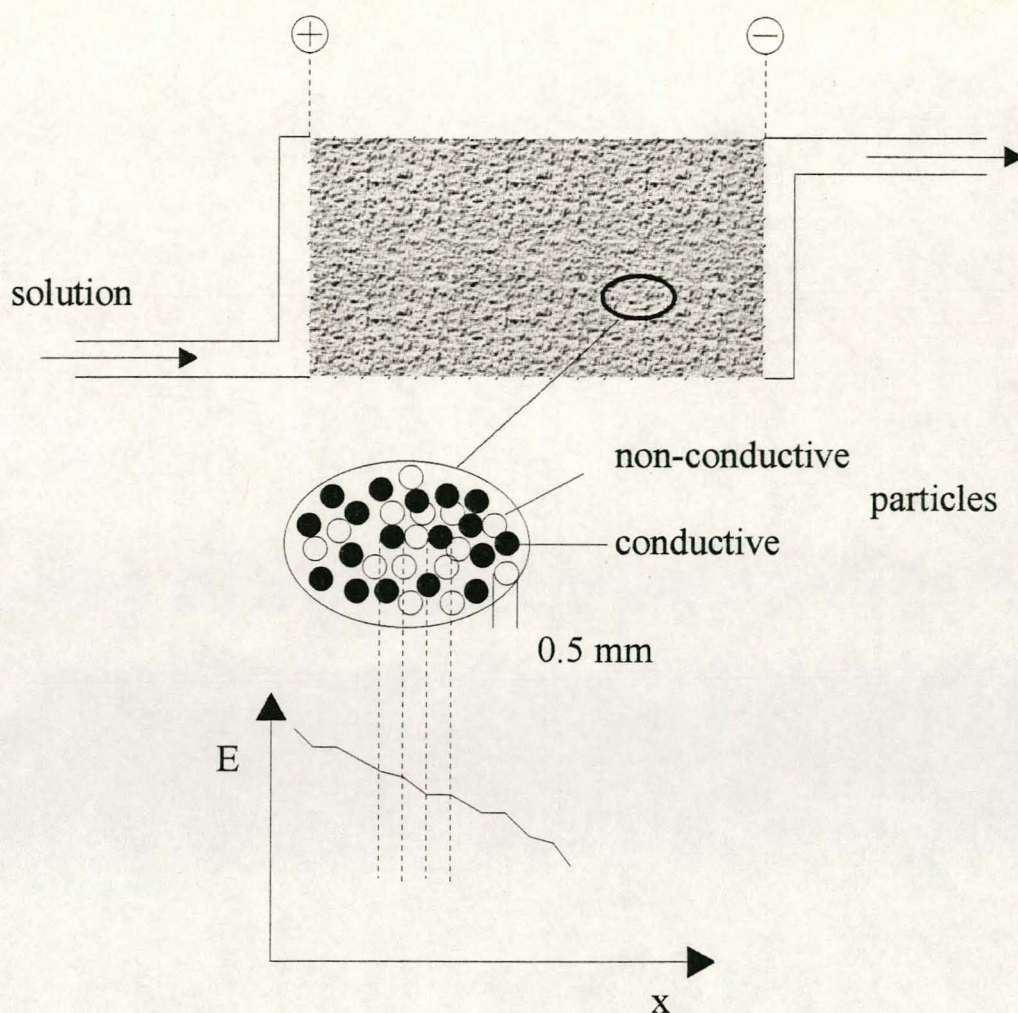
Fig. 1. Scheme of a packed bed reactor and the potential decay along the cross-section

is not too high and the voltage across it is sufficiently high, the conductive particles will act as a multitude of bipolar electrodes. In three-dimensional electrodes the penetration depth of the current in a direction parallel to the current flow is limited. Ohmic losses in the electrolyte are the main cause of the decrease in local current density. For a diffusion-controlled reaction, the penetration depth of the limiting current density can be calculated with the formula:

$$h_p = \left[\frac{2 v \chi_s \Delta \eta}{a_e kzFc} \right]^{0.5} \tag{5}$$

a_e specific electrode surface [cm^{-1}]

c   concentration [kmol/m^3]

F   Faraday constant [As/mol]

h_p penetration depth [m]

k   mass transfer coefficient

$\Delta\eta$ over-potential [V]

v   degree of vacancy

X_s electrolyte conductivity [S/m]

z   number of electrons

According to this equation, the penetration depth of the limiting current density increases with decreasing concentration of the metal ions. The application of this principle led to the design of the Enviro-Cell which is shown schematically in Fig. 2. The penetration depth of the bed increases as the metal ion concentration decreases. The metal concentration can be reduced to as little as 1/1000 of the initial concentration.
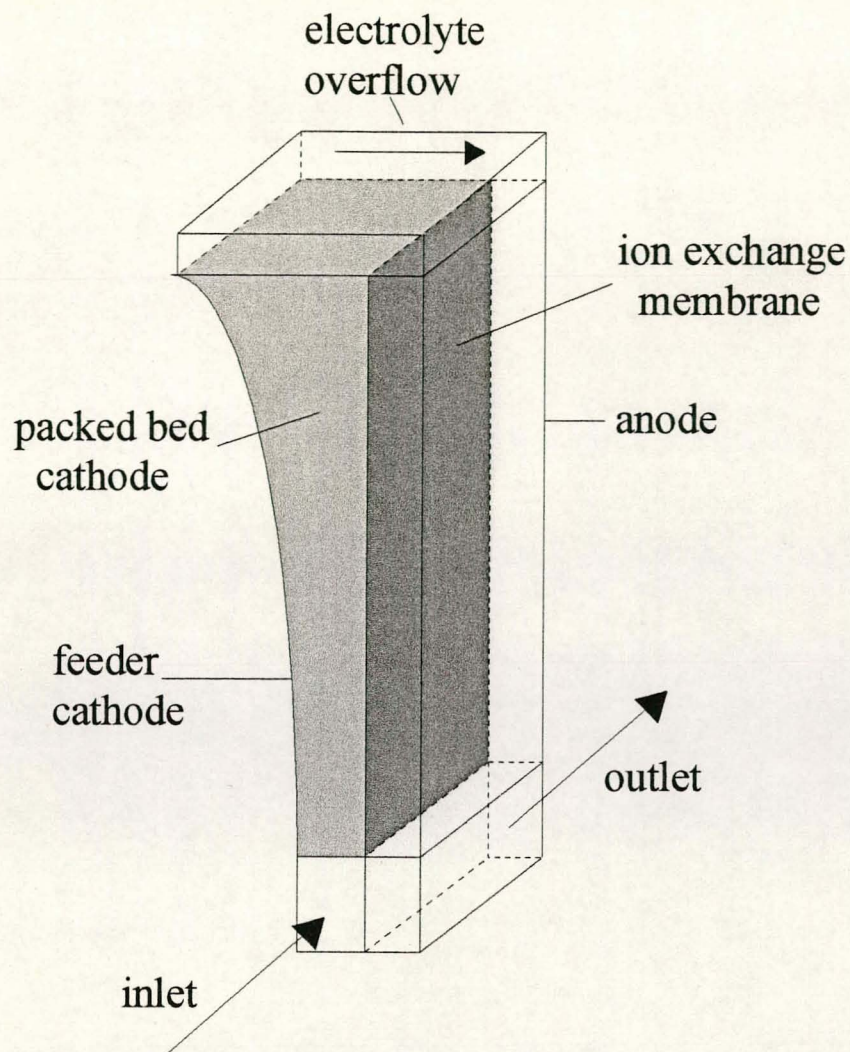
Fig. 2. Schematic representation of the Enviro cell

The principle design of the fluidised-bed reactor is illustrated in Fig. 3. In this reactor a loose bed of particles of size diameter 0.1-1 mm is flooded upwards, from the bottom. The fluidised particles are charged cathodically by a feeder electrode. Metal ions are adsorbed at the surface of the particles and, once the particles contact the working-electrode, its potential drives the charge-transfer reaction and the discharged metal is deposited. When the metals lose contact with the electrode, they either desorb and collect at the bottom of the reactor or the particles grow and the larger ones sink to the bottom and are replaced by fresh particles.

Anolyte

Anolyte

Catholyte
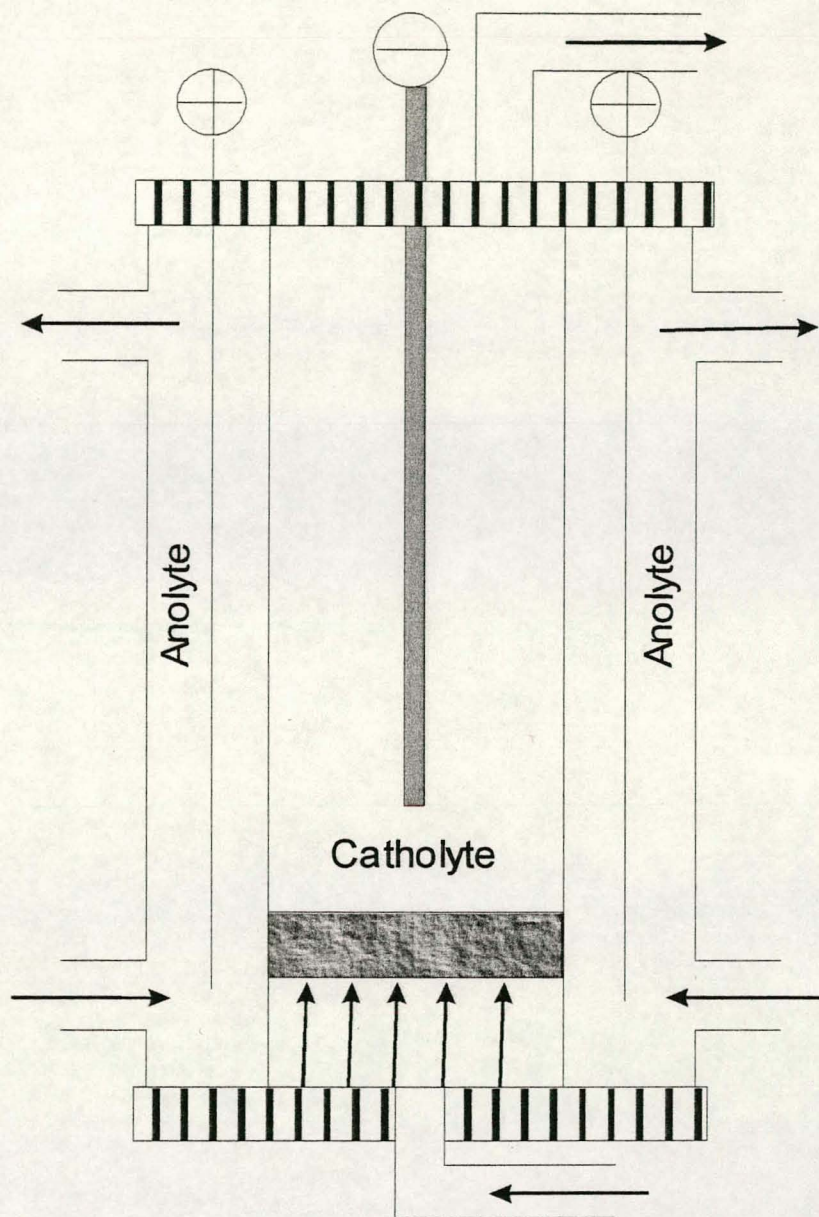
Fig. 3. The principle design of a fluidised bed reactor

The principle has been widely studied and purification by this means has been carried

out on an industrial scale [Kreysa, 1981]. For hydraulic reasons the height of such a cell is

30

usually restricted to 2m. Consequently, only a limited concentration drop per pass can be achieved. Continuous operation and serial arrangement of the cells can reduce these problems.

The A_V value of a fluidised-bed reactor is about 50 cm^{-1}. According to equation (2) the Space-Time-Gain for the removal of Cd-ions equals, for j = 0.2 A cm^{-1}, approximately 20 kg l^{-1} h^{-1}. Apart from the high values of A_V, another advantage of the fluidised-bed reactor is the rapid mass-transport and the low real-current density which means that even very low concentrations of metals can be removed from the waste-water.

2.5. Electrochemical Methods

2.5.1. Anodic Oxidation

Anodic oxidation is a powerful tool for the treatment of organics in water, especially as far as the removal of organic wastes in industrial effluents is concerned. The main objective of the process is to oxidize any organics to H_2O and CO_2. Two different approaches may be distinguished:

- direct anodic oxidation, where the organics are destroyed at the electrode's surface, or

- indirect oxidation, where a mediator, for example Ag^{2+}, is electrochemically generated to carry out the oxidation.

2.5.1.1. Direct oxidation

Two different pathways are described in the literature for the anodic oxidation of undesired organics [Comninellis, 1993]:

- electrochemical conversion and

- electrochemical combustion (Fig. 4).

Electrochemical conversion transforms only the toxic non-biocompatible pollutants into biocompatible organics, so that biological treatment is still required after the electrochemical oxidation.

In contrast, electrochemical combustion yields water and CO_2 and no further purification is necessary. This means that research should rather focus on studies of the mechanisms of the anodic combustion. Fig. 4 is a schematic representation of the electrochemical conversion/combustion, adopted from C. Comninellis [C. Comninellis, 1993].
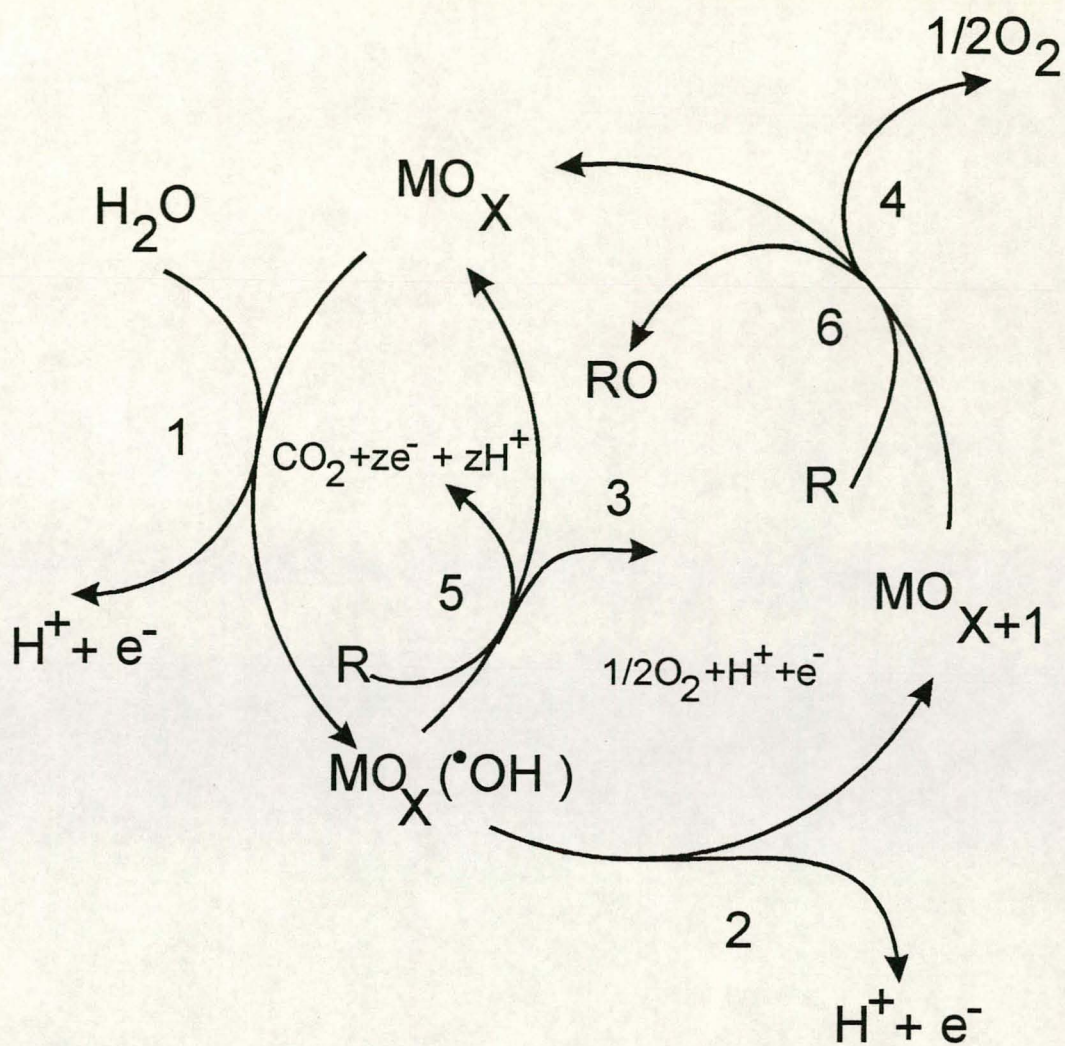
Fig. 4. Pathway of electrochemical combustion/conversion (scheme adopted from Comninellis, 1993). R represents an organic compound.

Experimental results indicate that the accumulation of •OH radicals favours the combustion reaction, while introduction of oxygen into the electrode's lattice results in combustion. This opens a challenging field for materials science, as electrodes need to be optimised. Chemically stable and electrically conductive material must be selected as a carrier for the electrocatalytic material. Usually, Ti is used as the base material. There are a variety of methods for coating the catalyst support to obtain dimensionally stable anodes.

Methods of film preparation include:

-    chemical vapour deposition

-     reactive sputtering

-     sol-gel dip coating

-     spray-pyrolysis.

H. Sharifan and D.W. Kirk [Sharifan, 1986] reported on results obtained after using PbO_2 as electrode material, while Comninellis et al. [Comninellis, 1996] focused their research on SnO_2 coatings obtained by spray pyrolysis. Surface properties of the electrodes such as pore-size, roughness and catalytic activity can be examined by electrochemical methods such as impedance spectroscopy or cyclic voltammetry. Favoured goals of electrode design are high surface roughness with many catalytic sites (that might be smoothed during application), high exchange current densities and steep Tafel slopes [Bard and Faulkner, 1980] for a high electron transfer rate. High porosity provides a large surface area and the pore sizes must not be too small, to allow for a rapid mass transport. Catalytic activity should be at a maximum, if the undesired molecules fit closely into the pores.

2.5.1.2. Indirect oxidation

During indirect electrochemical oxidation the organic pollutants are destroyed by an electron-transfer agent, such as ClO^-/Cl^- [23] or Ag^{2+}/Ag^+ [Almon, 1992]. The extremely high standard potential of the reaction (1.96V/NHE, in nitric acid medium): $Ag^+ \rightarrow Ag^{2+}$, establishes silver ions as the ideal mediator which attack organic species such as tributylphosphate (TBP), tetraphenylborate (TPB) and benzene [Almon, 1989]. The process has the potential for use in waste treatment as well as even for the disposal of radioactive organic waste. When used as an electron-transfer agent, silver acts as a reusable catalyst, and no silver waste is generated. Because the anodic reaction is balanced by the cathodic reduction of nitric acid,

$$HNO_3 + 2\ H^+ + 2e^- \rightarrow HNO_2 + H_2O \tag{6}$$

Nitric acid must be regenerated by the chemical reaction of nitrous acid with oxygen. Furthermore, separators must be inserted into the cell to prevent the HNO_2 from migrating to the anolyte compartment and reducing the Ag^{2+}.

The mechanism has been studied by means of spectroscopic and potentiometric methods [Lehmani, 1996].

2.5.2. Membrane-assisted methods

Membranes serve as separators and solid electrolytes in many fields of applied electrochemistry. For the treatment of polluted water two main principles are:

• Electrodialysis

• Solid-Polymer-Electrolyte (SPE) applications.

2.5.2.1. Electrodialysis

The use of direct-current electricity to increase the rate of dialysis of electrolytes or to produce demineralised water from potable water has been known for about 100 years.

Electrodialysis is an electrically driven ion-exchange membrane-separation technology that is capable of separating selected ions from aqueous mixtures and concentrating them. Electrodialysis, like evaporation or reverse osmosis, can recover pure water from a salt solution or concentrate the total dissolved solids in a waste stream.

The electrodialysis stack consists of both anion- and cation-exchange membranes assembled alternately and separated by a proprietary gasket-spacer which directs the flow of solution into

35

provided chambers and distributes flow. The driving force in an electrodialysis stack is electricity, applied as direct current flowing from an anode at one end of the stack, through the stack, to the cathode at the other end of the stack. The ion-exchange membrane, the current density and the electrolyte to be processed are all influenced by the electrodialytic system.

The direct current causes the positively charged cations to migrate toward the cathode, and the negatively charged anions to migrate towards the anode. When an ion contacts an anion-exchange membrane surface, the properties of the membrane determine whether the ion is rejected or allowed to pass through it. As with ion-exchange resin technology, the ion-exchange membranes are thin-film polymers containing electrically charged functional sites. These selectively charged membrane barriers thus effect a separation. This ability of the membrane to separate ions is called permselectivity, which can be custom designed to meet specific demands.

Figure 5. Electrodialytic removal of fluorine and HF gain by use of a bipolar membrane.
AEM: Anion Exchange Membrane; **CEM**: Cation Exchange Membrane

Electrodialysis has been successfully used for the removal of fluoride from drinking water in the coastal areas of the Zhejiang Province of China [Sun Li-Cheng, 1985]. The fluorides are forced through permselective anion-exchange membranes by the electric field. A product gain could be accomplished by adding a bipolar membrane to the fluoride-enriched chamber to produce HF as illustrated in Fig. 5. The construction and operation of a large scale ED water desalination plant has been descibed by Kawahara [Kawahara, 1994].

2.5.2.2. Solid-Polymer-Electrolyte (SPE) applications

The literature describes both oxidative and reductive treatment for water purification by SPE.
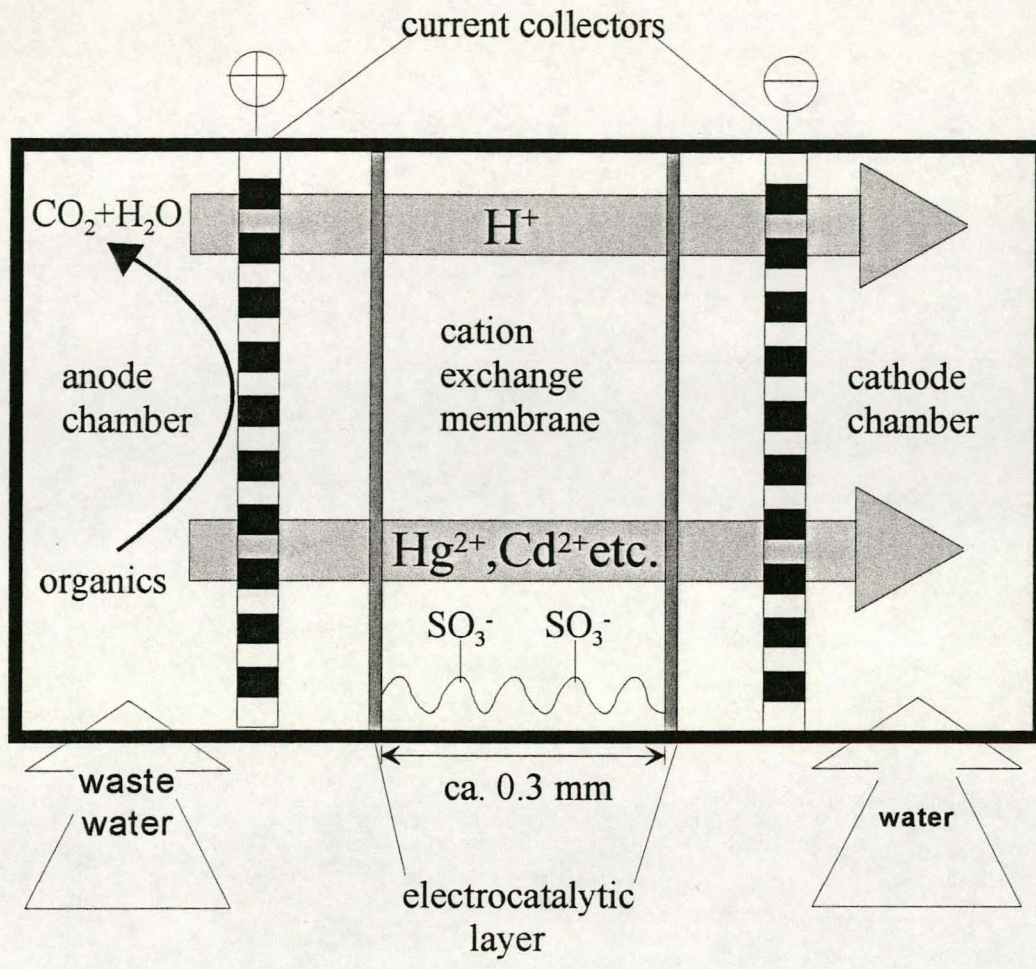
Fig. 6. SPE configuration for combined combustion and heavy metal removal supporting a cation-exchange membrane

An adverse effect of using an electrochemical oxidation approach for water purification is the low ionic conductivity of many types of waste water. For the electro-oxidation process to be effective for organic contaminants, acid, base or salt must be added to form an electrolyte. This is impractical for many purposes. Ion-exchange membranes work as solid

38

polymer electrolytes (**SPE**), even in non-conductive fluids. Of special importance in the **SPE**-process is the electro-osmotic transport through the membrane, which should be used to enhance the mass transfer at the electrodes and thus improve selectivity and yield.
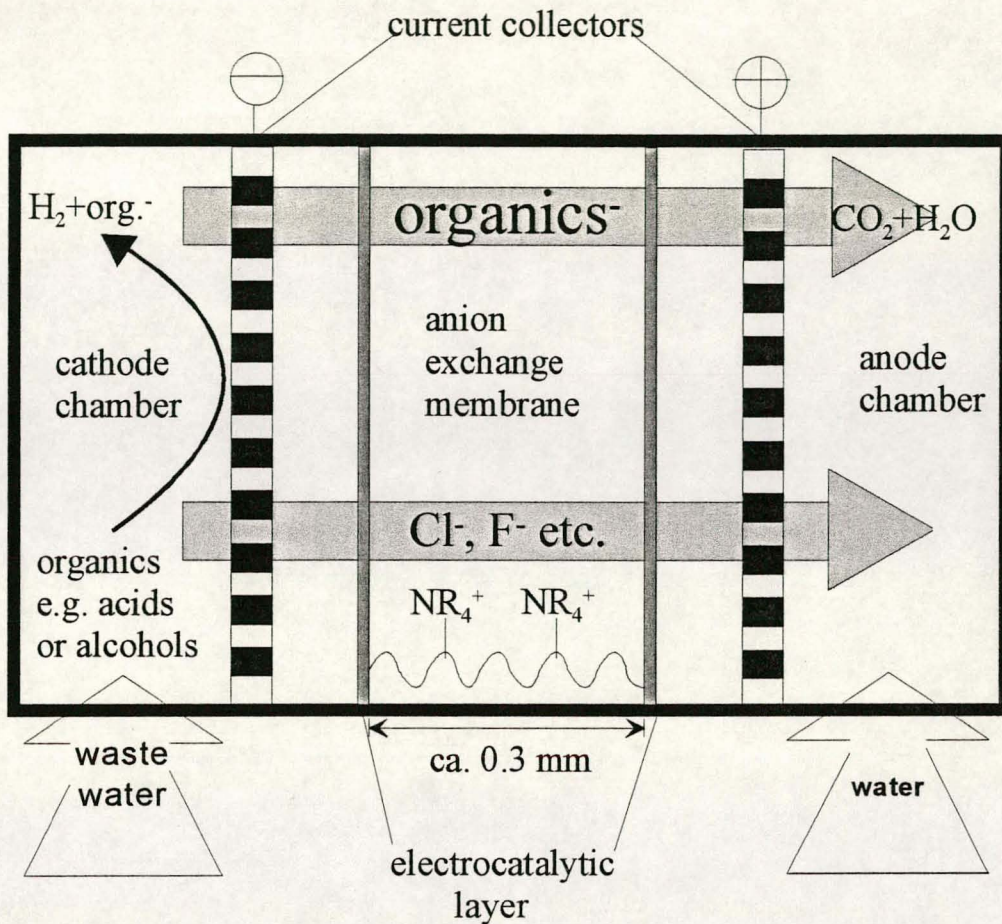
Fig. 7. SPE configuration for combined combustion and anion removal supporting an anion-exchange membrane

The direction of the mass transport is determined by the choice of a cation or an anion exchange membrane. Fig. 6 illustrates the principle of an **SPE** configuration. The ionic flux is maintained by the protons and the electrodialytic removal of heavy metals can be carried out simultaneously. When an anion-exchange membrane is used for separation, the organics are

ionised at the cathode and driven through the membrane to the anode where electrochemical oxidation takes place, as illustrated in Fig. 7.

Another membrane assisted approach has been made for the so-called electro-catalytic nitrate-elimination (NKE-process) [Stadlbauer, 1996]. Doing this, NO_3^- is electrochemically reduced at a catalytic active surface (Pd) according to the following equation (H_{ad} is H adsorbed):

$$2\,NO_3^- + 2\,H^+ + 10\,H_{ad} \rightarrow N_2 + 6\,H_2O \tag{7}$$
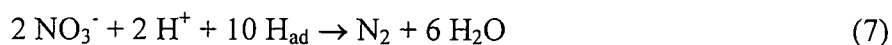
Hydrogen ions form at the anode, pass the cation exchange membrane to reach the cathode. At the cathode the hydrogen necessary for the nitrate reduction is produced electrochemically in the very reactive state of status nascendi. The major advantage of the reductive treatment of nitrates is that the only endproducts are nitrogen-gas and water. Fig. 8. Illustrates the set-up used for the nitrate-removal installation.
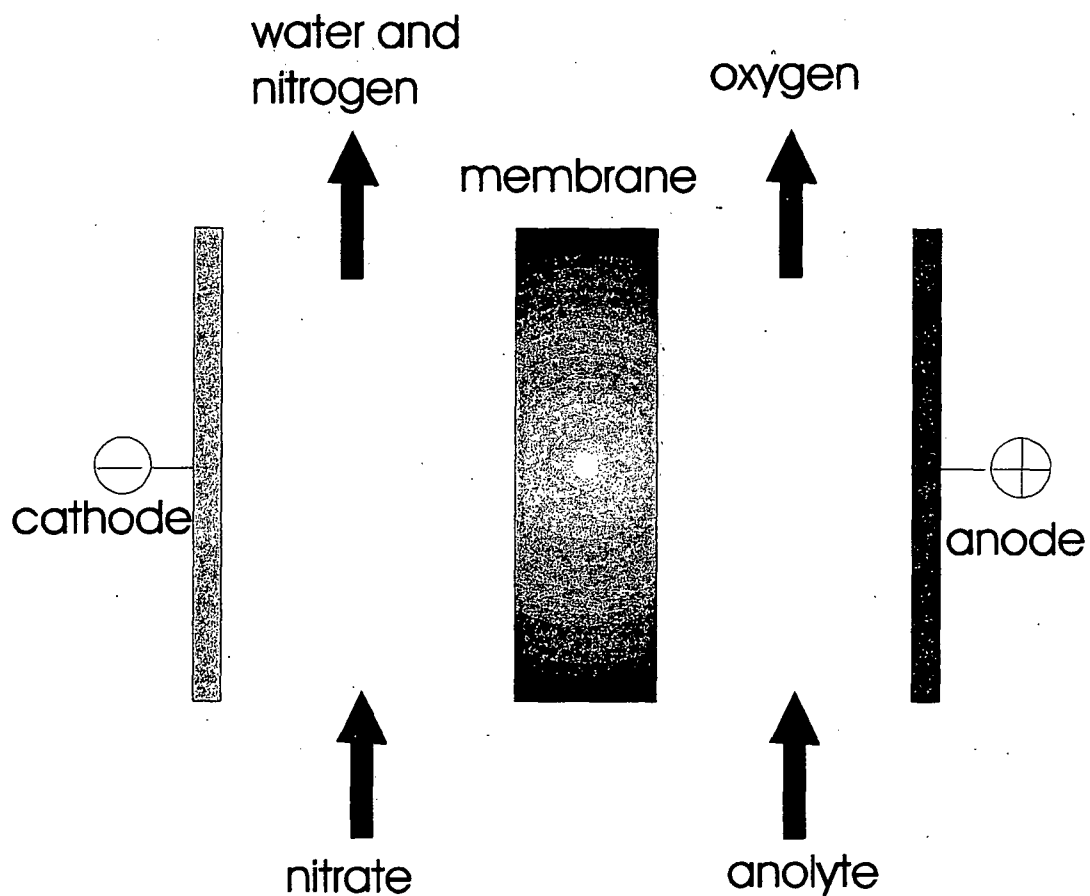
Fig. 8. Principle of the EKN-process

2.6. Electrochemically generated species for disinfection

Once water has been purified, measures must be taken to guarantee the safety of the water during storage. Electrochemically generated species for disinfection can serve that purpose. The production of chloride and hypochlorite at graphite or dimensionally stable titanium-anodes can be used for the destruction of micro-organisms and macro-organisms, especially for the disinfection of the water in pools, according to equation (8).

$$6Cl^- \rightarrow 3Cl_2 + 6e^-$$ (8)

$$3Cl_2 + 6OH^- \rightarrow 3ClO^- + 3Cl^- + 3H_2O$$
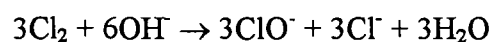
Hydrogen peroxide, a powerful oxidising agent, is another substance that can prevent bacterial growth in the water. It can be accumulated at the cathode as an intermediate of the oxygen-reduction reaction:

$$O_2 + H^+ + 2e^- \rightarrow H_2O_2 \tag{9}$$

The heterogeneous reaction is favoured at high temperatures and low pH-values, and preferably runs at electrodes such as Pt, Ag and activated carbon.

2.7. Adsorption methods

Electrosorption, for the removal for all kinds of contaminants, is best carried out with activated carbon, because of its extremely high surface area. A new device, called the flow-through capacitor, which might be important for future applications of water purification, has recently been patented [M. Andelman, 1996]. As the effluents pass the carbon electrodes a small voltage is applied to cause electrosorption. The electrosorbed species are released in small amounts of concentrated water by short-circuiting the electrodes.

Chapter 3

Electrode preparation for the electro-catalytic oxidation of hazardous organic contaminants in water and surface analysis.

Abstract

Novel SnO$_2$-based electrode material has been designed by a sol-gel dip-coating method. Titanium foil served as a support for the electro-catalytic film. As tin dioxide is a large band-gap semiconductor, the conductivity had to be improved by doping the film for an electrode application. In this study the effect of fluorine- and antimony-doping on the conductivity of the film was investigated. Conductivity measurements were carried out on the SnO$_2$ films deposited on quartz plates using the four-probe method across the surface. The surface polarity (hydrophobicity) of the bulk materials was measured by competitive adsorption [Glöckler, 1992; Weikamp, 1992; Berke, 1991] with especially built equipment [Klein, 1996]. The hydrophobicity index HI is defined as ratio of adsorbed n-octane over adsorbed water. A HI > 1 indicates a hydrophobic, < 1 a hydrophilic surface. Surface areas of the powdered materials were measured by Ar-adsorption isotherms in liquid Ar.

PbO$_2$ deposited galvanostatically on Ebonex was also prepared and used as a reference electrode material.

3.1. Theoretic background

3.1.1. Electronic band structure of oxides of the rutile lattice

The sol-gel dipping technique leads to very high-quality SnO_2 layers with respect to structure and morphology. Chemical modifications, achieved readily by the addition of selected dopants, like antimony alkoxides, antimony chlorides, $K_2[PtCl_6]$ or fluoride to the sol, should reduce the band gap between the valence- and conducting bands as an n-donor in the oxide and thus increase conductivity. Fluoride addition should furthermore reduce the surface polarity of the electrode and thus improve the adsorption of organics on the electrode surface. Fig. 9. shows the band structure scheme for the rutile modification of SnO_2 and PbO_2, where the 26 valence electrons just fill all anionic, all t- , and all e-type states. Since a gap is expected to occur between the e-type and s-type energy states, these materials should be insulators or semiconductors in accordance with the literature [Wabner, 1985]. As illustrated, n- or p-doping with fluoride or antimony can convert SnO_2 to a conductor. PbO_2 already has metallic conductivity. This means that the e_σ - s_σ gap has now been totally eliminated and that very broad bands have formed, facilitating electron movement.
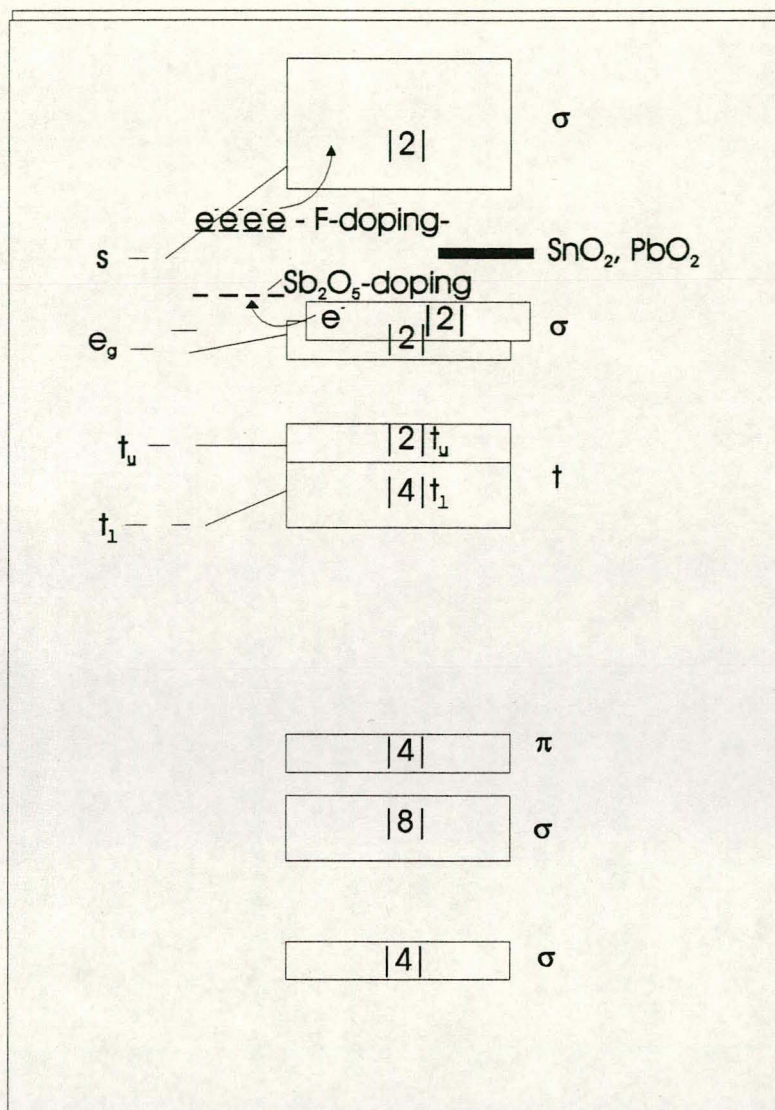
Fig. 9. Model of the band structure scheme of the rutile lattice of SnO_2 and PbO_2

3.1.2. The sol-gel process

Sol-gel chemistry is a versatile tool for the preparation and understanding of catalytic materials. The large variety of synthetic parameters provides control over the structural and chemical properties of catalysts. Sol-gel synthesis offers better control over pore volume, surface area, porosity and pore size distribution. Sol-gel can also facilitate multi-element

45

systems in a single step. The sol-gel process provides a new approach to the preparation of catalysts, membranes, thin layers (catalytic films) etc.

Starting from molecular precursors, an oxide network is obtained by hydrolysis-polycondensation of alkoxides. The solution chemistry of alkoxides is investigated, the precursors are commercially available and used in most studies. Sol-gel synthesis involves the formation of a sol followed by the formation of a gel. A gel is a diphasic material with a solid encapsulating a liquid. These polymerised alkoxides are dried to remove the encapsulating liquid, leaving a porous network. The external surface of the sol-gel catalyst is relatively small compared to the internal surface area. Thus, sufficient diffusion of molecules through the pores of the active catalyst centres is crucial and requires a proper design of the pore structure.

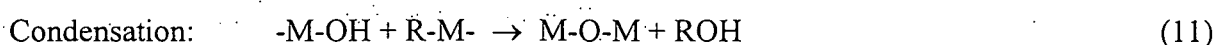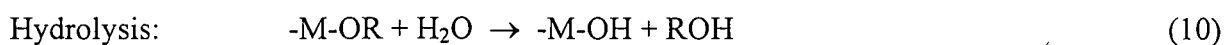Sol-gel chemistry is based on the hydrolysis of a precursor and the condensation of partially hydrolysed species to form a three-dimensional network. These two reactions can be represented as:

Hydrolysis: $\qquad$ -M-OR + H$_2$O $\rightarrow$ -M-OH + ROH $\qquad\qquad$ (10)

Condensation: $\qquad$ -M-OH + R-M- $\rightarrow$ M-O-M + ROH $\qquad\qquad$ (11)

Although this is a reduced representation, the complexity thereof makes its simplification necessary.

The basic premise is that the sol-gel product depends on the relative rates of hydrolysis and condensation. For example, precipitates form if the hydrolysis rate is low and the condensation rate is fast. Controlling these rates can change the characteristics of the product for specific applications. Factors that can be also varied include acid or water content, the type of precursor, the type of solvent, precursor concentration and temperature.

Three approaches are used to make sol-gel monoliths:

- gelation of a solution of colloidal powders

- hydrolysis and polycondensation of alkoxide or nitrate precursors followed by supercritical drying of gels

- hydrolysis and polycondensation of alkoxide precursors followed by aging and drying under ambient conditions.

Sols are dispersions of colloidal particles in a liquid. Colloids are solid particles with diameters of 1 – 100 nm [Davis, 1963]. A gel is an interconnected, rigid network with pores of submicrometer dimensions and polymeric chains whose average length is greater than a micrometer. The term gel embraces a diversity of combinations of substances that can be classified in four categories as discussed by Flory [Flory, 1953]:

- well-ordered lamellar structures;

- covalent polymeric networks, completely disordered;

- polymer networks formed through physical aggregation, predominantly disordered;

- particular disordered structures.

A gel may be formed by network growth from an array of discrete colloidal particles (method 1) or by formation of an interconnected 3-D network by the simultaneous hydrolysis and polycondensation of an organometallic precursor (methods 2 and 3). When the pore liquid is removed as a gas phase under supercritical conditions (critical-point drying, method 2), the network does not collapse and a low density *aerogel* is produced. Aerogels can have pore volumes as large as 98 % and densities as low as 80 kg/m^3 [Graham, 1864; Yoldas, 1975; Fricke, 1988].

When the pore liquid is removed near ambient pressure by thermal evaporation (called drying, used in method 1 and 3) and shrinkage occurs, the monolith is termed a *xerogel*. If the pore liquid is primarily alcohol based, the monoliths are often termed *alcogels*. The generic term gel usually applies to either xerogels or alcogels, whereas aerogels are usually

designated as such. A gel is defined as dried when the physically absorbed water is completely evacuated. This occurs between 100 and 180°C.

A dried gel may still contains a very large concentration of chemisorbed hydroxyls on the surface of the pores. Thermal treatment in the range of 500 – 800° C desorbs the hydroxyls and thereby decreases the contact angle and the sensitivity of the gel to rehydration stresses and results therefore in a stabilised gel.

3.1.3. Tin dioxide prepared by sol-gel

Stannic oxide is an important oxide semiconductor and its properties have been well understood over the temperature regions practical for applications. It has a wide band gap and one of the highest mobilities of the carriers (electrons) among oxides. Its semiconductance can be controlled by doping with antimony and/or fluorine. Besides electrode materials, tin oxide semiconductors with dopants and additives are widely used as transparent, electronically conductive electrodes in electrochromic devices (ECD), low emitting (i.e. heat reflection) coatings and as conductance type gas sensitive detectors [Granqvist,1990]. Although various techniques could be used for their fabrication, the sol-gel route in combination with a dip-coating technique is particularly attractive because it is possible to already tailor the properties of the final oxide at the beginning or the production process i.e. in solution. Generally, the sols could be produced either directly from inorganic salt solutions or from the metal alkoxides after which hydrolysis and polymerisation yield the gels and xerogels. Conversion of xerogels into final oxides requires removal of organic residues and is attained by heat-treatment of the xerogel films at temperatures rarely exceeding 500°C.

It is generally accepted that the alkoxide route is more appropriate for the fabrication of optical films. The yield of the corresponding dip-coating process is quite high and the dip-coated films exhibit high compactness and low porosity. However, the inorganic route has

been successfully used for film-preparation although it is known that films are less homogeneous and more porous when they are deposited from the aqueous colloidal inorganic solutions [Brinker, 1990]. In this study electrode material has been produced by both an inorganic and an organic sol-gel dip-coating route.

3.2   Experimental - preparation of the various electrode materials

3.2.1. Preparation of SnO_2 solution via the inorganic route

The Sb-doped SnO_2 films were prepared from two alkoxides [Hench, 1984; Mazdiyasni, 1982; Mehrotra, 1990] obtained directly from chlorides. The SnO_2 solution was obtained by dissolving 8.37 g of $SnCl_2 \bullet 2H_2O$ in 100 ml of absolute ethanol. The antimony solution was simultaneously prepared from a given amount of $SbCl_3$ dissolved in 20 ml of absolute ethanol. Both mixtures were separately stirred and heated in a closed vessel. Then the vessels were opened, and the solutions again stirred and heated until the solvent was completely evaporated. Finally, two powders were obtained and then mixed in 50 ml of absolute ethanol in accordance with the desired doping level. For the fluoride doping triethoxyfluorosilane $(FSn(OEt)_3)$ was added under nitrogen-atmosphere. For the Pt doping Na_2PtCl_6 was added to the solution The doped solution was finally stirred and heated to 50°C for 2 h. The doping level (Dp_{sol} ratio = $n_i/\sum n$) in the initial antimony solution was kept constant at 5 %, while the doping level for the fluoride ranged from 0-2.5 %.

It must be stressed at this point that the percentage of antimony introduced in the final solution used for the sol-gel dip-coating must be precisely controlled, as the reactions occuring in the solution are not known. Unknowns include, to what extent the dopant is

correctly mixed, and also if, owing to any time- (or temperature-) dependent possible reaction, a partial precipitation of Sb or other dopants occurs.

3.2.2 Preparation of SnO_2 solution via the organic route

Commercial $Sn(2\text{-ethylhexanoate})_2$, extra pure triethanolamine (TEA) and hexanol were used without further purification.

To an hexanol solution of the alkoxide (0.5M) one molar equivalent TEA was added at room temperature, and the mixture stirred at room temperature for 2h. Then 20 ml of deionised water, diluted with hexanol, was added drop-wise to the solution and the mixture was stirred at room temperature for 2h. The resultant clear solution was used for the dip-coating of the SnO_2 films. In the preparation of Sb-doped films, a mixture of the tin alkoxide and $Sb(\text{butanoate})_3$ for a doping level of 5% were used; for the Pt-modifacation the amount $Na_2[PtCl_6]$ necessary to achieve a doping level of 5% was added. The procedure to prepare the final solution was the same as described above.

3.2.3. The dip-coating process

All substrates were pretreated with nitric acid and rinsed with absolute ethanol prior to dip-coating. The beaker containing the sol was placed into a large glass container that was covered with a glass plate designed with a hole (Fig. 10.). The substrate was attached to a string passing through the hole in the glass plate and connected to a vibration-free motor (Wemo). Plates of quartz glass were used as substrates for the conductivity-measurements. Plates of titanium foil served as substrates for the electrodes. Before dip-coating the atmosphere in the container was saturated with ethanol. The substrate was immersed and pulled out of the sol continuously, and at a constant speed of 3 mm/min. When the plate was

completely removed from the solution the motor was stopped. The hanging substrate was allowed to dry for 6 hours. Afterwards it was dried at 100°C for 15 min in air. This coating procedure was carried out twice to heal cracks and defects in the film. Calcination was carried out in air by heating the substrate to 600°C at a rate of 1°C/min.
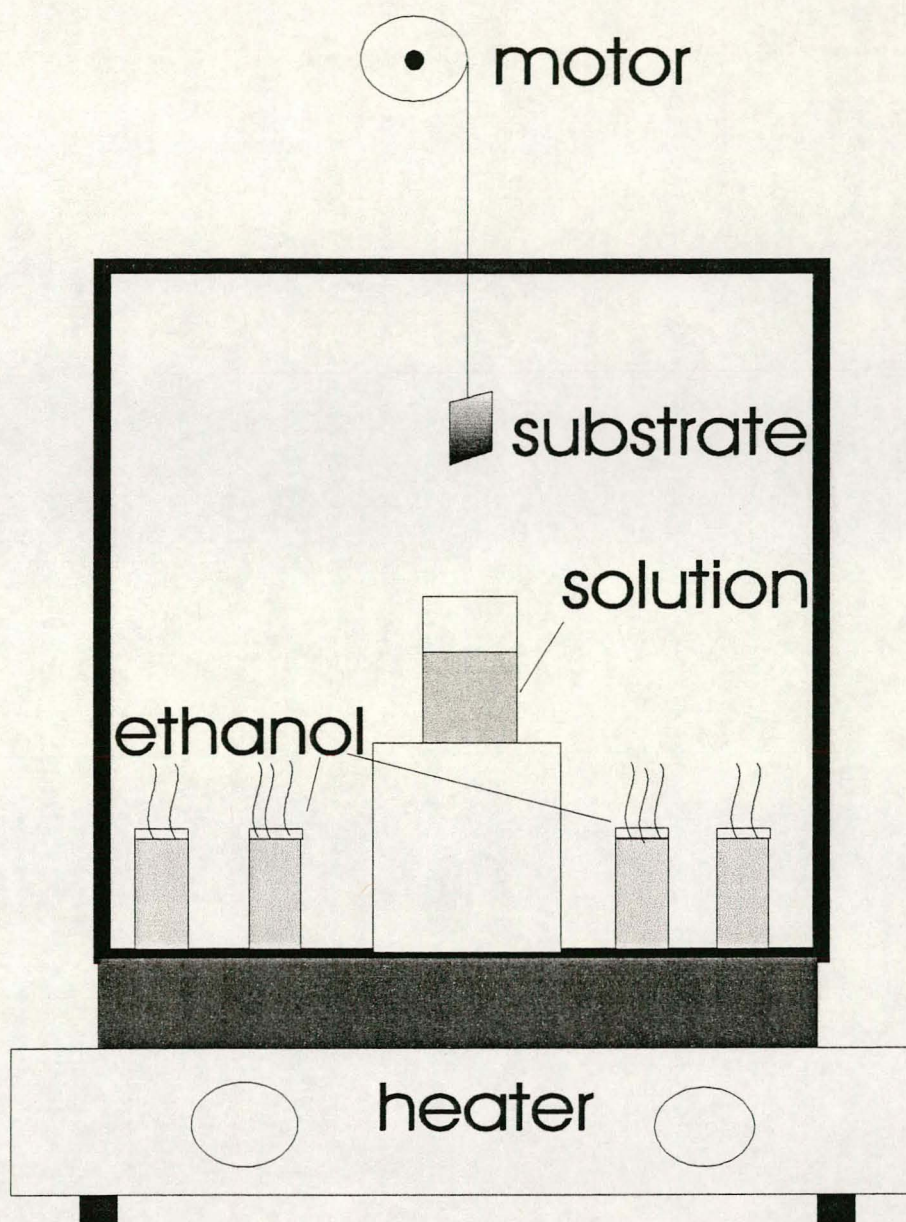

Fig. 10. Dip-Coating equipment with motor and atmospheric control

51

3.2.4. Galvanostatic deposition of PbO_2

Plates of Ebonex were coated anodically for 30 min with PbO_2 in an acid solution of $Pb(NO_3)_2$ (c.d. = 10 mA cm^{-1}, electrolyte: 0.4 mol l^{-1} $Pb(NO_3)_2$, pH = -0.3) [Trassati, 1980]. Ebonex, as Magneli phase titanium suboxides which are blue-black in colour and electrically conductive, has been reported to be an excellent support for any kind of electrocatalytic coating [Park,1995]. The remarkable combination of its electrical conductivity and very high corrosion resistance makes this material most suitable for use in electrochemical cells with particularly corrosive electrolytes [Graves,1992]. Additionally, the ceramic-rutile based structure of Ebonex ceramic makes it very compatible with rutile-structured surface coatings such as iridium dioxide, ruthenium dioxide and lead dioxide. For example, work recently carried out by Heraeus has shown that lead dioxide-coated Ebonex electrodes have projected lifetimes of at least 4 years at 1 kA/m^2 in fluoride-containing electrolytes [Mayr, 1990].

3.1.   Results

3.3.1. Conductivity measurements

In Fig. 11 the resistances of the SnO_2 films are plotted against the number of sequential dip-coatings (calcinations). Fig. 12 gives a better resolution of the resistivity of the inorganic samples as the organic films are not included.

The films were coated onto quartz glass and the resistances measured by the four-probe technique, using Pt-foil for contact and a multimeter. The antimony content was kept constant at 5 %. Changes in the conductivity were observed when fluoride was added as a dopant,

while the addition of Pt did not seem to influence the conductivity of the films. The fluoride content was 2.5 %, while the Pt content reached 5 %.

The specific resistance was calculated under the assumption that one layer of the film, after each calcination, had a thickness of 100 nm. This film thickness is based on AFM investigations of the films (film edge height) and a gravimetric measurement, carried out at the MPI-Mülheim, Germany. The results of the specific resistance are shown graphically in Fig 13 and Fig. 14. Fig. 14 only illustrates the specific resistance of the inorganic route. The specific resistance of the fluoride films (0.0048 Ohm cm) is in the range of metallic conductivity, whereas the results obtained from the organic precursors were quite poor. The results of the first two calcination steps were even omitted, because their resistivities were out of range. The incorporation of Pt into the matrix resulted only in little improvement with regard to conductivity.
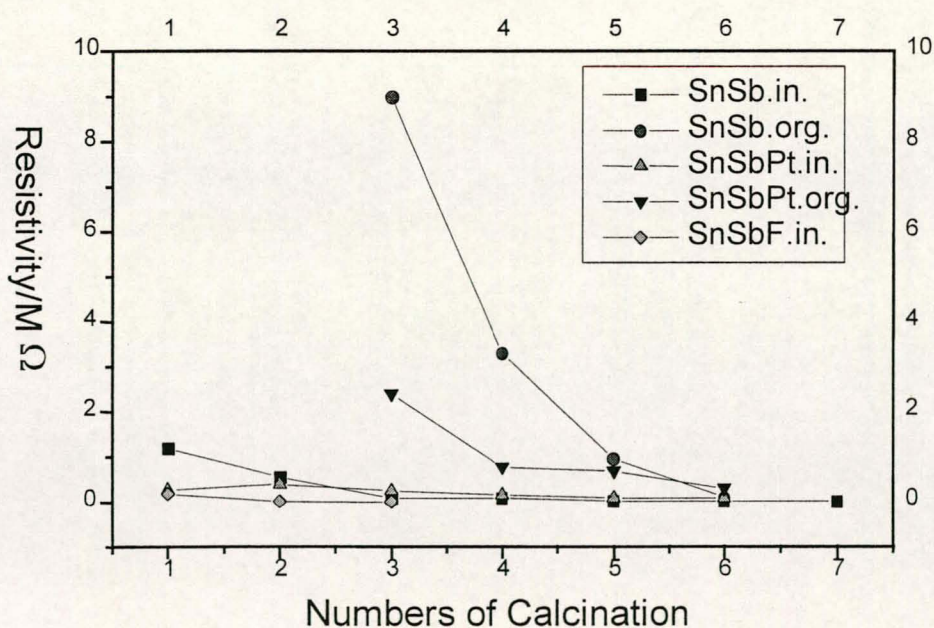
Fig. 11. The effect of the various dopants on the resistances of the SnO_2-films plotted against the number of calcinations: SnSb: 10 % Sb; SnSbPt: 10 %Sb, 5 % Pt; SnSbF: 10 % Sb, 2.5 % F. The index *in* stands for the inorganic route, *org* for the organic route

Fig. 12. Amplified parts of Fig. 11., excluding the organic films

The incorporation of fluoride into the SnO_2-film obviously improved the conductivity by reducing the band-gap between the valence- and the conducting band of the oxide.

Fig. 13. Specific resistivity of all the films
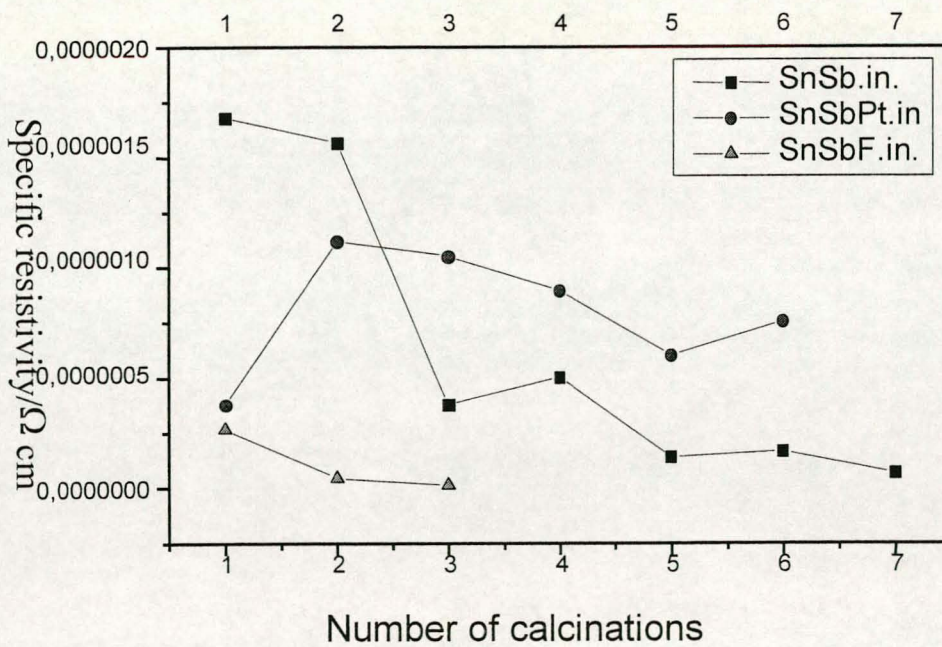
Fig. 14. Specific resistivity of the inorganic films only.

55

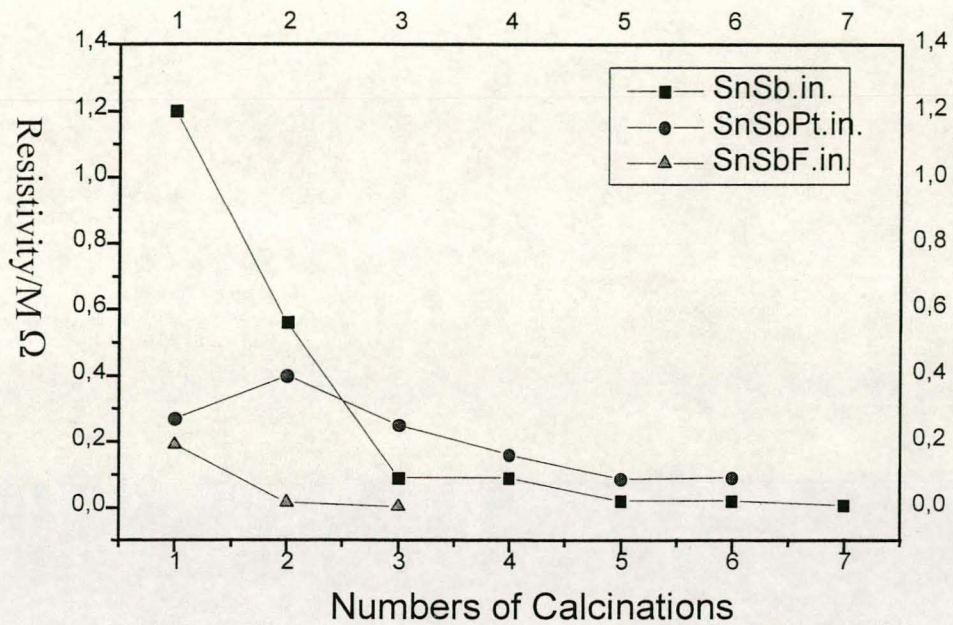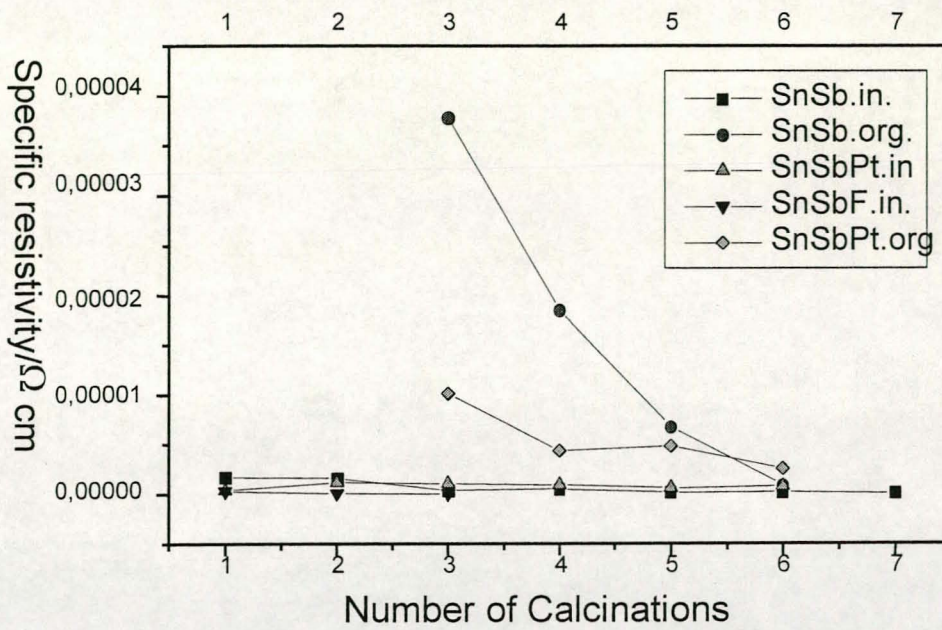Although the specific resistance should remain constant over time, a slight shift to lower values with increasing numbers of calcinations can be observed which indicates that the films become increasingly more dense during calcination.

Conductivity values for the undoped SnO_2 could not be obtained, as the resistance was out of range and could not be displayed on the multimeter.

3.3.2. Surface analysis of the Ti/SnO$_2$/Sb$_2$O$_5$ by microprobe

The surface of the electrodes with a doping level (Dp_{sol} ratio = $n_i/\Sigma n$) of 10 % Sb was investigated by microprobe analysis. The samples are bombarded by protons and the resulting X-ray spectra are analysed. The X-ray spectrum is shown in Fig. 15. The ratio of Sn/Sb calculated by integration methods ranged from 9.9 - 12.8 % for the Sb content, thus confirming that the dopant had been well mixed in the sol without detectable precipitation taking place.
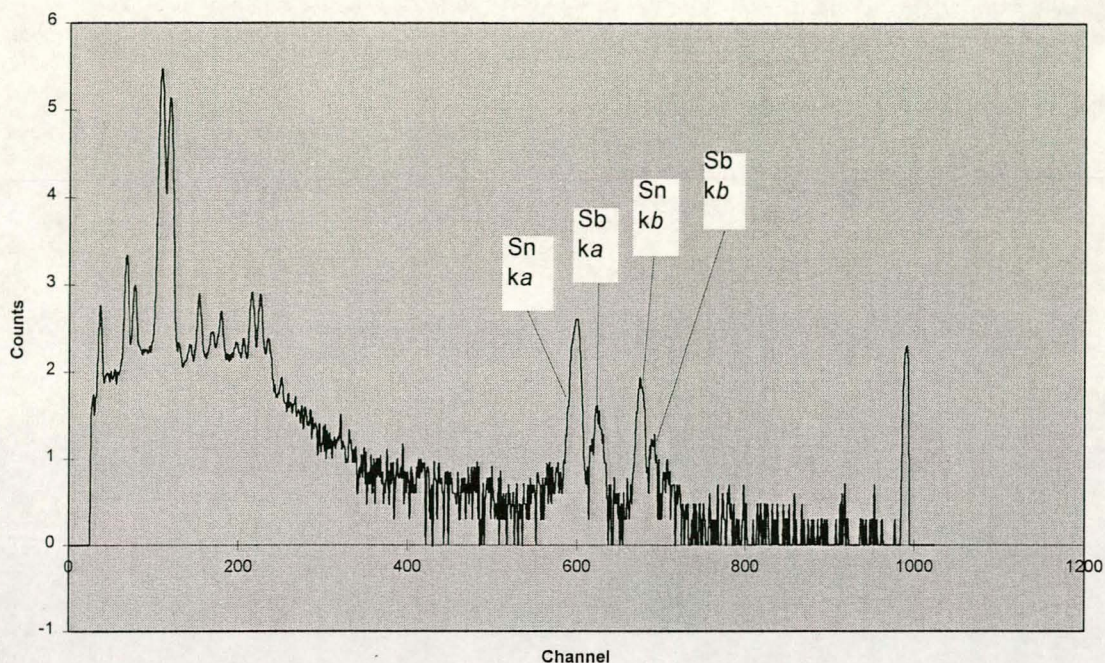
Fig. 15: X-ray spectrum of the surface of Ti/SnO$_2$/Sb$_2$O$_5$, indicating the Sn and Sb peaks.

Unfortunately, no information on the oxidation states of the elements could be obtained by this experimental method.

3.3.3 XPS Spectroscopy

The ionisation energies of electrons in compounds are measured by using photoelectron spectroscopy. According to the results, the scientist obtains a picture of the energies of the orbitals.

The energy hν supplied by the photon corresponds to the sum of work necessary for the removal of the electron from the orbital plus the kinetic energy of this electron. This is explained by the following equation:

$$h\nu = 0.5\ m_e\ v^2 + I_i \qquad\qquad (12)$$

57

when I_i is the ionisation energy of an electron from orbital i.

Using X-ray photoelectron spectroscopy (XPS), the photons have enough energy to knock out the core electrons. The energy of the core shells is to a large degree independent of the chemical environment of the atom. Consequently, the resulting absorption lines are characteristic for distinct elements in a film, molecule or alloy. Elementary analysis of films is thus possible. The value of the absorbing energy can furthermore help to determine the oxidation state of the analysed element. This is why this method is also often referred to as ESCA (electron spectroscopy for chemical analysis).

ESCA is limited to investigations of the surface, because while merely the X-rays can penetrate thicker samples, the resulting expelled electrons can only pass a few nanometers through a compact sample.

To confirm the results from the microprobe analysis, further surface analysis was undertaken with XPS at the Heinrich-Heine-Universität Düsseldorf, Germany. The method provided additional information on the oxidation states of the coating. The entire spectrum of the electrode prepared by the inorganic sol gel route is shown in Fig. 16.
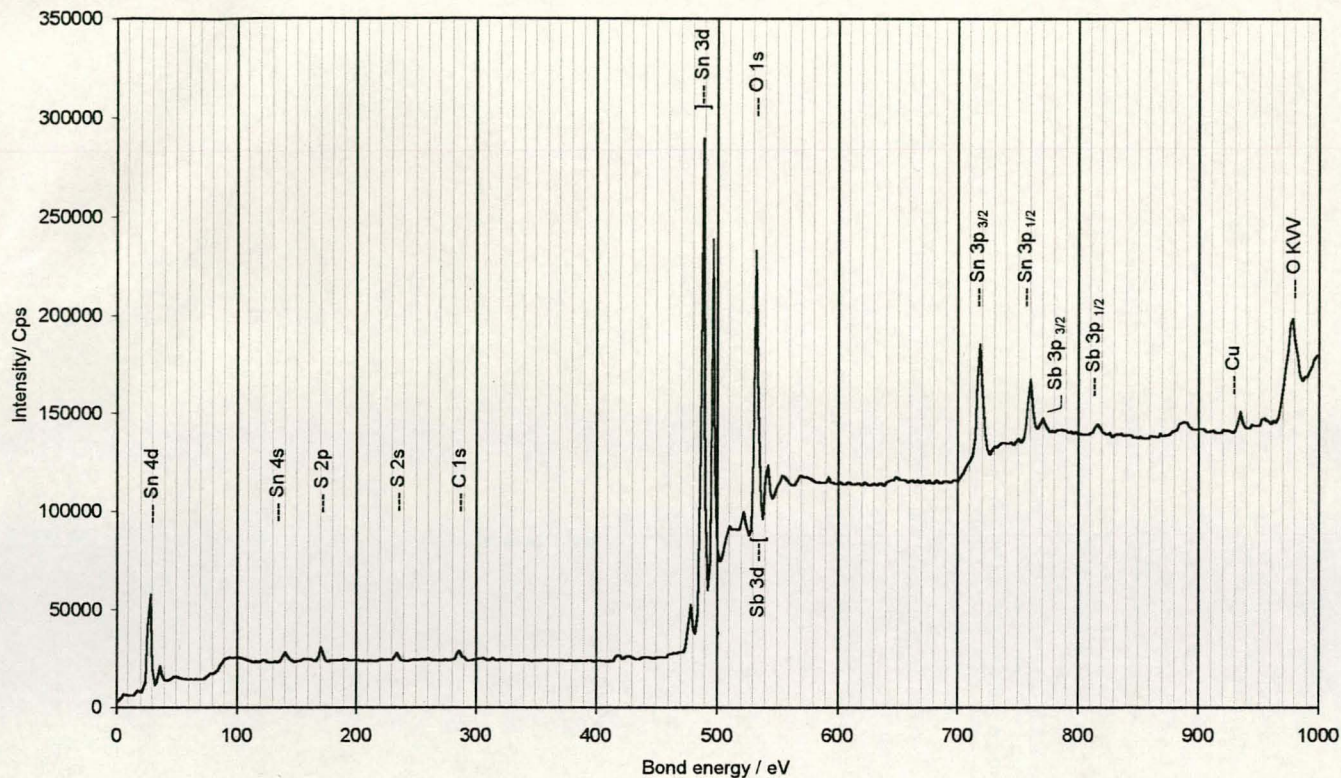
Fig. 16. XPS-spectrum of the Ti/SnO$_2$/Sb$_2$O$_5$ electrode, prepared by the inorganic route

The catalytic layer of the electrode material was investigated. Information about the distribution of the elements and the oxidation state of the elements was obtained. The determination of the antimony was not straight forward, as its signal appears at the same binding energy as the oxygen peak. The peak at 532 eV (Fig. 17) had to be separated into an oxygen peak and an antimony peak. In our case this was done by making use of the relation between the pre-wave (Sb 3d$_{5/2}$) at 532 eV and the wave at 541 eV (Sb 3d$_{3/2}$) for antimony is fixed to be 1.44. This precondition was used for the fit in Fig. 17.

59
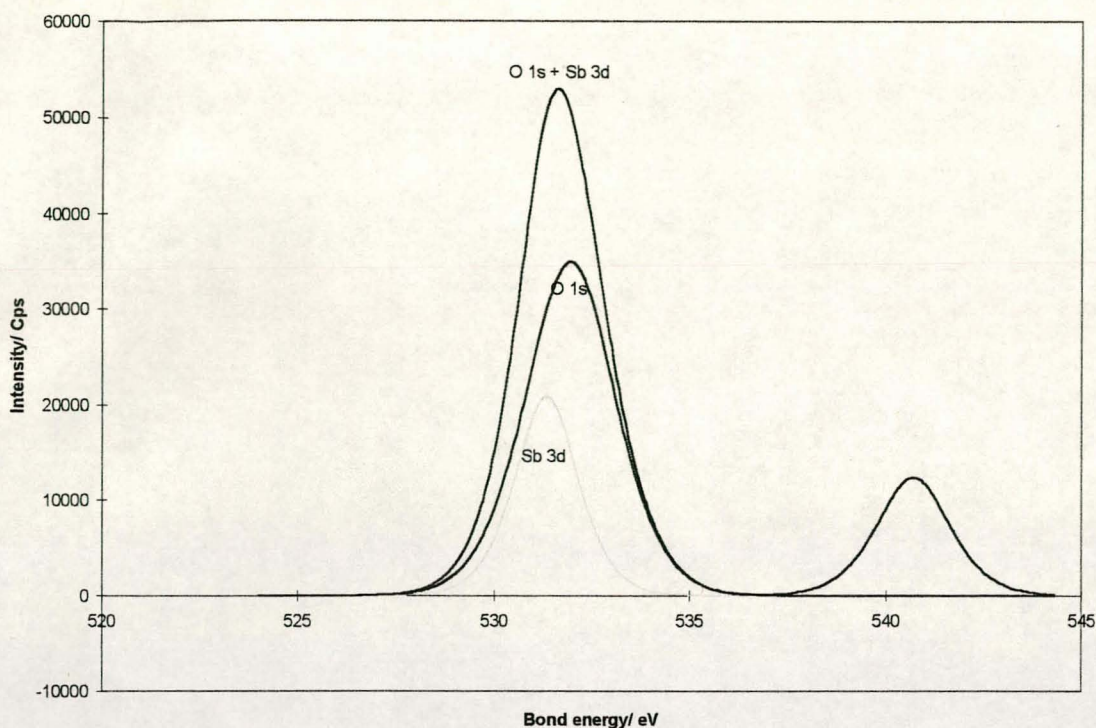
Fig. 17. Curve fitting for the separation of the oxygen and the antimony peak.

The real areas of the peaks had to be calibrated according to the sensitivity of the instrumentation towards the particular elements. The atomic ratio between Sn and Sb was found to be 4:1. Since the doping level (Dp_{sol} ratio = $n_i/\sum n$) of Sb in the initial solution was 10 %, part of the Sn must have precipitated out of the solution prior to the process of dip-coating. The shift in the binding energy of the elements determined the oxidation number and Sn was found to have the oxidation number 4, while the shift for Sb indicated an oxidation number of 5, corresponding to the oxides SnO_2 and Sb_2O_5. The fact that traces of sulphur and copper were detected on the surface, is explained by the treatment of the samples before the XPS-analysis. The samples and sample-holders (Cu) were purified with 2M H_2SO_4. Obviously, despite an attempt to remove them in an ultrasonic bath, small amounts of S and Cu had remained on the surface.

The samples prepared via the organic sol-gel route revealed a high Ti-peak, obviously given rise to by the titanium foil based substrate (Fig 18). This indicates defects in the film as

the substrate is not completely coated. The inefficient coating adds to the poor catalytic performance of this electrode material as is described in Chapter 4.
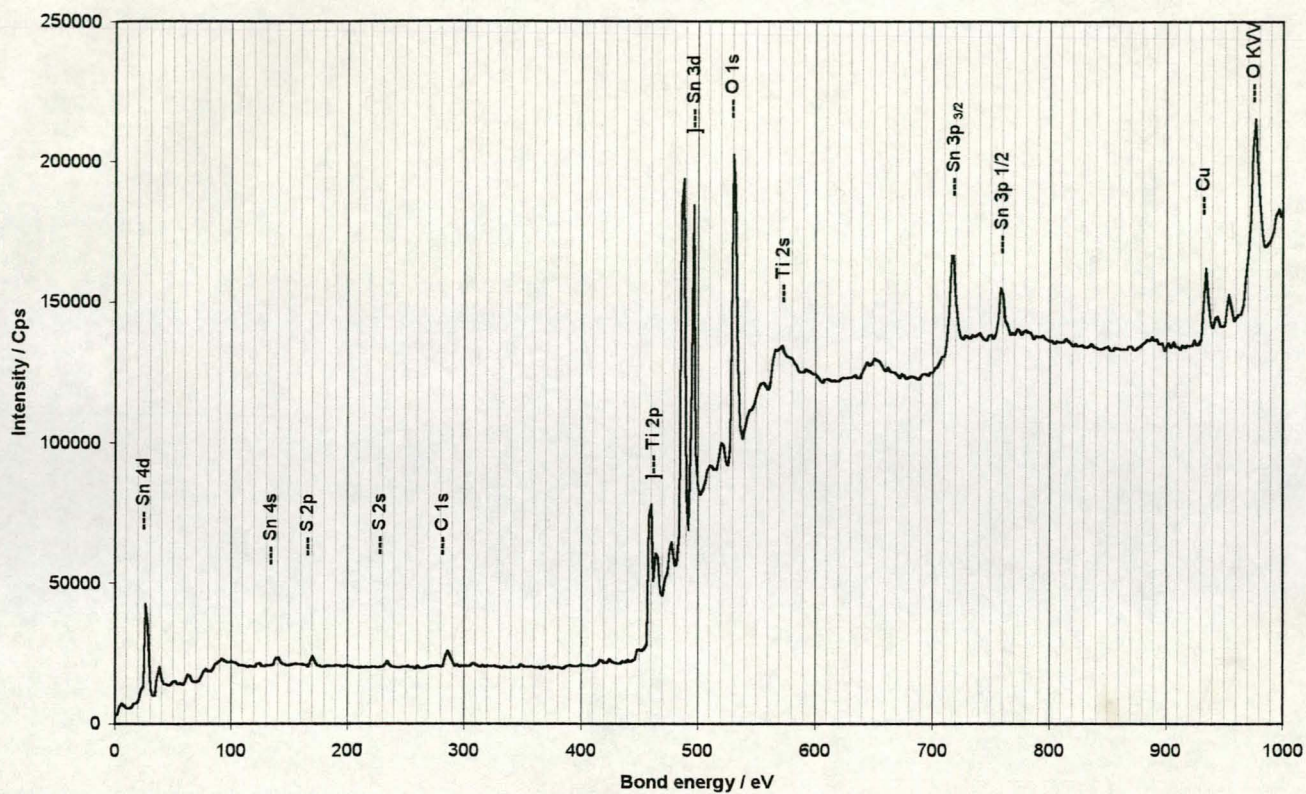
Fig. 18. XPS-spectrum of the Ti/SnO$_2$ electrode, prepared by the organic route

3.3.4. Hydrophobicity measurements

3.3.4.1. Experimental set-up for the measurement of the hydrophobicity index

The modified hydrophobicity index is a simple method for the estimation of the surface polarity. It is based on the competitive adsorption of n-octane and water from the gas phase.

The surface polarity measurements were implemented at the Max-Planck-Instiut für Kohlenforschung at Mülheim, Germany.

A weighed sample is placed in a protective gas stream and is heated to 300°C for desorption and the removal of impurities. After cooling to 30°C the sample is exposed to a stream of argon which contains defined and similar concentrations of water and octane. The water and octane content of the gas streams are dependent on the flowrate of the argon passing through the particle packed vessel. Consequently, accurate control of the flowrate is crucial for a correct measurement. The final ratio of the single components (water and octane) is determined by GC.
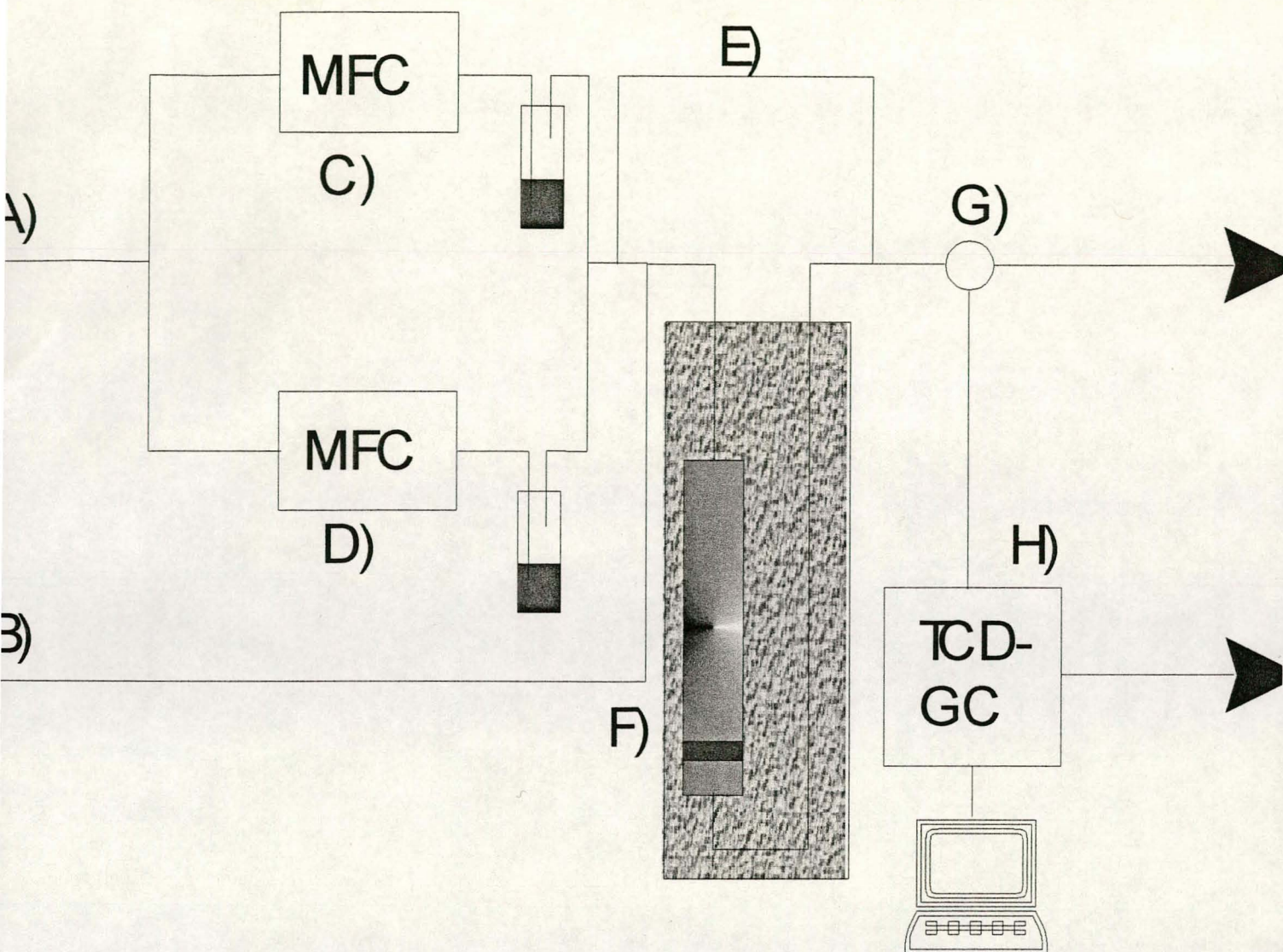
Fig. 19. Apparatus assembly for the determination of the surface polarity

a) Argon supply (saturation) $p_{mm} > 2$ bar

b) Argon supply (desorption) $p_{mm} - 0.4$ bar

c) + d) Separate mass flow controller for the saturation of octane and water

(saturation temperature 298 K)

e) Bypass

f) Vertically positioned, catalytic solid bed reactor with bronze filter for sample

protection in a temperature controlled metal block.

g) Six way valve (manual) for GC sample injection.

h) TCD-GC HP5890 (Thermal conductivity detector).

The reactor is heated to 323 K to avoid condensation.

3.3.4.2. Procedure

A known mass of the solid sample, normally a powder, is placed in the reactor, which is then closed by screwing on the lid. A moderate high temperature resistant copper paste is used on the threads to assist subsequent dismantlings. The reactor is installed into the metal heating block and secured by a cliplock (Swagelok)-fitting. To obtain a powdered sample, part of the sol-gel solution was allowed to dry without a dip-coating step involved. Thereafter, the sample was placed into the furnace and underwent the same temperature programme as the electrodes for calcination which is described in chapter 3.2.3. The surface polarity of the powdered material is thus identical to that of the coated films.

For the desorption of any contaminants on the sample, the sample is purged by an argon stream at 400°C for 12 hours. After that the temperature is set to 35°C, while the argon flow is continued and the heating band is wrapped around the capillary wires. The GC is set to a temperature of 50°C and the main valve to the helium flask is opened. After confirmation of the helium stream (approximately 5 min) the TCD can be switched on. Subsequently, the weighed saturation bubblers are inserted in the line, containing water and octane respectively. The saturation bath is kept at 25°C and the argon valve opened. After switching on the flow controllers the argon starts flowing through the saturation flasks. This has to be recorded as the starting time of the measurement. To avoid high pressure in the saturation section the outlet of the gas through the bypass must be assured. After cooling the reactor to 30°C, the measurements can start.

At first the H_2O background value of the chromatogram of the argon that purges the reactor has to be determined. This has to be done by simultaneously pressing the start button

of the integrator and opening the 6-way valve for 8 seconds. The obtained value is used for the calculation to be subtracted from the water peak.

After turning the valves (1) and (2) (saturation flow from the bypass through the reactor and argon through the saturation section, respectively), the initial chromatogram at t = 0 is recorded. The same procedure is repeated every 3.5 min until the saturation of water and octanol of the sample is reached.

3.3.4.3. Quantification

The quantitative calculation of the process curve was done with the numerical calculation programme TABLECURVE 3.0 (Jandelscientific). The programme determines the depicted integrals between y = 0 and y = 1 (Fig. 20) after fitting the data, obtained from the measurement to power functions.

The point of saturation for the sample is reached for the respective adsorbing species once its GC-peak converges at a constant value which is standardised to one. Physically, that means that because of the saturation of the sample, the powder does not adsorb either the octanol or the water and the argon stream transports them directly to the detector of the GC. Normally, saturation occurs for the octanol first, while the water peak is still going up.

The difference between the rectangular total area, formed by y = 1 and t_{max}, and the integral of the measured curve in the corresponding time frame, leads to the adsorbed component quantity (shaded area in Fig. 19). The total area in the saturation time frame equals the component quantities extracted from the saturation vessels (Δm_i). The value Δm_i is easily obtained by the mass difference of the saturation vessels prior to and after the measurement.

Given those integrals, the amount of water and octane adsorbed by the sample can be calculated (13). The hydrophobicity index is obtained by the ratio of the octane and water adsorption (14):

$$X_i = \frac{t_{sat}[\min] - AREA * \Delta m_i[mg] - background[mg]}{t_{whole}[\min]}$$

(13)

t_{sat} = time until the last measurement

AREA = integral of the fitted curve

Δm_i = mass loss of the saturation vessels

t_{whole} = the total time recorded for the saturators to determine Δm_i

$$HI^* = \frac{X_{octane}}{X_{water}}$$

(14)

X_{octane} = octane adsorption of the sample

X_{water} = water adsorption of the sample

The diagrams of Fig. 20 illustrate a typical concentration absorption experiment.
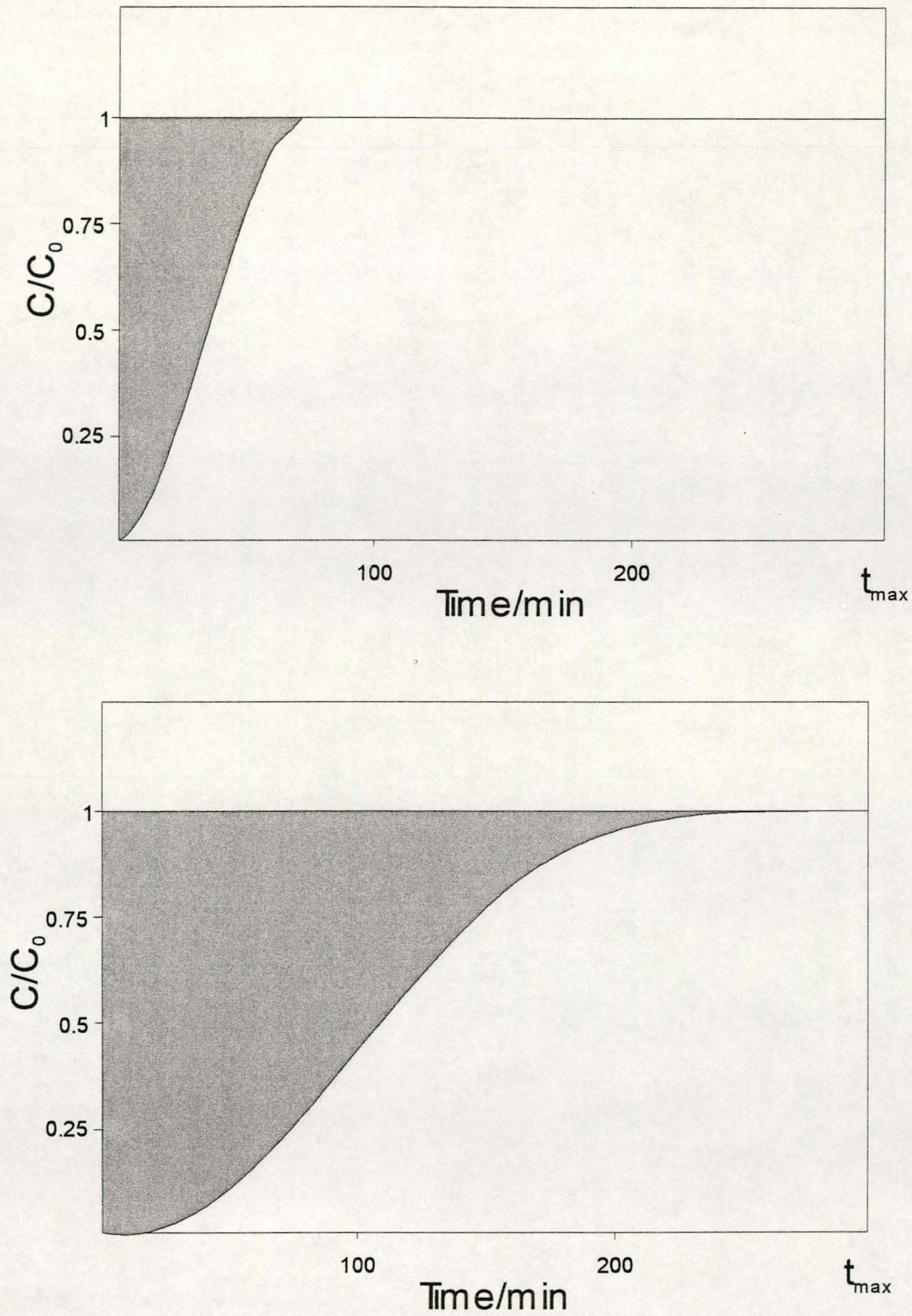
Fig. 20. Schematic illustration of the two adsorption curves. The octane curve is on top, the water curve below.

3.3.4.4. Hydrophobicity Results

Hydrophobicity measurements were conducted on powders, obtained by the inorganic sol-gel synthetic route. Both samples were doped with antimony (doping level of 5%). The second sample, however, was additionally doped by 5% of fluorine. The hydrophobicity measurements were carried out to determine if the fluorine doping had an effect on the surface polarity of the powders which would be expected to enhance adsorption of organics on the surface of the electrodes. An increase of the hydrophobicity index (HI) from 0.70 to 0.79 was observed upon addition of 5 % fluorine containing alkoxide. Thus an increase of the hydrophobicity can be detected, although the doping did not have a dramatic effect on the surface polarity, as the hydrophobicity index only showed a slight increase upon the addition of fluorine. Measurements and data evaluation were carried out at the Max-Planck-Institut at Mülheim, Germany.

Chapter 4

Characterisation of the electrode material by cyclic voltammetry

Abstract

The electrochemical oxidation of phenol as a model contaminant has been studied using different electrode materials (Ebonex, Ebonex/PbO$_2$, Ti/SnO$_2$) in water by means of cyclic voltammetry. Best results have been obtained with doped SnO$_2$-films on titanium foils prepared by a sol-gel dip-coating technique. The cyclic voltammograms reveal a high overpotential for oxygen-evolution, resulting in a well separated peak for the oxidation of phenol. Improvements of the conductivities of the films and higher current densities for the oxidation were obtained by doping the film sol-gel solution with 5% Sb. Doping with fluoride increased the conductivity and hydrophobicity, as described in chapter 2, but decreased the oxidation peaks. The PbO$_2$-coated Ebonex-electrodes were obtained by the galvanostatic deposition in an acidic PbNO$_3$-solution. Upon the addition of phenol to the electrolyte, however, the electrodes did not show a separated oxidation peak. The oxidation peak is partially hidden by oxygen evolution. The electrochemical characteristics of the electrode material Ebonex is not significantly changed by the addition of phenol to the electrolyte.

4.1. Theoretical background of cyclic voltammetry

4.1.1. The three-electrode arrangement

The only method to measure and impose an accurate potential difference at the working electrode is to use a three electrode system. A variable current source is used to pass a current through the working and counter electrodes. Changes in the potential of the working electrode are measured and adjusted versus a reference electrode, which carries practically no current. In this way the polarising current flows through one circuit (which includes the working and the counter electrodes) while the resulting change in the potential is measured in a different circuit (consisting of the working and the reference electrodes), through which the current is essentially zero. Since no current flows through the reference electrode, its potential can be considered to be constant, irrespective of the current passed through the working and the counter electrodes. Thus, the measured change in potential between the working and the reference electrode is truly equal to the change of potential of the working electrode. It should be noted that during measurement in a three-electrode cell, the potential of the counter electrode may change substantially. This, however, does not in any way influence the measured potential of the working electrode with respect to the reference electrode.

As the origin of the electrochemical potential scale, the Normal Hydrogen Electrode (NHE) has arbitrarily been selected. A Pt-foil in acidic aqueous solution with the proton activity of 1 is bubbled with hydrogen at a pressure of 1013.25 mbar.

For the potential determining reaction and the equilibrium potential φ_0 can be expressed by:

$$2\,H_3O+ + 2\,e- \;\rightleftharpoons\; H_2 + 2\,H_2O \tag{15}$$
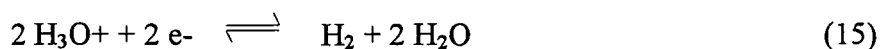
and

$$\varphi_0 = \varphi_{00} + \frac{RT}{F}\ln\frac{a[H_3O^+]}{\sqrt{p[H_2]}} \qquad (16)$$

φ_0 = potential of equilibrium.

φ_{00} = potential of equilibrium under standard conditions.

The standard potential φ_{00} of equation (15) is zero by definition.

The standard potential of any reference system is thus related to the NHE system and can be determined by equation (17):

$$E_{00} = \varphi_{00} \text{ (reference system) - } \varphi_{00} \text{ (NHE)} = \varphi_{00} \text{ (reference system)} \qquad (17)$$

The use of the normal hydrogen electrode is, however, awkward, because the hydrogen pressure at the electrodes surface and the pH in the system need to be constant. A good reference electrode consists of a reversible electrode with a readily reproducible and stable potential. A typical commercial reference electrode, such as a calomel electrode, is a complete system, with electrode and electrolyte enclosed in a small compartment and connected to the rest of the cell through a porous plug or Haber-Luggin capillary. The Haber-Luggin capillary is a small glass capillary which ends right in front of the working electrode, to reduce the iR_s potential drop in the solution.

Mostly, metal-ion-electrodes are in use, whereby the potential determining metal ion activity a $[Me^{Z+}]$ of the dissolved phase is in equilibrium with a solid phase (an almost

71

insoluble salt of the metal as a residue). Then a[Me^{Z+}] and thereby the equilibrium potential of the reference electrode is determined by the solubility K_a of the solid phase.

That means for instance for a silver-ion-electrode $Ag \rightleftharpoons Ag^+ + e^-$:

$$\varphi_0^{Ag/Ag^+} = \varphi_{00}^{Ag/Ag^0} + \frac{RT}{F} \ln a[Ag^+] \tag{18}$$

In the presence of a solid residue with , $K_a^{AgCl} = a[Ag^+] * a[Cl^-]$ the silver ion concentration can be expressed as:

$$a[Ag^+] = \frac{K_a^{AgCl}}{a[Cl]^-} \tag{19}$$

thus for the equilibrium potential for the silver-silver chloride electrode, it follows that:

$$\varphi_0^{Ag/AgCl/Cl^-} = \varphi_{00}^{Ag/Ag^+} + \frac{RT}{F} \ln K_a^{AgCl} - \frac{RT}{F} \ln a[Cl^-] \tag{20}$$

or, combining the term $\varphi_{00}^{Ag/Ag^+} + \frac{RT}{F} \ln K_a^{AgCl}$ and expressing it as the standard reference potential of the silver-silver chloride electrode, equation (20) becomes:

$$\varphi_0^{Ag/AgCl/Cl^-} = \varphi_{00}^{Ag/AgCl/Cl^-} - \frac{RT}{F} \ln a[Cl^-] \tag{21}$$

With $\varphi_{00}^{Ag/Ag^+} = 0.7996$ V NHE and $K_a^{AgCl} = 1.78 \times 10^{-10}$, $\varphi_{00}^{Ag/AgCl/Cl^-}$ has the value of + 0.2224 V NHE, the suffix NHE indicating the normal hydrogen electrode as the reference point.

For the choice of the reference system, compatibility with the various components in the solution is crucial. Thus, a calomel reference electrode ($Hg/Hg_2Cl_2/KCl$) should not be used in a solution of $HClO_4$ or of $AgNO_3$, because $KClO_4$ or $AgCl$ respectively, could precipitate in the porous plug and isolate the reference electrode from the solution in the main cell compartment. Also, since chloride ions are strongly adsorbed on electrode surfaces and can hinder the formation of passive films in corrosion studies, a calomel electrode should not be used, unless the test solution itself contains chloride ions, such as in seawater corrosion studies. Another concern is that the pH value of the reference system and the electrolyte should correspond, to avoid a concentration/potential drop at the entrance of the Haber-Luggin capillary.

In this study, either a mercury sulphate electrode ($Hg/HgSO_4/K_2SO_4$) or **R**eversible **H**ydrogen Electrode (**RHE**) were used. RHE is the hydrogen evolution potential in the solution for the present pH in the solution. It can be calculated by $V_{NHE} = V_{RHE} + 0.058\ pH$.

Table 1 gives a survey of the most commonly used reference systems:

Half-cell	Comments	Equilibrium-reaction	Volt
$Ag/AgCl/Cl^-$ (silver-silver-chloride-electrode)	$a[Cl^-] = 1$ saturated KCl KCl (c = 1 mol/l) KCl (c = 0.1 mol/l)	$AgCl + e^- \rightleftharpoons Ag + Cl^-$	0.2224 0.1976 0.2368 0.2894
$Hg/Hg_2Cl_2/Cl^-$ (calomel-electrode)	$a[Cl^-] = 1$ saturated KCl KCl (c = 1 mol/l) KCl (c = 0.1 mol/l)	$Hg_2Cl_2 + 2\ e^- \rightleftharpoons 2\ Hg + 2\ Cl^-$	0.2682 0.2415 0.2807 0.3337
$Pb/PbSO_4/SO_4^{2-}$ (lead-sulphate-electrode)	$a[SO_4] = 1$	$PbSO_4 + 2e^- \rightleftharpoons Pb + SO_4^{2-}$	-0.276
$Hg/HgSO_4/SO_4^{2-}$ (mercury-sulphate-electrode)	$a[SO_4] = 1$ H_2SO_4 (c = 0.5 mol/l) Saturated K_2SO_4	$Hg_2SO_4 + 2\ e^- \rightleftharpoons 2\ Hg + SO_4^{2-}$	0.6158 0.682 0.650
$Hg/HgO/OH^-$ (mercury-oxide-electrode)	$a[OH^-]$ NaOH (c = 1 mol/l) NaOH (c = 0.1 mol/l)	$HgO + H_2O + 2\ e^- \rightleftharpoons Hg + 2\ OH^-$	0.097 0.140 0.165

Table 1. Standard potentials of some customary reference electrodes against NHE

Fig. 21 and 22 illustrate the technical implementation of a mercury sulphate-electrode and a reversible hydrogen electrode. Both designs were realised by the glassblower of the University of Stellenbosch.

The Haber-Luggin capillary establishes the connection to the main compartment of the measurement cell. From there the electrolyte of the main compartment has to be sucked up a small pipe, where it is separated from the solution in the reference compartment by a porous plug.

Opening for sucking up the electrolyte from main compartment

Porous plug

H_2SO_4

Electrolyte from the main compartment

Hg_2SO_4

Mercury

Pt-wire

Haber-Luggin Capillary
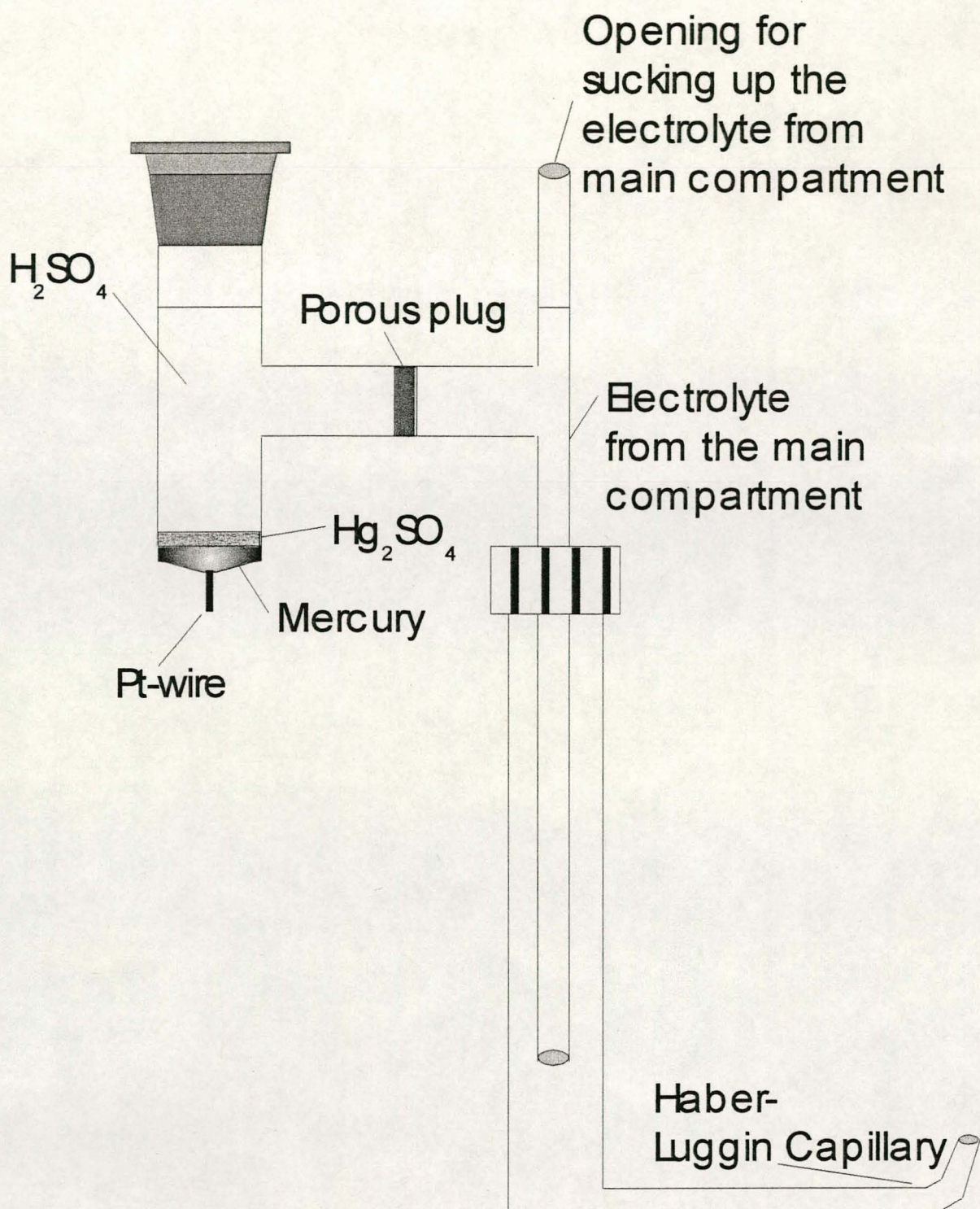
Fig. 21. Scheme of a mercury-sulphate-electrode.

The RHE is also mounted into the Haber-Luggin compartment in order to maintain contact

with the electrolyte of the electrochemical cell. The electrode itself is composed of a Pt-wire

in a small glass bell. The electrolyte is pipetted into that bell. By connecting the Pt-wire cathodically and applying a constant current, hydrogen evolves at the Pt-wire and is collected in the glass bell, while the lower part of the wire is still in contact with the electrolyte. Consequently, the hydrogen stays at atmospheric pressure (1013.25 mbar). The pH at the reference electrode is the same as in the solution.

Fig. 22. Scheme of a reversible hydrogen electrode (RHE).

4.1.2. Linear potential sweep and cyclic voltammetry

Linear potential sweep is a potentiostatic technique, in the sense that the potential is the externally controlled parameter. The potential is changed at a constant rate
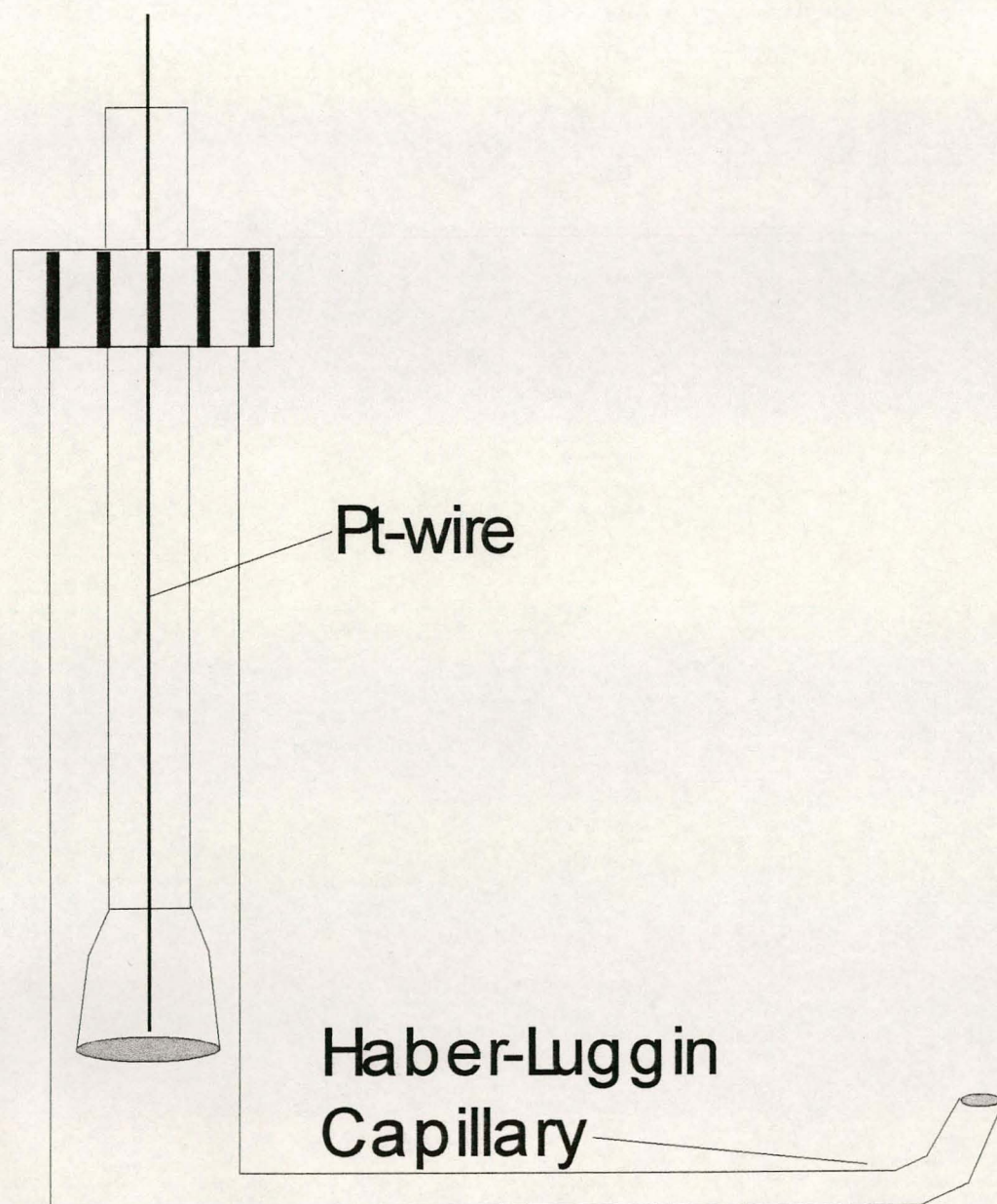
$$v = dE/dt \qquad\qquad (22)$$

and the resulting current is followed as a function of time.

When the potential is swept forward and backward between two fixed values, the technique is referred to as cyclic voltammetry. In this way the current measured at a particular potential on the anodic sweep can readily be compared with the current measured at the same potential on the anodic sweep. Almost all literature data are presented in this form.

Linear potential sweep measurements are generally of three types:

(a)   Very slow sweeps

When the sweep rate is very low, in the range of v = 0.1 – 2 mV/s, the system can be considered to be almost at equilibrium and measurement is conducted under quasi-steady-state conditions. The sweep rate plays no role in that case, except that it must be slow enough to ensure that the reaction is effectively at steady state at each potential in the course of the sweep. This type of measurement is used in corrosion and passivation studies and also in the study of some fuel cell reactions in stirred solutions. Reversing the direction of the sweep should have no effect on the i/E relationship, if the sweep is slow enough. This is rarely the case, however, because the surface changes during the sweep. In most cases an oxide is formed, and its reduction occurs at a more negative potential than the potential of its formation.

(b)   Studies of oxidation or reduction of species in the bulk

In the second case, the sweep rate is usually in the range of 0.01 – 100 V/s. The lower limit is determined by the need to maintain the total time of the experiment below 10 – 50 seconds (i.e., before mass transport by convection becomes important). The upper limit is determined by the double layer charging current and by the uncompensated solution resistance.

(c)   Studies of oxidation or reduction of species on the surface

The redox behaviour of species which are adsorbed on the surface are activation controlled processes, which may be performed in stirred solutions. The typical sweep rates are also 0.01 – 100 V/s, but here the lower limit is determined by background currents from residual impurities in solution (and perhaps by the desire of the experimenter to collect more data in a given time) while the upper limit is determined by uncompensated solution resistance and by instrumentation. The relative current for double-layer charging is independent of sweep rate.

We shall here only consider cases (a) and (b), since very slow sweeps are just a convenient method for scanning the potential automatically, under conditions in which the sweep has practically no effect on the current observed.

4.1.2.1. Double-layer-charging currents

The double-layer charging current is described by the following simple equation:

$$I_{dl} = C_{dl}(dE/dt) = C_{dl} * v \qquad (23)$$

If double-layer charging is the only process taking place in a given potential region (this would be the case for an ideal polarisable interphase) and one cycles the potential between two fixed values, the results should be such as shown in Fig. 23. Plotting $\Delta i = i_a - i_c = 2\,|i|$ as a function of v as shown in Fig. 24, one can obtain the value of the double layer capacitance from the slope. If a faradaic reaction is taking place, a result such as shown by line 2, from which C_{dl} can still be obtained, might be observed.

It is important to evaluate the numerical value of i_{dl}. For a very slow sweep experiment, using $v = 1$ mV/s and $C_{dl} = 20$ μF/cm^2, one has $i_{dl} = 20$ nA/cm^2. This is negligible, even with respect to the small currents observed on passivated electrodes and can hence be ignored.

The interplay between double layer charging and oxidation or reduction of an electroactive material in the bulk of the solution is illustrated in Fig. 25. The faradaic currents shown by the solid lines are the peak currents I_p calculated according to equation (33) and equation (37) which are discussed in section 4.1.2.2.

It is important to note that these currents change with $v^{1/2}$, while i_{dl} is proportional to v. As a result, double-layer charging becomes increasingly more important with increasing sweep rate. The hatched area in Fig. 25 represents the region of sweep rates and concentrations in which accurate measurements can be made, on the basis of the following assumptions:

- the peak current of the faradaic process being studied should be at least ten times the double-layer charging current to allow reliable corrections for the latter;

- the sweep rate should be $v > 10$ mV/s, chosen so as to limit errors due to convective mass transport;

- the peak faradaic current should be $i_p < 20$ mA/cm^2, in order to limit the error due to uncompensated solution resistance; and

- the bulk concentration should be < 100 mM, to ensure that it will always be possible to have an excess of supporting electrolyte, to suppress mass transport by migration.

The numerical values used to construct Fig. 25 are somewhat arbitrary. They do represent, however, the right order of magnitude and are probably correct within a factor of two or three. The important thing to learn from Fig. 25 is the type of factors which must be considered in setting up an experiment. Thus, one notes that it is difficult to make measurements at concentrations below 0.1 mM or at sweep rates above 100 mV/s. The best concentration to use is in the range of 1 – 10 mM. Interestingly, this conclusion does not depend strongly on the four assumptions we have made above, since it refers to the middle of the field of applicability of the method.

The section should perhaps be concluded by noting that the above considerations are valid for large electrodes, operating under semi-infinite linear diffusion conditions.
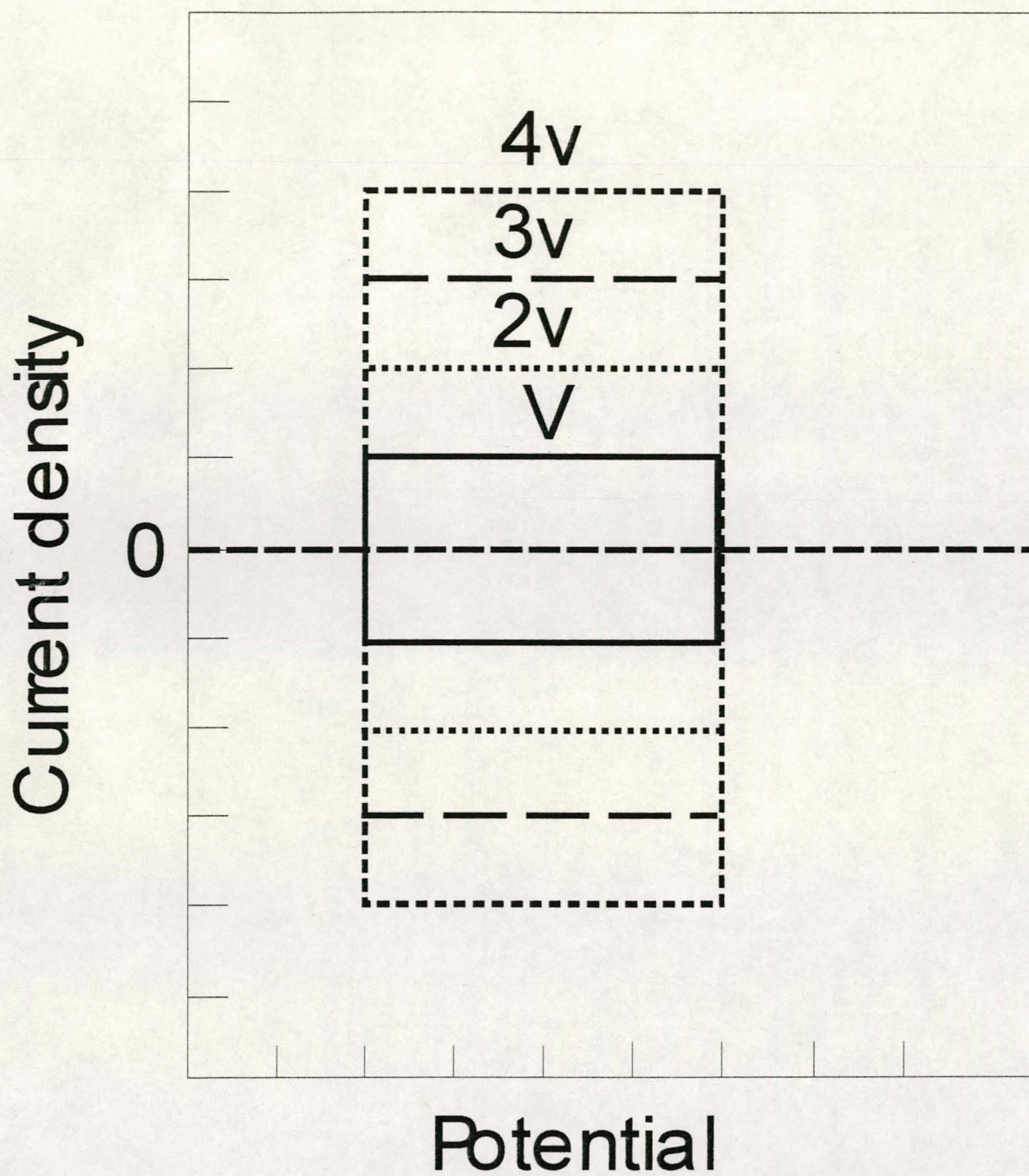
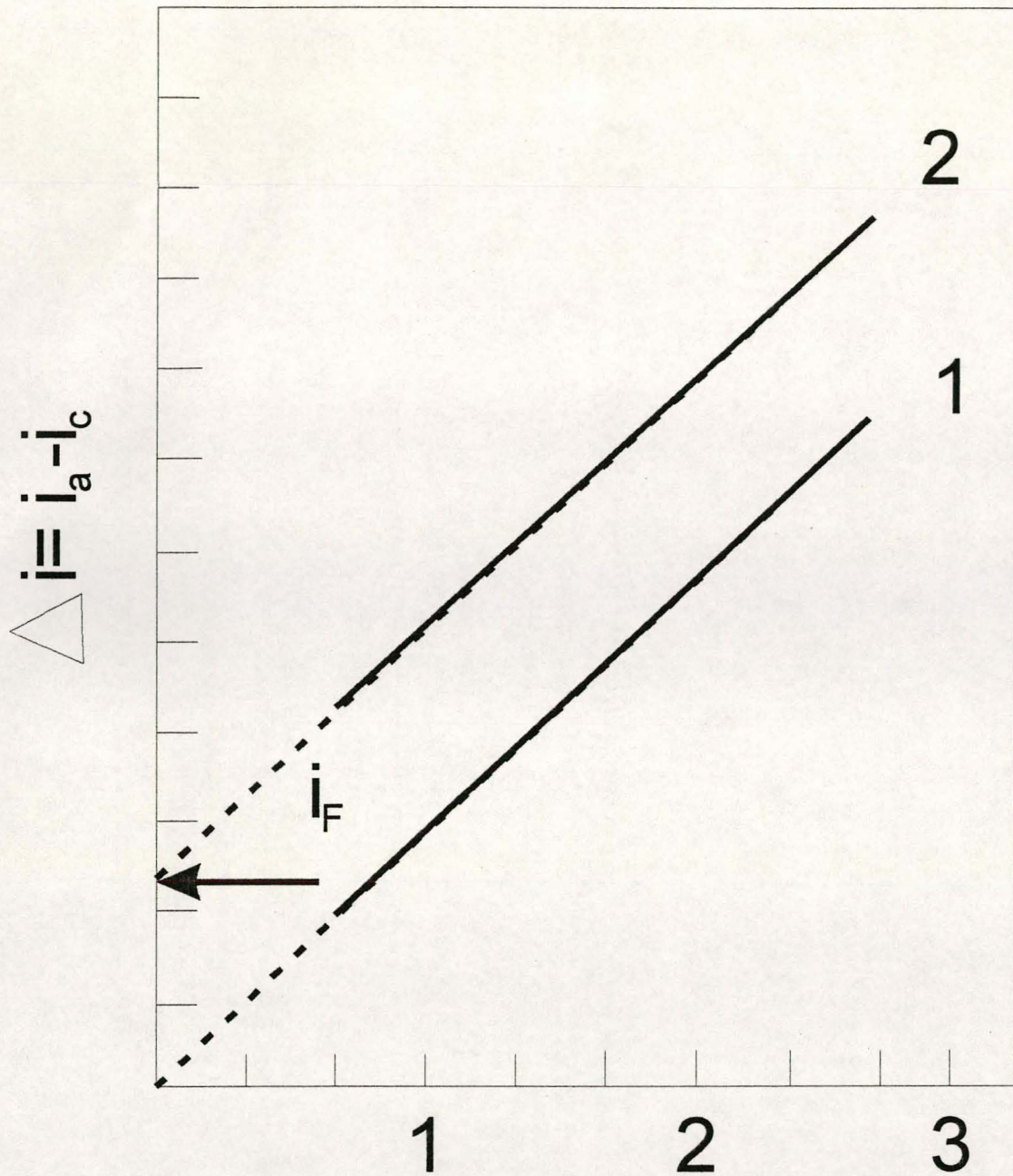Fig. 23: Cyclic voltametry for an ideally polarisable interphase.

Fig. 24: The plot of $\Delta i = i_a - i_c$ as a function of the sweep rate v for an ideally polarisable

interphase (line 1) and for the case of some residual faradaic current i_F (line 2).
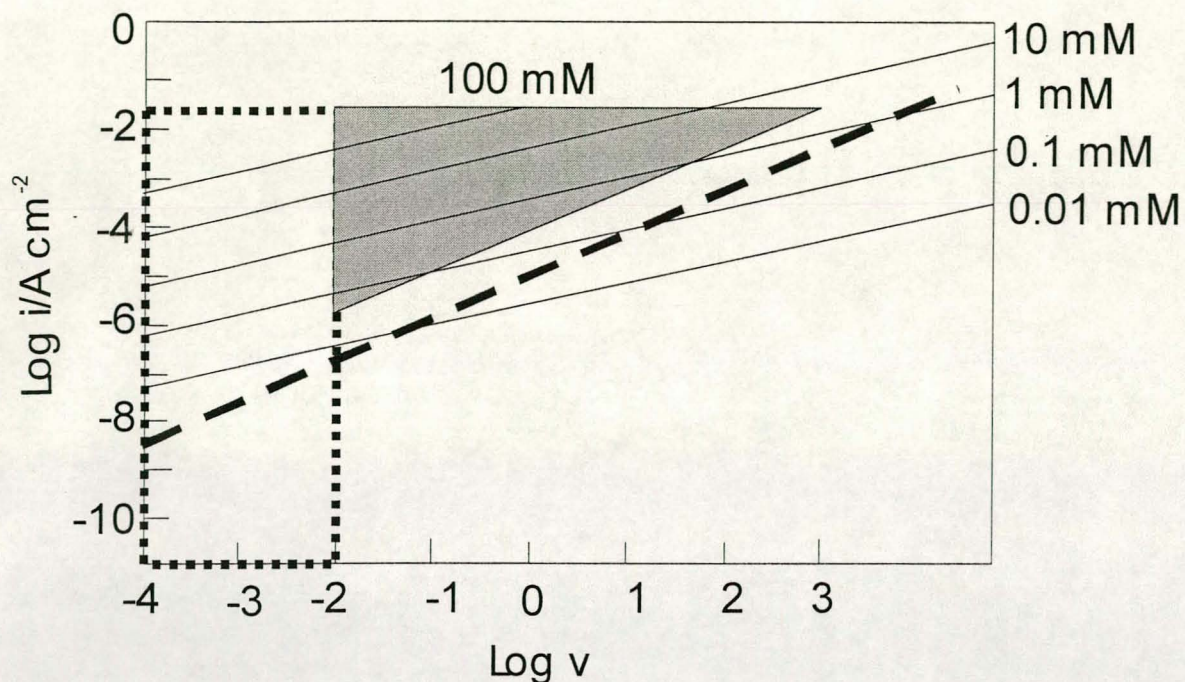
Fig. 25: The optimum range of concentration and sweep rate (shaded area) for measurement in cyclic voltammetry on a smooth electrode. The double-layer-charging current i_{dl} was calculated for $C_{dl} = 20 \ \mu F/cm$

4.1.2.2. The form of the current-potential relationship

The $Ti/SnO_2/Sb_2O_5$ electrode was investigated by making use of the redox couple Fe^{2+}/Fe^{3+} ($K_4[Fe(CN)_6]/K_3[Fe(CN)_6]$), (section 4.3).

In cyclic voltammetry, the potential is made to change linearly with time between two set values. Often the current during the first cycle is quite different from that in the second cycle, but after 5 – 10 cycles the system settles down, and the current traces the same line as a function of potential, independent of the number of cycles. This is often referred to as a *steady-state voltammogram*, which is an odd name to use, considering that the current keeps

changing periodically with potential and time. The term is used here in the sense that the voltammogram as a whole is independent of time.

In a solution containing, for instance 3 mM Fe^{2+} ions in 1M H_2SO_4, the anodic peak corresponds to the simple reaction

$$Fe^{2+} \rightarrow Fe^{3+} + e^- \tag{24}$$

in which both reactant and product are stable species and both are soluble. The initial concentration of Fe^{3+} is zero, but its surface concentration is very close to the bulk concentration of Fe^{2+}. As a result, the cathodic peak is nearly equal to the anodic oxidation peak. In fact, the ratio i_p(anodic)/i_p(cathodic) is a good indication of the chemical stability of the product formed by charge transfer. By studying the dependence of this ratio on sweep rate, one can determine the homogeneous rate constant in a reaction sequence.

The sweep is started at a potential of −0.2 V versus the standard potential for the Fe^{2+}/Fe^{3+} couple, where no reaction takes place. At about −0.05 V the anodic current starts to increase with potential. Initially the current is activation controlled, but as the potential becomes more anodic, diffusion limitation sets in. The observed current is the inverse sum of the activation and the diffusion limited currents. As the time goes on, the activation controlled current increases (due to the linear increase of potential with time) but the diffusion controlled current decreases. As a result, the observed current increases first, passes through a maximum and then decreases. At higher sweep rates each potential is reached at a shorter time, when the effect of diffusion limitation is less, hence the peak current is found to increase with sweep rate.

In a few simple cases, however, it is possible to calculate the maximum of the peak current. Simple is meant in a sense that the phenomena are only determined by diffusion of the reactants to the electrode's surface and the following charge transfer reaction. As

mentioned above, the current peak maximum comes about due to the beginning of the faradaic process and a depletion of the surface concentration c^s of the reacting species that rapidly becomes $c^s = 0$ with a further increase in potential, while at the same time the Nernst-diffusion layer grows ($\delta_N = \sqrt{\pi D t}$). This means that the current density $j = nFD\frac{dc}{dx}|_{x=0}$ passes through a maximum.

The following discussion refers to a single potential scan in unstirred solution with planar electrodes (linear diffusion in x-direction). Transport by migration is neglected. For a simple redox-reaction $S_{ox} + ne^- \rightarrow S_{red}$ the following differential equations need to be solved:

$$\frac{\partial c_{OX}}{\partial t} = D_{ox}\frac{\partial^2 c_{OX}}{\partial x^2}$$

(25)

$$\frac{\partial c_{red}}{\partial t} = D_{red}\frac{\partial^2 c_{red}}{\partial x^2}$$

(26)

The boundary condition is described by:

$$j = -nFD_{ox}\frac{\partial c_{ox}}{\partial x}\Big|_{x=0} = nFD_{red}\frac{\partial c_{red}}{\partial x}\Big|_{x=0}$$

(27)

As a precondition the substance S_{red} is not present in the solution before the reaction starts. Thus the following applies:

$$t = 0,\ x \geq 0,\ c_{ox} = c_{ox}^0$$

(28)

$$t \geq 0,\ x \rightarrow \infty,\ c_{ox} = c_{ox}^0$$

and
$$t = 0, \ x \geq 0, \ c_{red} = 0 \tag{29}$$

$$t \geq 0, \ x \rightarrow \infty, \ c_{red} = 0$$

A further boundary condition depends on the speed of the charge transfer. Two cases have to be distinguished:

Case A: Uninhibited charge transfer

In the case of uninhibited charge transfer the potential φ determines the equilibrium concentration at the surface of the electrode according to the Nernst equation. With $v = \frac{d\varphi}{dt}$ and $\varphi = \varphi_u + vt$ one obtains:

$$\varphi = \varphi_u + vt = \varphi_{00} + \frac{RT}{nF} \ln \frac{c_{ox}^s}{c_{red}^s} \tag{30}$$

φ_U = starting potential.

which gives the additional boundary condition:

$$t > 0, \ x = 0 \quad \frac{c_{ox}}{c_{red}} = \exp\left[\frac{nF(\varphi_u + vt - \varphi_{00})}{RT}\right] \tag{31}$$

As a solution for the differential equations (25) and (26) equation (32) is then valid for the description of the current density – potential relationship:

$$j = nF\left(\frac{nF}{RT}\right)^{1/2} D_{ox}^{1/2} c_{ox}^0 v^{1/2} P[(\varphi - \varphi_{00})n] \tag{32}$$

The function P illustrates the course of the peak current. The maximum (peak-potential φ_P) appears for a one-electron-step and a cathodic sweep, independent from the scan rate v, 28.5 mV more negative than the φ_{00} value of the redox-reaction. The numerical value for P then becomes 0.4463. Consequently, equation (33) is valid for the peak current:

$$j_P = 2.69 \times 10^5 \, n^{3/2} D_{ox}^{1/2} c_{ox}^0 v^{1/2.} \qquad (33)$$

In accordance with experiments the increase of the peak current is proportional to $v^{1/2}$.

By reversing the potential scan after the cathodic sweep the consumption of the reaction product S_{red} on the electrode's surface results in a further current wave. Both peak currents are equally high, which can be expressed as j_P (cathodic) = j_P (anodic). The maximums are 57 mV apart for a one-electron step (n = 1). For too high a scan-rate v, equation (30) becomes invalid and the distance between the two peaks is enlarged.

Case B: Inhibited charge transfer

In the case of inhibited charge transfer and diffusion, a peak current is also expected in the course of the potential scan. Whereas the peak maximum is fixed for case A, the peak current is now expected to be shifted with increasing speed of the scan rate along the direction of the scan, because the concentrations at the electrode's surface emerge slower than expressed in equation (30). In addition, the influence of the transfer coefficient has to be considered in the equations for the current density.

Investigating the cathodic reduction of the substance S_{ox} again, the reduction rate follows equation (34):

$$v_{red} = -\frac{j}{nF} = c_{ox}(x = 0, t)k_0^- \exp[-\frac{(1-\alpha)nF}{RT}(\varphi_u + vt)] \qquad (34)$$

k_0^- = standard reaction rate for the cathodic reaction.

v_{red} has to correspond to the transport of the reacting species at any time. This leads to a new boundary condition:

$$t > 0; x = 0; D_{ox}\frac{\partial c_{ox}}{\partial x} = c_{ox}k_0^- \exp[-\frac{(1-\alpha)nF}{RT}(\varphi_u + vt)] \qquad (35)$$

As a solution for the set of the differential equations (25) and (26) equation (36) is obtained:

$$j = \pi^{1/2}nF(\frac{(1-\alpha)nF}{RT}v)^{1/2}D_{ox}^{1/2}c_{ox}^0 Q(\frac{(1-\alpha)nF}{RT}vt) \qquad (36)$$

The function Q has a similar course as the function P from case A. For the maximum (Q = 0.282) the peak current density is calculated by:

$$j_P = 3.01 \times 10^5 n^{3/2}(1-\alpha)^{1/2}D_{ox}^{1/2}c_{ox}^0 v^{1/2} \qquad (37)$$

As already valid for case A, the peak current density is also increasing proportional to $v^{1/2}$. Additionally the factor $(1-\alpha)^{1/2}$ occurs. The calculation of the peak potential φ_P results in a shift of 60 mV for a change of the scan rate by a factor of 10 (n = 1, α = 0.5).

Consequently, in simple cases the cyclic voltammetry can be treated qualitatively. The peak current then becomes proportional to $D^{1/2}$, c^0 and $v^{1/2}$. For electrochemical reactions with similar rates of charge transfer and diffusion the proportionality to $v^{1/2}$ is no more valid. The

peak potential is independent of the scan rate in the case of rapid charge transfer. On the other hand slow charge transfer leads to dependence of the scan rate. Furthermore, the transfer coefficient influences the peak current.

4.2. Characterisation of the catalytic activity of the electrode material towards phenol

4.2.1. Experimental details

All electrochemical measurements were carried out with a Solartron SI 1280B electrochemical measurement unit with a three-electrode cell. The reference electrode was based on a $Hg/HgSO_4/K_2SO_4$ (sat.) system. The electrolyte consisted either of 1M H_2SO_4 or 1M H_2SO_4 and 5mM phenol. The solution temperature was maintained at 25°C. Prior to any measurement being made, nitrogen was bubbled through the electrolyte.

Phenol was chosen as standard contaminant, because of its toxicity and stability due to the aromatic ring structure.

4.2.2. Results of the electrocatalytic oxidation

4.2.2.1. Cyclic voltammograms on pure Ebonex

The cyclovoltammic scans were carried out in 1M sulfuric acid and 1M sulfuric acid plus 5 mM phenol (Figs. 26 and 27). Phenol is used as a standard contaminant. The activity of the catalytic film towards combustion is indicated by the appearance of an additional peak or increase in the current in the anodic range after the addition of phenol to the electrolyte. The hydrogen adsorption and desorption can be attributed to the respective peaks between -0.5 V (NHE) and +0.7 V (NHE). The hydrogen and oxygen evolution reactions are shifted to high overpotentials. The hydrogen evolution starts at 0.650 V (NHE), whereas the oxygen evolution begins at 2.7 V (NHE). The addition of phenol to the electrolyte of sulfuric acid

does not have a great impact on the shape of the cyclic voltammograms of Ebonex. However, a slight increase in the anodic current density is observed and this can be attributed to the oxidation of phenol, although Ebonex is reported in the literature to be electrocatalytically inactive [Park, 1995].
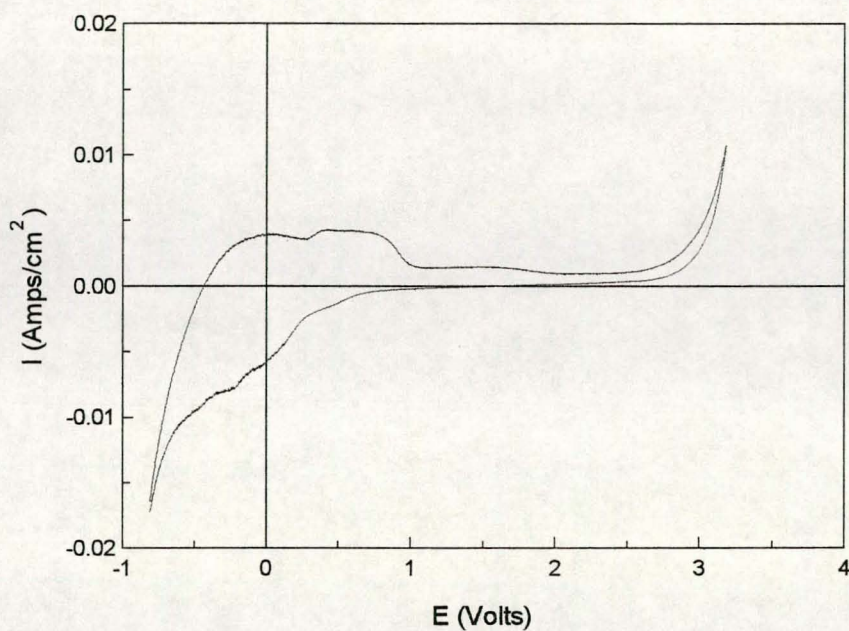

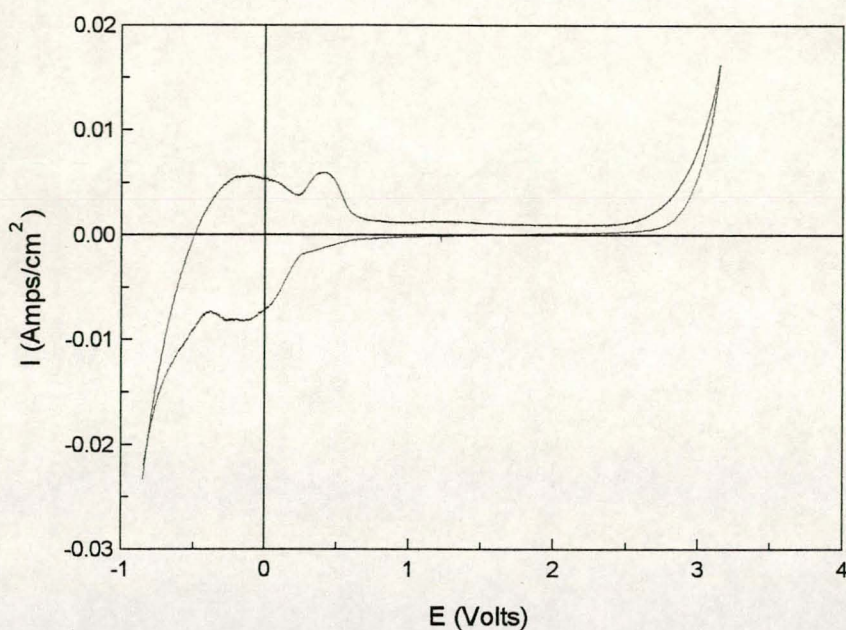Fig. 26. Cyclic voltammogram of pure Ebonex, V = 20 mV/sec, Electrolyte: 1 M H_2SO_4, plotted versus NHE

Fig. 27. Cyclic voltammogram of pure Ebonex V = 20 mV/sec, Electrolyte: 1 M H_2SO_4 + 5 mM phenol plotted versus NHE.

4.2.2.2. Cyclic voltammograms of Ebonex coated with PbO_2

After coating the Ebonex with PbO_2 the CV completely changed. The PbO_2 only seemed to be stable towards reduction at potentials above 1.5 V versus NHE. Below that potential reduction peaks are observed and these shift to lower voltages with increasing numbers of scans, as seen in Fig. 26.
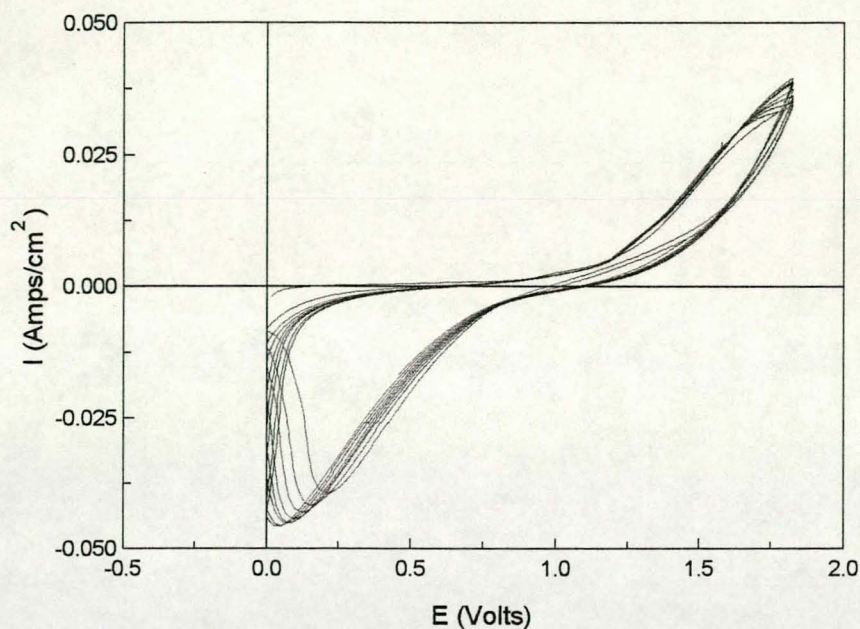
Fig. 28. Ebonex electrode, coated with PbO_2. Electrolyte: 1 M H_2SO_4 v = 20 mV/s, 10 scans

After the addition of 5mM phenol to the electrolyte there appeared no additional clearly separated oxidation peaks, but there was a significant increase in the anodic current in the range of 1.2 V - 1.5 V, indicating the destruction of phenol (Fig. 29). The anodic current is partially obscured by the oxygen evolution peak which means that, at the potential of the combustion, oxygen evolution had also taken place. As the concentration of phenol decreases with each scan, the anodic current also decreases.
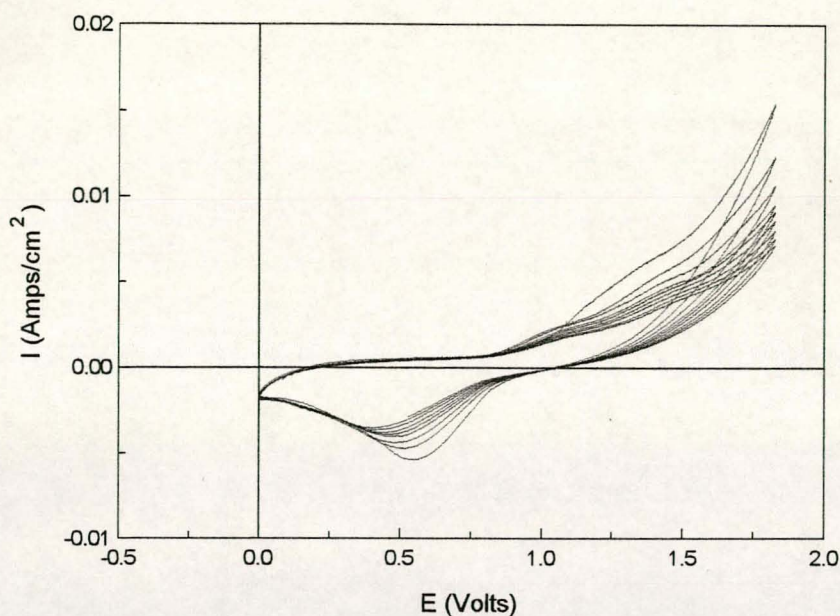
Fig. 29. Ebonex electrode, coated with PbO$_2$. Electrolyte: 1 M H$_2$SO$_4$ + 5mM Phenol, v = 20 mV/s, 10 scans

4.2.2.3. Cyclic voltammograms of titanium coated with SnO$_2$

Without the addition of any dopants to the sol-gel solution, the electrode did not show any catalytic activity for the oxidation reaction, as illustrated by the comparison between Fig. 30 and Fig. 31. The addition of phenol to the electrolyte did not change the shapes of the cyclic voltammograms; both voltammograms remained featureless. There is apparently no indication of combustion. The peak for the oxygen-evolution reaction appears at a high over-potential of 2.3 V (NHE).

In contrast to this, the doping with Sb resulted in a new combustion peak after the addition of phenol to the electrolyte. This can be seen in Figs. 32 and 33. The peak is well separated from the oxygen and thus, at its maximum of 1.5 V (NHE), it can be assumed that the combustion takes place without any side-reactions. By doping the sol-gel solution with fluoride,

additionally, the shape of the CV remains the same, but the combustion peak reaches a current density lower than that obtained after Sb-doping only. After the addition of 10 % fluoride, the peak totally disappears. The peak current for pure Sb-doping is 1mA cm^{-1} , 0.81 mA cm^{-1} for 2.5 % F$^-$ and 0.14 mA cm^{-1} for 5 % F$^-$. Although the doping with fluoride improves the conductivity of the film, it seems to lower the electrode's capacity for combustion.

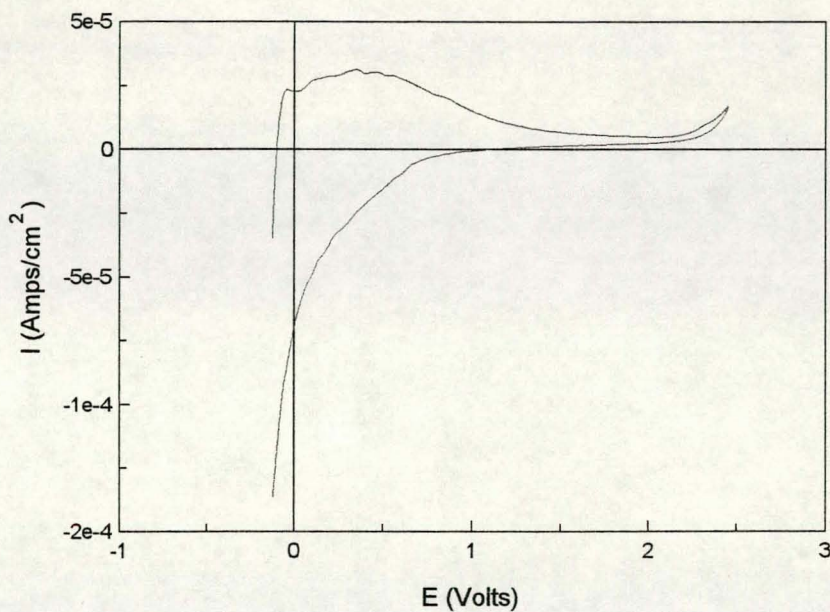Fig. 30. Ti coated with pure SnO$_2$, electrolyte: 1 M H$_2$SO$_4$, v = 20 mV/sec

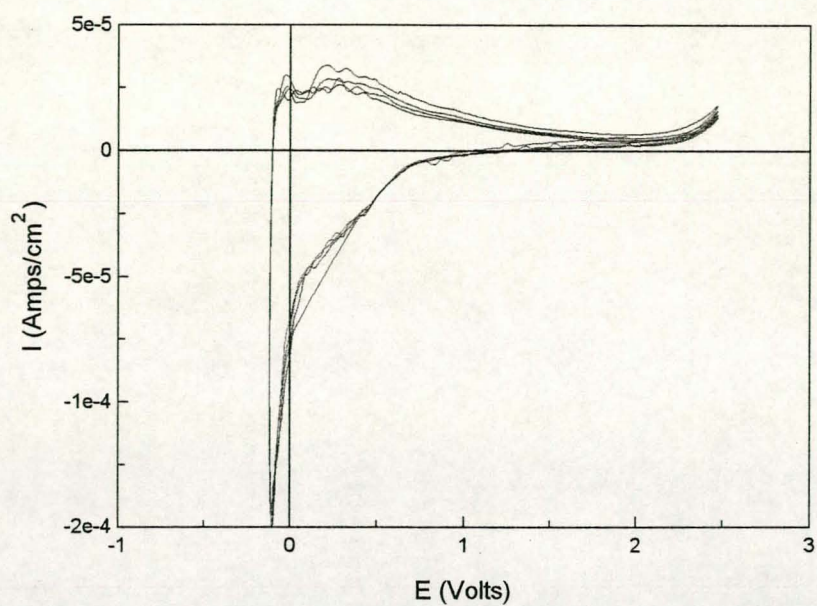Fig. 31. Ti coated with pure SnO_2, electrolyte: 1 M H_2SO_4 + 5 mM phenol, v = 20 mV/sec
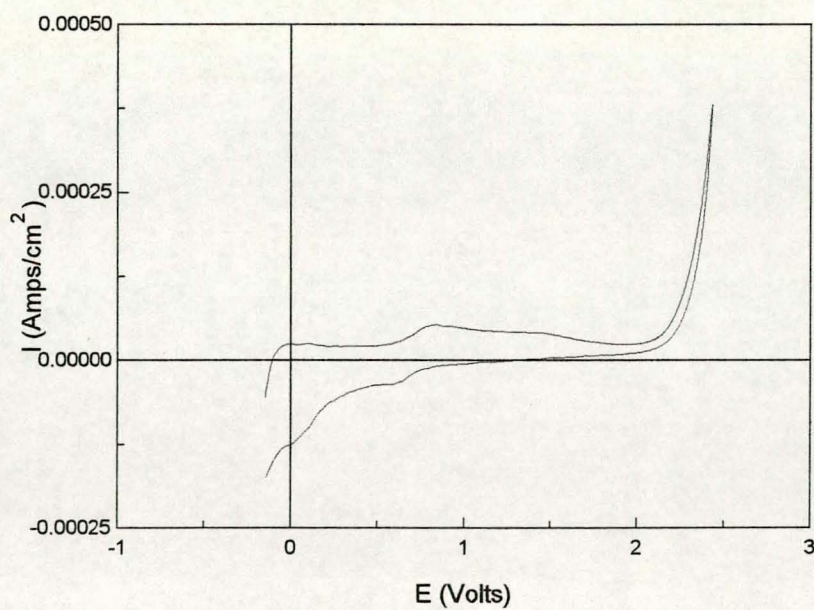

Fig. 32. Ti coated with SnO_2 + 10 % Sb-content, electrolyte: 1 M H_2SO_4, v = 20 mV/sec
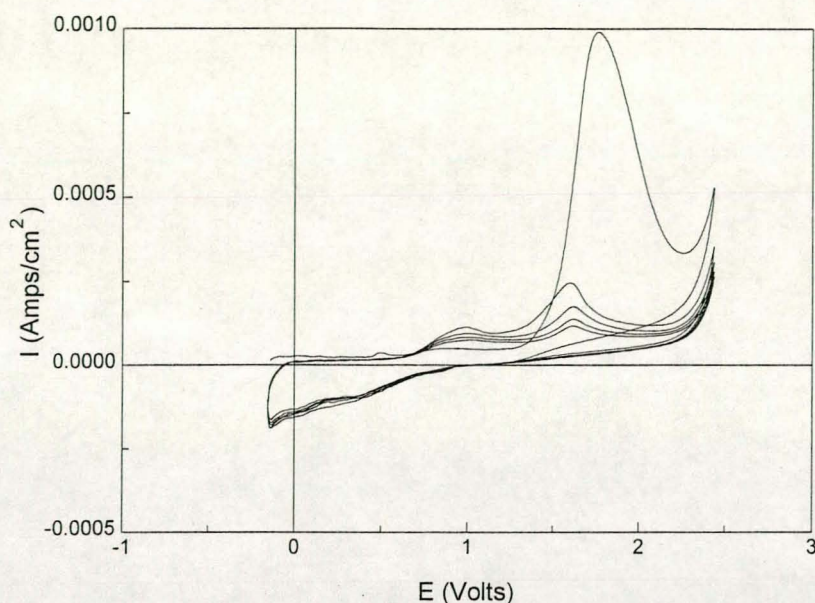
Fig. 33. Ti coated with SnO_2 + 10 % Sb-content, electrolyte: 1 M H_2SO_4 + 5 mM phenol, v = 20 mV/sec

The beneficial effect of Sb-doping can be attributed to the incorporation of an element with a higher oxidation number (Sb^5) into the film to create electron vacancies in the lattice that make the electron transfer from the organic pollutant to the electrode for the oxidation easier. In addition, the introduction of Sb_2O_5 results in a higher oxide present in the film. Consequently the electrochemical conversion pathway is suppressed as the chemisorption of oxygen (MO_{x+1}) into the lattice is less likely to occur.

4.3   Kinetic measurement with the redox couple $K_4[Fe(CN)_6]/K_2[Fe(CN)_6]$

Cyclic voltammetry on the redox couple $K_4[Fe(CN)_6]/K_2[Fe(CN)_6]$ was carried out with different scan rates. This was carried out for further characterisation of the Ti/SnO_2/Sb_2O_5 based material. The value of the peak current especially gives an indication of the electron

98

transfer rate on the electrode's surface. Moreover, the diffusion coefficient of the active species in the electrolyte can be calculated and compared to results from the literature to check whether the experiment gives consistent results. The electrolyte consisted of 10 mM of each ferri- and ferrocyanide. The supporting electrolyte was 0.1 M H_2SO_4. The scan rates ranged from 1 – 100 mV (1, 5, 10, 50 and 100 mV/s). Fig. 34 shows all the cyclic voltammograms combined in one plot.
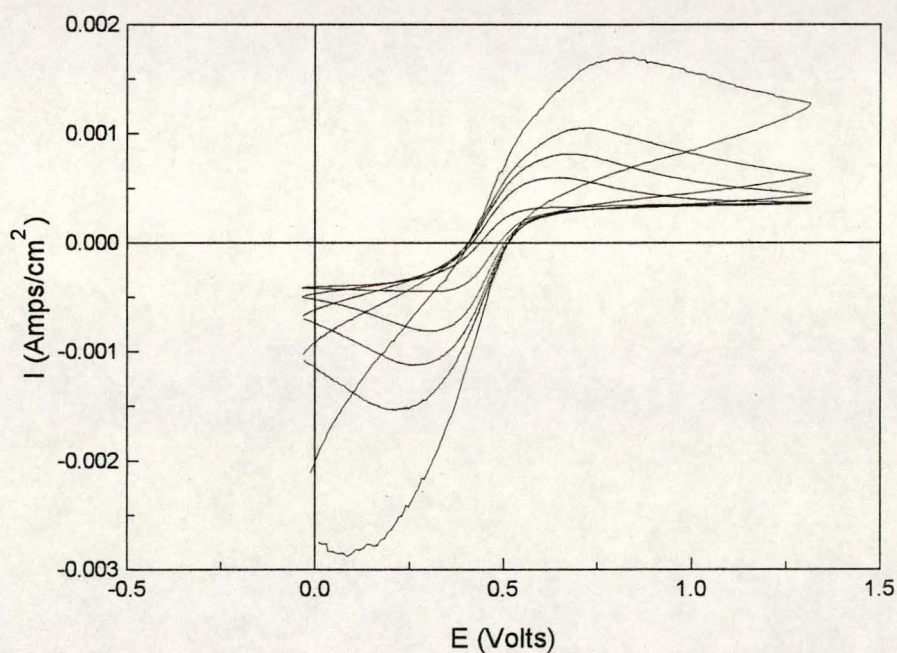
Fig. 34. Cyclic voltammograms with different scan rates (1, 5, 10, 20, 50, 100 mV/s); electrolyte: 10 mM $K_4[Fe(CN)_6]$, 10 mM $K_3[Fe(CN)_6]$

Table 2 presents an overview of the resulting peak currents and peak potentials.

Scan rate $v/mV\ s^{-1}$	$v^{1/2}/V^{1/2}\ s^{-1/2}$	Peak current density $I/mA/cm^2$	Peak potential E/V
1	0.032	0.357	0.013
5	0.071	0.600	0.032
10	0.1	0.817	0.061
20	0.141	1.057	0.111
50	0.224	1.406	0.136
100	0.316	1.701	0.232

Table 2. Overview of the peak currents and peak potentials for different scan rates.

Fig. 35 is a plot of the square route of the scan rate versus the peak potential to confirm the linearity between $v^{1/2}$ and i_P.
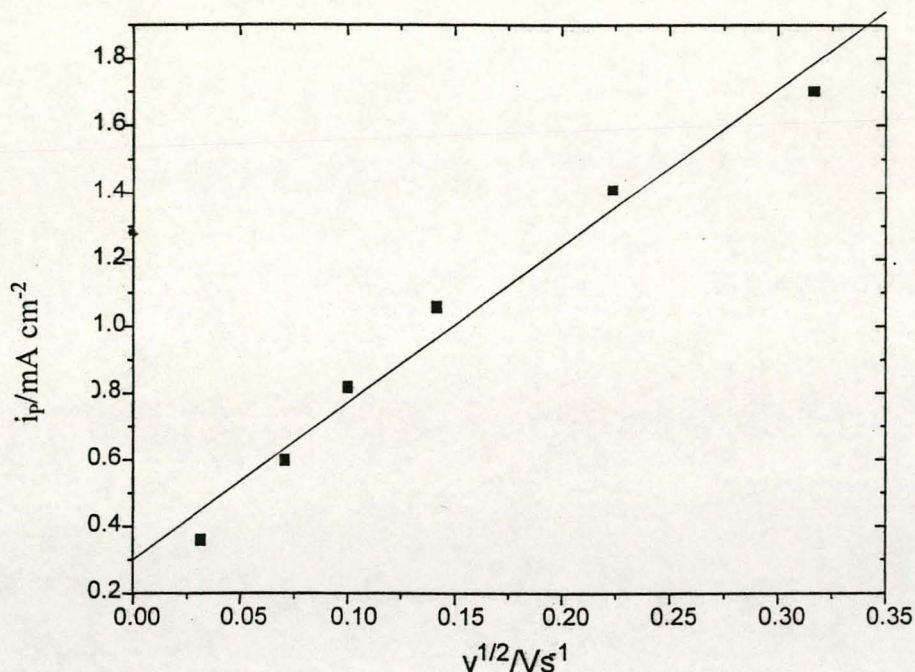
Fig. 35. Plot of the square route of the scan rate ($v^{1/2}$) versus the peak current i_P

The peak currents i_P from table 2 are rather low which indicates problems with the charge transfer on the electrode's surface. Maybe this is due to oxidation reactions that the electrode material is subjected to at high potentials.

The linearity between $v^{1/2}$ and i_P has been predicted for a simple reaction in section 4.1.2.2. and can be well observed in Fig. 35. The linear regression resulted in a standard error coefficient of $r = 0.98815$.

As the potential changes with the scan rate, the reaction is inhibited on the surface of the electrode (see section 4.1.2.2. case B). Consequently, equation (36) applies for the calculation of the diffusion coefficient. From the slope of the plot in Fig. 35 a diffusion coefficient for the electroactive species $D = 4.9 \times 10^{-9}$ m^2 s^{-1} was obtained which is close to the value reported in literature (1.178×10^{-9}) [Hamed, 1951]

4.4 Conclusions

A variety of different electrode materials were developed and tested for their catalytic potential as oxidation catalysts for organic pollutants in waste waters. The Ebonex/PbO$_2$-electrodes revealed combustion activities as seen in the cyclic voltammograms. The oxidation did not appear to be specific as oxygen evolution occurred as a side reaction at the same electrochemical potential. In contrast, the doped Ti/SnO$_2$-electrodes proved to be capable of specific oxidations of organics in the water, indicated by a well-separated anodic peak. The electrodes are only active when doped with antimony, because the n-donor provides for the conductivity of the film. Catalytic activity of the coating is enhanced as Sb2O5 forms a higher oxide than SnO2. Thus the incorporation of oxygen into the film is reduced and the combustion reaction favoured. Doping with fluoride has a reverse effect on the oxidation efficiency, although this modification did improve the hydrophobicity of the films. The independent determination of the phenol concentration will be presented in chapter 6.

The kinetic experiments have given a diffusion coeficient for the electrroactive speciies which is close to the value in literature.

Chapter 5

Spin-trapping of •OH-radicals by N,N-dimethyl-p-nitrosoaniline (RNO)

Abstract

Assessment of the cell performance was carried out using N,N-dimethyl-p-nitrosoaniline (RNO) as a spin trap for •OH-radicals. Kinetic studies were done for the formation of the •OH-radicals. For the kinetic measurements of the reactions by which •OH-radicals were formed at the anodes, PbO_2 based electrode material on Ebonex and the $Ti/SnO_2/Sb_2O_5$ anode material were compared. RNO as a detection method for spin-trapping •OH-radicals is already well established in biology and biochemistry.

5.1. Mechanism of the oxidation of organics in water and analytical methods for its verification

Two different pathways for the anodic oxidation of undesired organics are described in the literature [Simond, 1986; Arfsten, 1984; Chaudhuri, 1990]:

(i) electrochemical conversion, and

(ii) electrochemical combustion.

(i) Electrochemical conversion transforms only the toxic non-biocompatible pollutants into biocompatible organics, and biological treatment is still required after the electrochemical oxidation.

(ii) Electrochemical combustion yields CO_2 and water and no further purification is necessary. Previous work [Simond, 1997; Arfsten, 1984; Chaudhuri, 1990] has indicated, that the accumulation of •OH radicals favours the combustion reaction, while the introduction of

oxygen into the electrode lattice results in conversion. Anodes with a high oxygen-overpotential, such as Ti/SnO_2, Ti/PbO_2 and graphite-felt, favour electrochemical combustion [Arfsten, 1984; Chaudhuri, 1990; Karlsson, 1992]. The following mechanism for the formation of •OH radicals on an oxide anode (MO_x) has been suggested by Comninellis [Simond, 1986]:

$$MO_x + H_2O \xrightarrow{k_{OH}} MO_x(\bullet OH) + H^+ + e^- \tag{38}$$
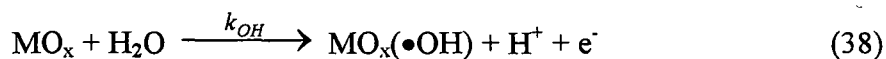
The destruction of organics proceeds by the reaction:

$$R + MO_x(\bullet OH)_z \xrightarrow{k_C} Z/2 \, CO_2 + Z \, H^+ + Z \, e^- + MO_x \tag{39}$$
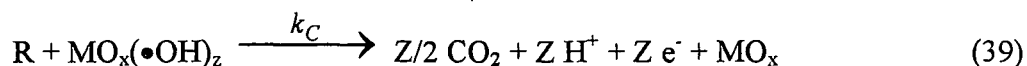
The •OH radicals were detected by a method which is already well established in biology and biochemistry, that is spin-trapping with N,N-dimethyl-p-nitrosoaniline (RNO) [Maier, 1993]. RNO has a sensitive absorption band at 440 nm ($\varepsilon = 3.44 \times 10^4 \, M^{-1}cm^{-1}$), and its bleaching upon acceptance of an e^- from the •OH-radicals can easily be observed by means of UV/VIS spectrophotometry.

Thus, the rate of the bleaching reaction in the presence of N,N-dimethy-p-nitrosoaniline (RNO) is determined by k_{RNO}.

$$RNO + \bullet OH \xrightarrow{k_{RNO}} \text{spin-adduct} \tag{40}$$
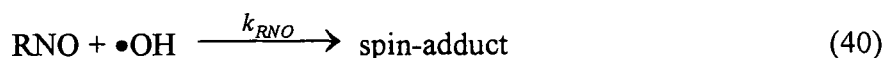
5.2. Detection methods for •OH-radicals

There are several methods for the detection of •OH-radicals, naamely:

- ESR-spectroscopy

- Thiobarbituric acid (TBA) and dihydroxybenzoic acid

- Spin-trapping with p-nitrosodimethylaniline.

Electron spin resonance spectroscopy (ESR) is the direct proof for an existing radical, because the measurement is based on the determination of the two energy levels of an unpaired electron. The energy levels of the spin of the electron exposed to a magnetic field B are given by:

$$E_{ms} = g_e \, \mu_B \, m_s \, B, \quad m_s = +/- \tfrac{1}{2} \tag{41}$$

g_e: Electron g-factor

μ_B: Bohr's magneton

B: Magnetic field

m_s: Spin quant number

Thus, increasing the field strength of the magnetic field results in an increase of the energy level of an α-electron ($m_s = \tfrac{1}{2}$), whereas the that of a β-electron ($m_s = -1/2$) becomes depressed.

The difference between the two energy levels is:

$$\Delta E = E_\alpha - E_\beta = g_e \, \mu_B \, B \tag{42}$$

The resonance condition is given by:

$$h\nu = g_e \, \mu_B \, B \qquad\qquad (43)$$

The drawback of this analytical method has always been that it only responds to unpaired electrons. Consequently, only the detection of radicals is possible. The instrumentation is expensive and not suitable for use in an electrochemical system. It must be used offline.

Thiobarbituric acid (TBA) reactive products and dihydroxybenzoic acid products of salicylate can be employed as indices of nonspecific oxidants and hydroxyl radical generation. The hydroxyl radical reacts with salicylic acid (2-hydroxybenzoic acid) to produce two dihydroxybenzoic acid products, 2,3- and 2,5-dihydroxybenzoic acid, and a small amount of catechol by decarboxylation [Halliwell, 1989]. These hydroxylated products provide evidence of hydroxyl generation [Floyd, 1986; Halliwell, 1991]. The detection of 2,3- and 2,5-dihydroxybenzoic acid is performed using high performance liquid chromatography.

p-Nitrosodimethylaniline (RNO) is a selective scavenger for •OH-radicals [Wabner, 1985]. A number of •OH-radical spin traps are available in the literature [Bors, 1978], but RNO has the following advantages:

(i)   The reaction of RNO has been reported to be selective [Comninellis, 1993] as neither singlet oxygen ($^1O_2$) nor various "peroxo" compounds destroys the chromophoric group of RNO [Kvaljic, 1965].

(ii) Another favourable quality for its application is the high rate of the reaction with •OH-radicals ($k = 1.2 \times 10^{10} \ M^{-1} \, s^{-1}$).

(iii)A convenient feature of RNO is the ease of application as one merely observes the bleaching of the sensitive adsorption band at 440 nm ($\varepsilon = 34\,200 \ M^{-1} cm^{-1}$).

Another advantage of RNO for the detection of •OH radicals formed by water hydrolysis is that RNO is electrochemically inactive at Pt, IrO_2 and SnO_2 anodes as has been shown by cyclic voltammetry measurements [Comninellis, 1993]; similar results have been reported in literature at Pt and PbO_2 anodes [Wabner, 1985].

In our experiment, RNO has been used as a spin trap and the bleaching of the yellow colour was measured during electrolysis:

$$RNO + •OH \rightarrow R\text{-}NO•$$
$$|$$
$$OH$$

(44)

5.3. Experimental set-up

The electrolytic cell (Fig. 36) was especially constructed to afford direct spectroscopic observation of the electrolysis at the anode. For the electrolysis the electrochemical cell consisted of a chamber with a working and a counter electrode, and was equipped with a fibre-optic sensor for spectrophotometric UV/VIS analysis. The fibre-optic sensor is illustrated in Fig. 37. This set-up was used for the kinetic studies with RNO. The •OH radical trapping was measured in a phosphate buffer (pH = 7.0) containing 2×10^{-5} mol/l RNO ($\varepsilon = 34\,200\ M^{-1}cm^{-1}$ at 440 nm).
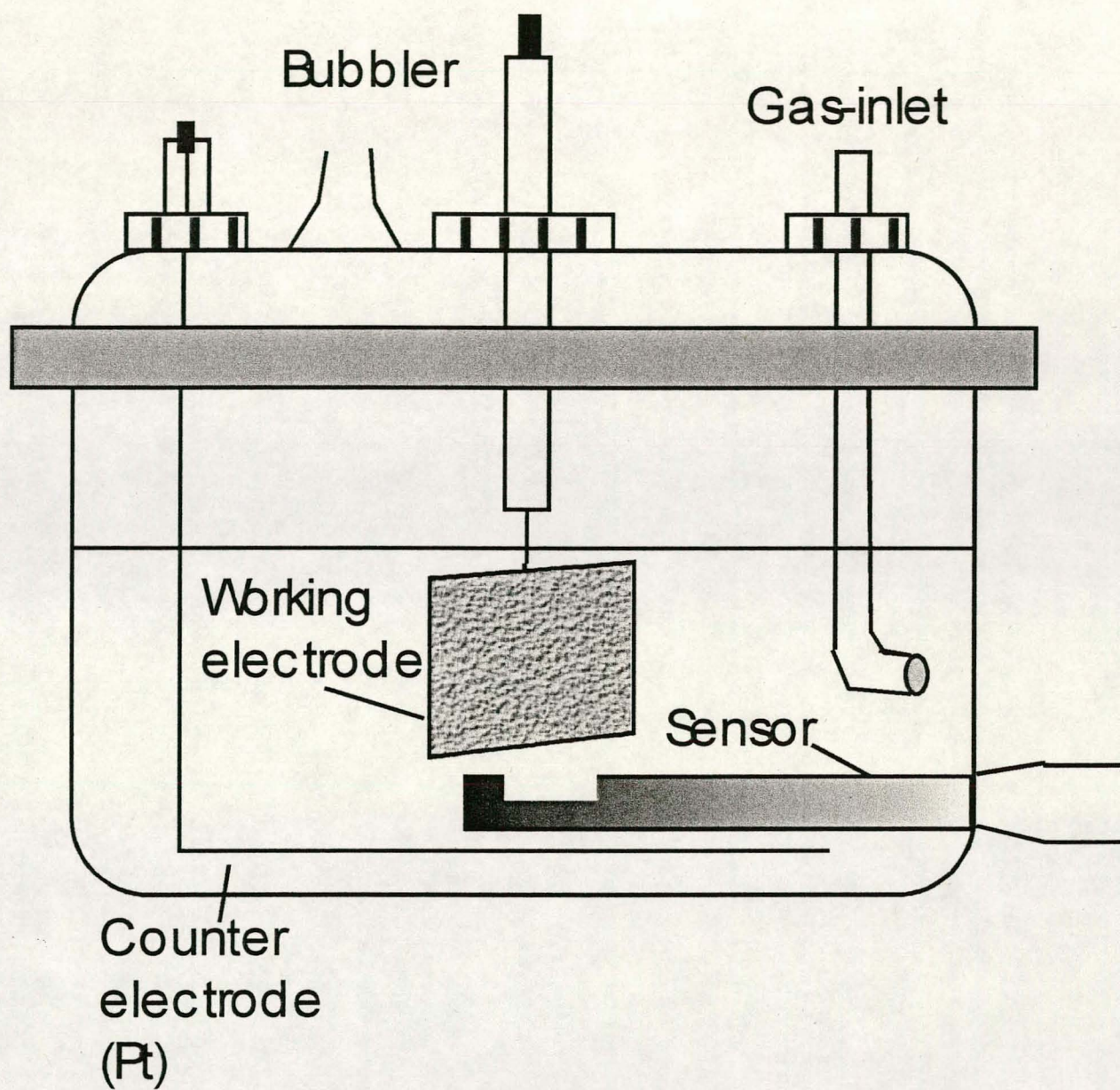
Fig. 36. Set-up for the electrochemical cell

Sample

Light-
Path
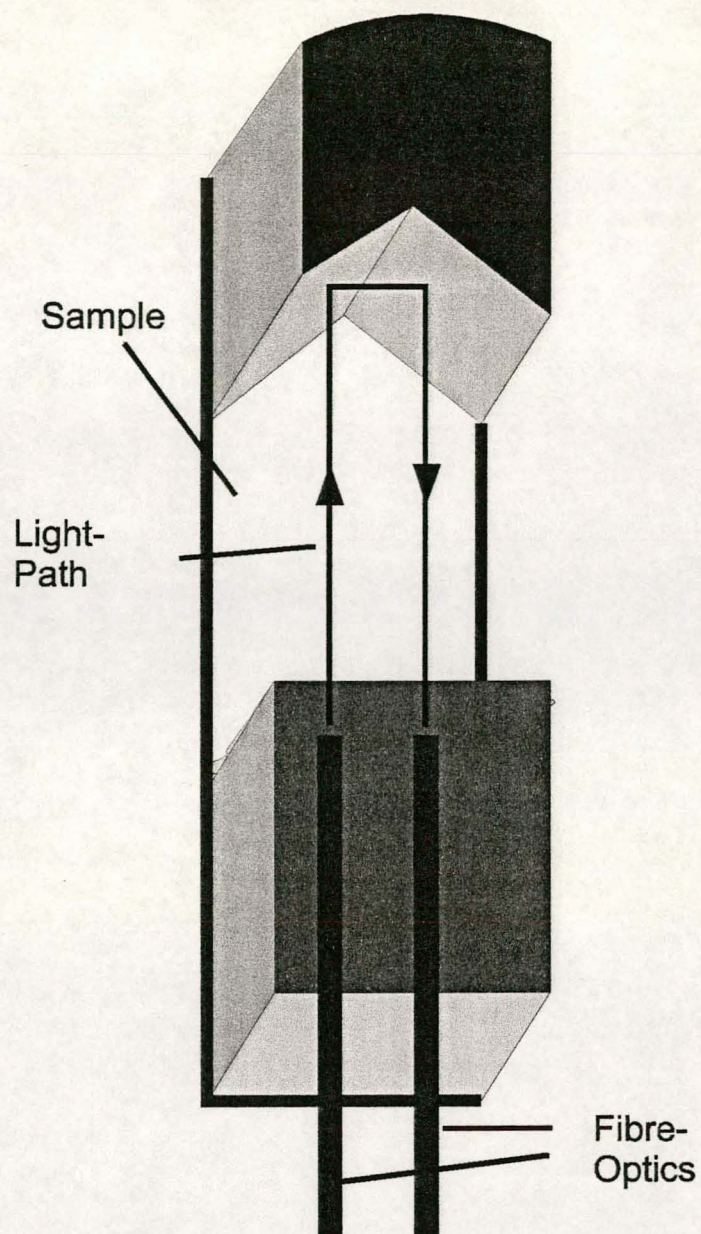
Fibre-
Optics

Fig. 37. Sensor for the RNO-determination for the fibre-optics
spectrophotometer

5.4. Results

After the galvanostatic electrolysis on $Ti/SnO_2/Sb_2O_5$ and $Ebonex/PbO_2$ in a phosphate buffer solution with 2×10^{-5} mol/l RNO, absorption curves were obtained for the bleaching of RNO (Fig. 38).

The software program 'Mathcad 5.0 Plus' was used to determine the rate constants of equation (38) or (40) and the order of the reaction. The program permitted the estimates of the reaction order and the rate constant, the differential method being used to analyse the reaction data. Interpolation was carried out by spline function to generate equally spaced points.

Kinetic data obtained for PbO_2 -based electrodes was:

Reaction order: $a = 2.4$; specific velocity for a rate equation $dC/dt = k \times C^a$: $k = 0.134 \ M^{-1}s^{-1}$; correlation: 0.967.

Correspondingly, the results for SnO_2 -based material were:

$a = 1.92$; $k = 0.155 \ M^{-1}s^{-1}$; $r = 0.959$.

The reaction order of 2 is valid for both electrode materials.

Fig. 38. Absorption against time during electrolysis for Ebonex/PbO$_2$ and Ti/SnO$_2$/Sb$_2$O$_5$.

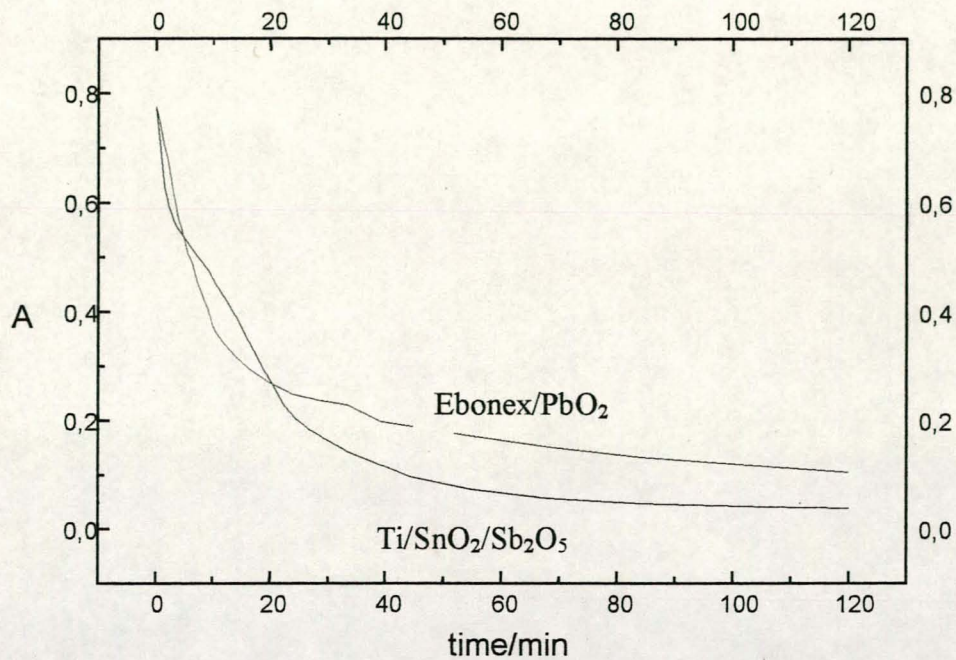Current density: i = 20 mA cm^{-2}, electrolyte: Phosphate buffer (pH = 7) + 2 × 10^{-5} M RNO.

5.6. Discussion

The pathway of the electrochemical combustion was confirmed by the detection of •OH-radicals by spin trapping by RNO during electrolysis. The reaction order of the overall reaction is 2. Unfortunately, this reaction order could satisfy either of the second order equations, equation (38) or equation (40), two successive reactions, so that one of them must be predominately rate-determining, meaning that either $k_{OH} \gg k_{RNO}$ or $k_{OH} \ll k_{RNO}$. Equation (38) was independent of the electrode material, because the radical reacted directly with the RNO. The difference in the rate constants could thus be explained only by the initial reaction during which the radicals are formed. Consequently, equation (38) must be the rate determining step of the whole reaction, and the calculated data valid for that particular step. This was in accordance with the literature [Comninellis, 1994], where the rate constant for equation (40) of $k_{RNO} = 1.2 \times 10^{10}$ $M^{-1}s^{-1}$ is reported, a far higher value than calculated here. Therefore, the overall reaction was assumed to be second order, with $k_{RNO} \gg k_{OH}$ and the first equation is the rate-determining step.

The absorption curves in Fig. 38 also indicate that •OH radical production is kinetically increased by the SnO_2 -based material, which led also to a lower final concentration of RNO.

Chapter 6

Characterisation of the Sb-doped SnO$_2$-based electrode material by Electrochemical Impedance Spectroscopy (EIS)

Abstract

By combining a frequency response analyser with a variable frequency sine-wave generator, one obtains an electrochemical impedance spectrometer. Proper analysis of the acquired data allows conclusions on the equivalent circuit of the electrode process.

6.1. Theoretical background

6.1.1. Introduction

The use of a phase-sensitive voltmeter for the study of the electrochemical response of the interphase is an accurate method for the determination of the double layer capacitance of an electrode system, but beyond that allows conclusions on the equivalent circuit of the system and elucidates the kinetics of the electrodes process [Wien, 1896; Warburg. 1899]

By combining a phase-sensitive voltmeter (also called a *lock-in amplifier*) or a *Frequency Response Analyser* (FRA) with a variable frequency sine-wave generator, one obtains an electrochemical impedance spectrometer [Randles, 1947; Ershler, 1947; H. Gerischer, 1951]. Such instruments are commonly combined with a microcomputer, which makes it easy to probe the interphase over a wide range of frequencies, and to record and

analyse the data [MacDonald, 1986; C. Gabrielli, 1980; Sluyters-Rehbach, 1984]. Modern instrumentation, which is commercially available, covers a frequency range of about 12 orders of magnitude, from 10^{-5} Hz to 10^7 Hz. This is a very wide range of frequencies indeed, when compared to other fields of spectroscopy. We recall, for instance, that visible light scarcely extends over a factor of 2 in frequency, and the whole range from vacuum UV to the far infrared covers no more than three orders of magnitude in frequency. In fact, the range of frequencies which can be employed in EIS measurement is limited more by the electrochemical aspects of the system than by instrumentation. Thus, measurements at very low frequencies take a long time, during which the interphase may change chemically. The minimum time needed to make a measurement at any frequency is the inverse of the frequency (i.e., the period) of the perturbing wave. While it is technically possible to make measurements at, say, 10^{-5} Hz, this would take longer than a day, and the changes in the interphase during the measurement at a single frequency could make the results meaningless. At the high frequency end, stray capacitances and inductances combine with possible nonuniformity of current distribution at the electrode surface, to make the results unreliable. For these reasons, EIS experiments are usually conducted in the range of 10^{-3} to 10^{-5} Hz.

For a circuit containing both capacitors and resistors, the ratio between the applied voltage signal and the resulting current signal is the impedance $Z(\omega)$, which is a function of frequency. The impedance of a pure resistor is simply its resistance R, while the impedance of a pure capacitor id given by:

$$Z_C = -(j\omega C) \tag{43}$$

The total impedance can be written in concise form as:

$$Z(\omega) = ReZ - j(ImZ) \tag{44}$$

where ReZ and ImZ refer to the *real* and *imaginary* parts of the impedance, respectively, and $j \equiv (-1)^{1/2}$.

It follows that the absolute value of the impedance vector is given by

$$|Z(\omega)| = \{(ReZ)^2 + (ImZ)^2\}^{1/2} \qquad (45)$$

The angle φ is the phase shift between the applied sine-wave voltage and the resulting sine-wave current.

$$E = \Delta E * \sin(\omega t) \quad \text{and} \quad i = \Delta i * \sin(\omega t + \varphi) \qquad (46)$$

where ΔE and Δi are the amplitudes of the voltage and current waves, respectively. For a pure resistor, the phase shift is zero and for a pure capacitor it is $-\pi/2$. For any actual interphase the value is somewhere in between, depending on the chemical nature of the interphase and on the frequency employed. Real systems do not behave ideally.

The FRA can measure the absolute value of the of the impedance vector $|Z|$ and the phase angle φ simultaneously. Since the impedance of a capacitor alone can be represented as an imaginary number, $Z_C = -j/\omega C$, according to equation (44) for a capacitor and a resistor in series one has:

$$Z(\omega) = R_S - j/\omega C \qquad (47)$$

And for a capacitor and resistor in parallel the impedance is given by:

$$1/Z(\omega) = 1/R_F - \omega C/j \qquad\qquad (48)$$

It is most convenient to represent $Z(\omega)$ as a vector in the complex plane, in which the X-axis is ReZ and the Y-axis is ImZ, as shown in Fig. 39. Both the absolute value of the impedance vector and the phase angle vary with frequency, of course, for any given equivalent circuit.
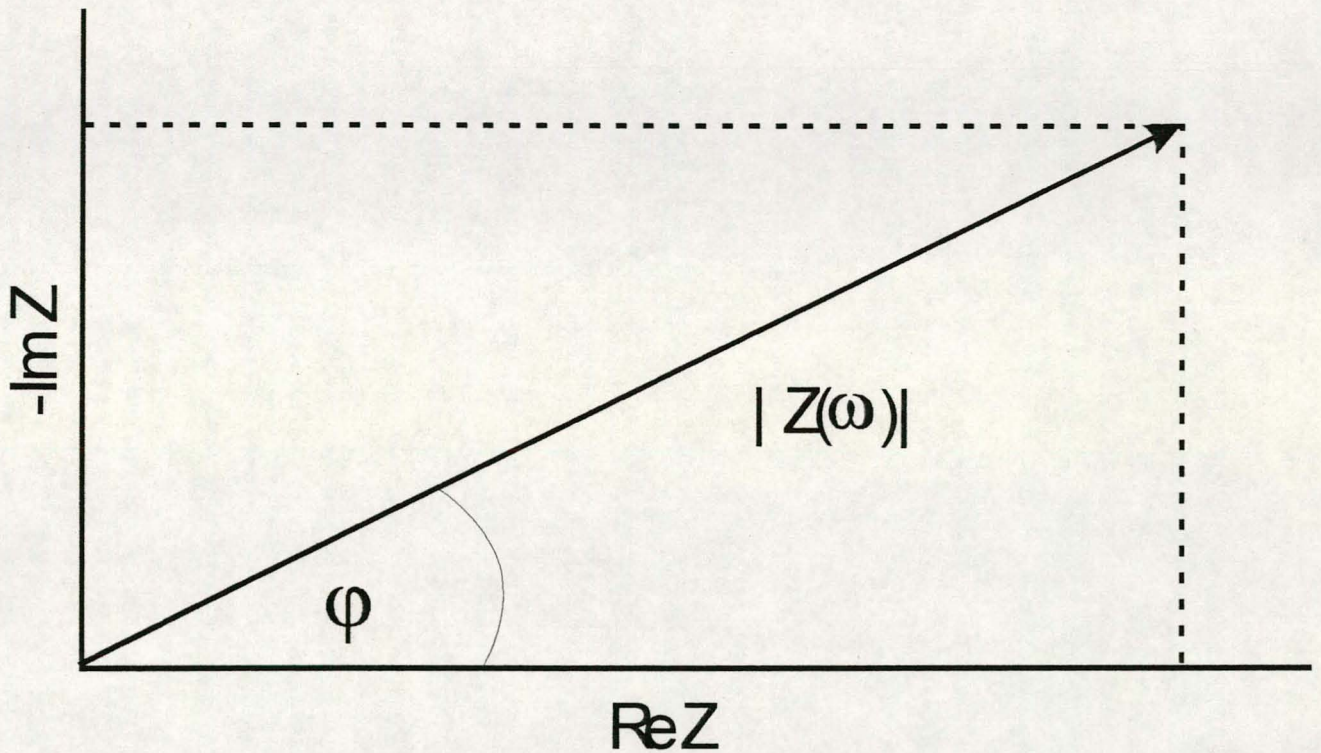
Fig. 39: Vector representation of the impedance $Z(\omega)$ in the complex plane. ReZ and ImZ are the real and imaginary components of the impedance respectively.

Fig. 40 and Fig. 41 show the vector representation of a capacitor and a resistor in series and parallel.
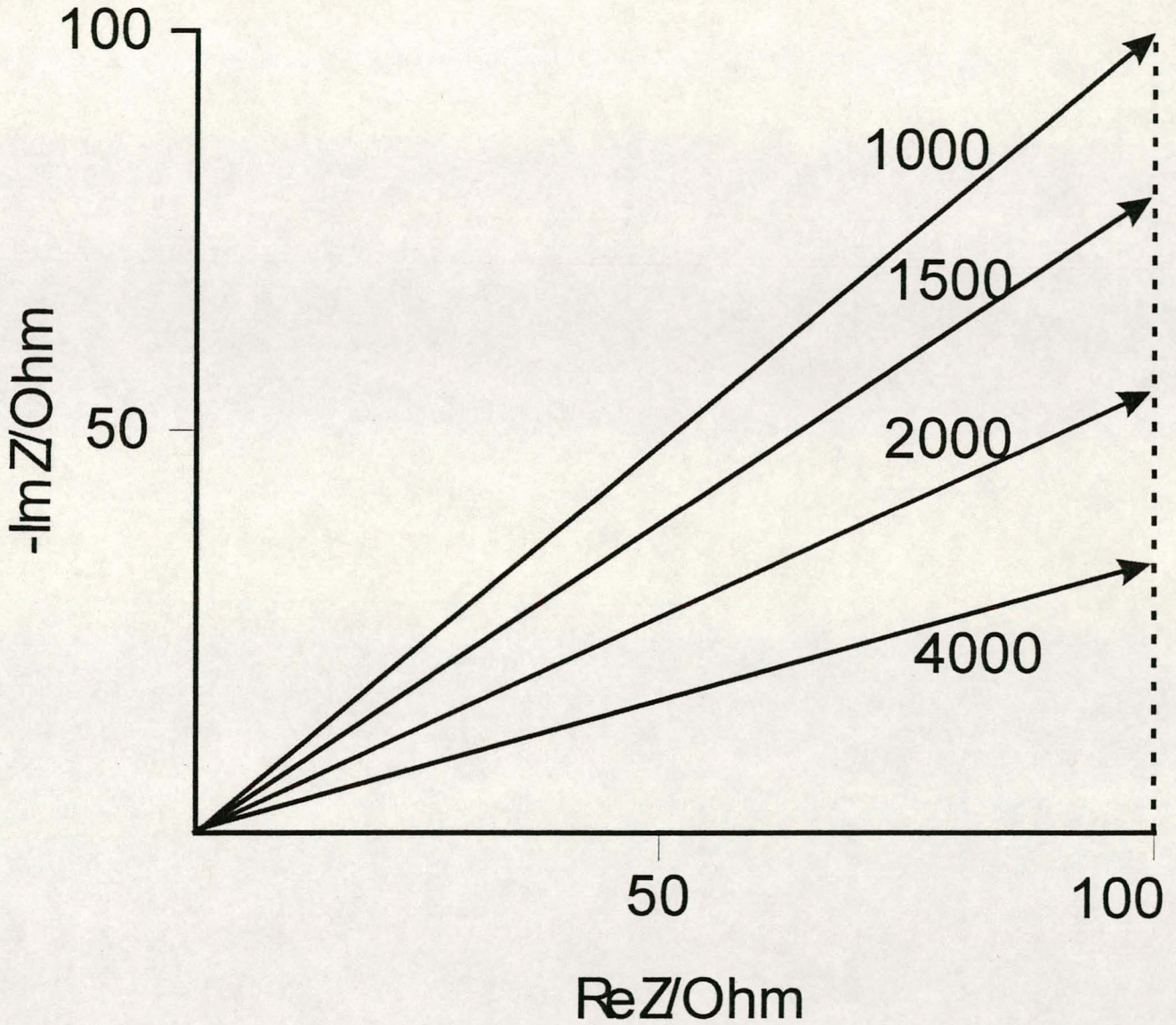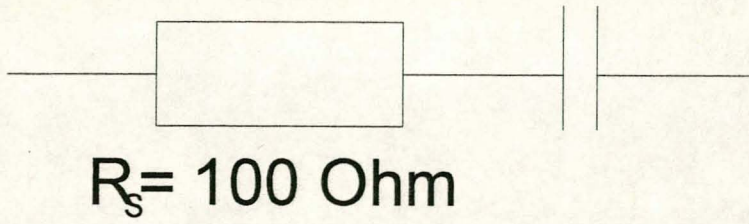
Fig. 40: Vector representation of the impedance of a series combination of a capacitor and a resistor, showing how the phase angle changes with frequency (expressed in Rad/s on the vectors). The ends of the arrows show the absolute values of the vectors.

Fig. 41: Vector representation of the impedance of a parallel combination of a capacitor and a resistor, showing how the phase angle changes with frequency (expressed in Rad/s on the vectors). The ends of the arrows show the absolute values of the vectors.

As the frequency is increased, the capacitive impedance decreases, while the resistive impedance is unchanged. In the series combination this makes the circuit behave more and more like a pure resistor, causing a decrease in phase angle as seen in Fig. 41.

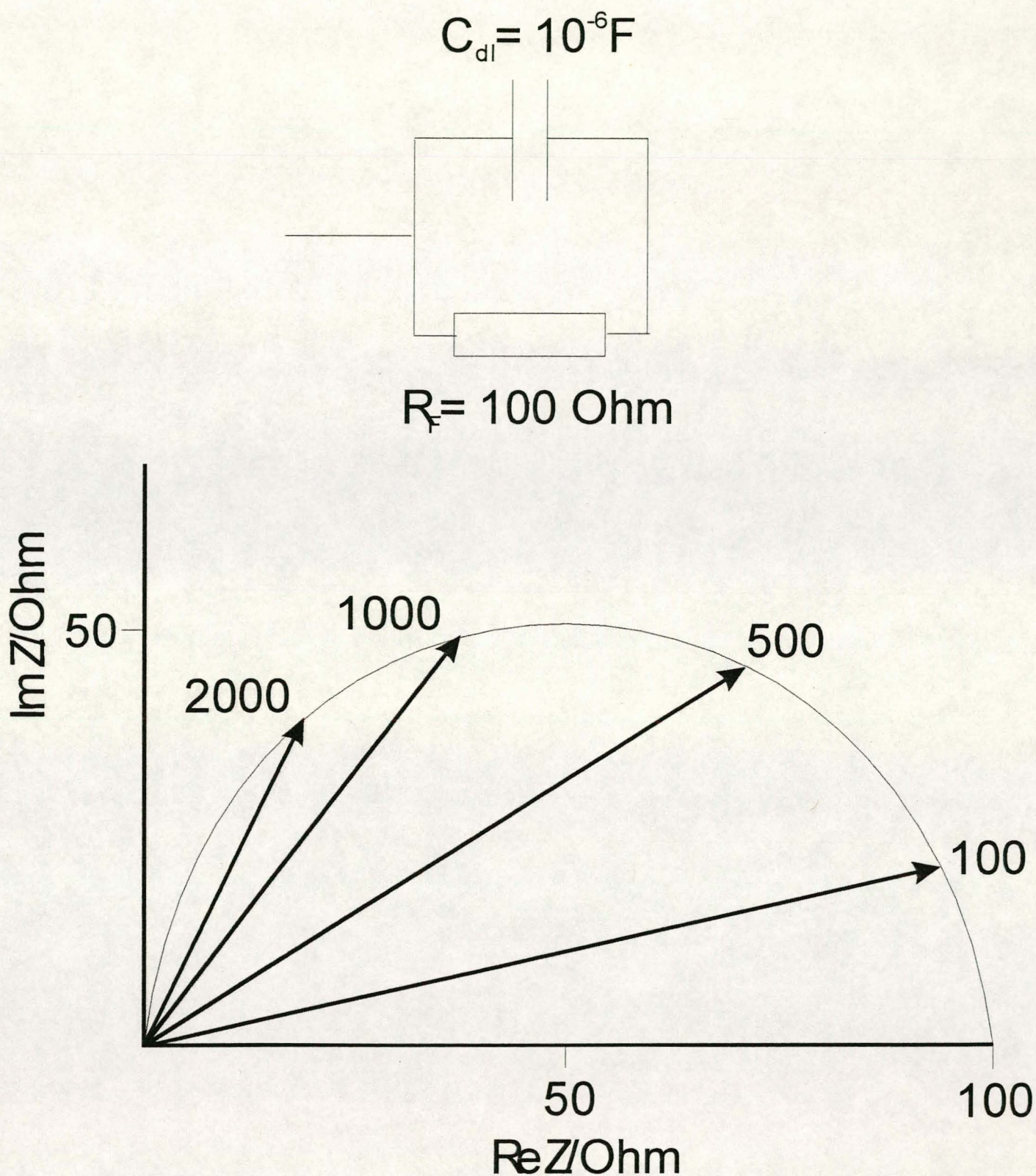In the parallel, it makes the circuit behave more and more as a capacitor, causing an increase in phase angle, as seen in Fig. 42.

It now has to be considered a more realistic situation, in which both the series and parallel resistance must be taken into account. The equivalent circuit and the corresponding complex-plane plot are shown in Fig. 43. The mathematical expression for the impedance applicable to this circuit can be derived as a function of ω:

$$Z(\omega) = R_S + \frac{1}{1/R_F - \omega C_{dl}/j} = R_S + \frac{R_F}{1 + j\omega C_{dl} R_F} \tag{49}$$

The following simple manipulation allows the separation of the real part from the imaginary part of the impedance:

$$Z(\omega) = R_S + \frac{R_F}{1 + j\omega C_{dl} R_F} \times \frac{1 - j\omega C_{dl} R_F}{1 - j\omega C_{dl} R_F} \tag{50}$$

which leads to the expression

$$Z(\omega) = R_S + \underbrace{\frac{R_F}{1 = (\omega C_{dl} R_F)^2}}_{\text{ReZ}} - j \times \underbrace{\frac{\omega C_{dl} R_F^2}{1 + (\omega C_{dl} R_F)^2}}_{\text{ImZ}} \tag{51}$$

The result is a semicircle having a radius equal to $R_F/2$, with its centre on the x-axis and displaced from the origin of coordinates by $R_S + R_F/2$. Each point on the semicircle of Fig. 42 represents a measurement at a given frequency. At very high frequencies, the faradaic resistance is effectively shorted out by the double layer capacitance, leaving the solution resistance in series as the only measured quantity. At very low frequency the opposite occurs, namely, the capacitive impedance becomes very high and one measures the sum of the two resistors in series.

The double layer capacitance can be obtained from this plot in different ways. The maximum of the semicircle satisfies the equation

$$R_F C_{dl} \omega_{max} = 1 \qquad (52)$$

from which C_{dl} can readily be evaluated. The capacitance can also be calculated at any frequency, by first obtaining $\text{Im} Z$ from the plot and then using the appropriate relationship given in equation 51.
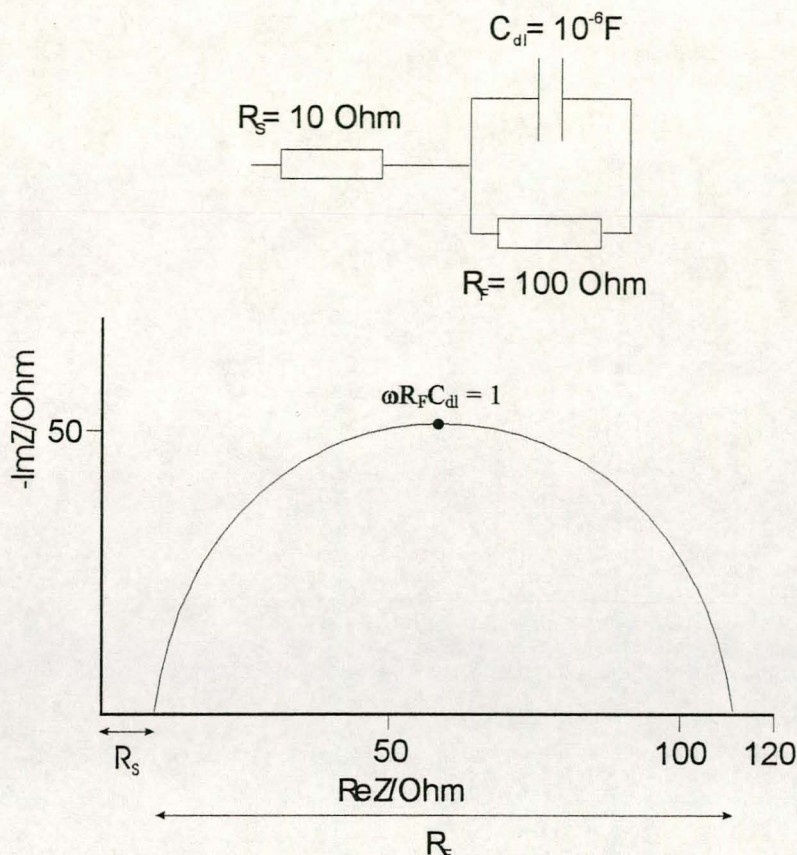
Fig. 43: Complex-plane representation of the impedance of an interphase. ReZ and ImZ are the real and imaginary components of the impedance, respectively.

6.1.2. Graphical representations

The results of electrochemical impedance spetroscopy (EIS) can be displayed in a number of different forms. We discuss first the one commonly referred to as the complex-plane impedance plot. Similar representations, in which the coordinates are the real and imaginary admittance (ReY and ImY) or capacitances (ReC and ImC) are referred to as the complex-plane admittance and the complex-plane capacitance plots, respectively. Other ways of displaying the results are the so-called Bode magnitude plot, in which $\log |Z(\omega)|$ is shown as a function of $\log (\omega)$ and the Bode angle plot, in which the phase angle, φ, is plotted versus $\log (\omega)$. There has been some argument in the literature as to the best method of displaying

EIS data. Nowadays, it is easy to display the data in all the above ways, to compare and choose the one that best suites the particular system being studied, making the above argument somewhat obsolete.

The perfect semicircle, shown in Fig. 41, is constructed by connecting the tips of the impedance vectors at different frequencies. The frequency itself is not shown, and this is one of the disadvantages of this form of presentation. This is sometimes corrected by marking the frequencies at which specific measurements were taken on the semicircle (Fig. 42). The diameter of the semicircle is equal to the resistance and is independent of the capacitance. As a result, plots measured for a fixed value of R_F but different values of C_{dl} cannot be distinguished in this type of presentation, even though corresponding points on the semicircle have been measured at different frequencies.

For the complex-plane admittance plot the real and the imaginary parts of the admittance are defined as

$$\mathrm{Re}\,Y = \left\{\frac{\mathrm{Re}\,Z}{(\mathrm{Re}\,Z)^2 + (\mathrm{Im}\,Z)^2}\right\} = \frac{\mathrm{Re}\,Z}{(|Z|)^2} \tag{53}$$

$$\mathrm{Im}\,Y = \left\{\frac{\mathrm{Im}\,Z}{(\mathrm{Re}\,Z)^2 + (\mathrm{Im}\,Z)^2}\right\} = \frac{\mathrm{Im}\,Z}{(|Z|)^2} \tag{54}$$

and for the complex-plane capacitance plot one has:

$$\mathrm{Re}\,C = \left\{\frac{\mathrm{Im}\,Z}{(\mathrm{Re}\,Z)^2 + (\mathrm{Im}\,Z)^2}\right\} \times \frac{1}{\omega} = \frac{\mathrm{Im}\,Z}{(|Z|)^2} \times \frac{1}{\omega} \tag{55}$$

$$\mathrm{Im}\,C = \left\{\frac{\mathrm{Re}\,Z}{(\mathrm{Re}\,Z)^2 + (\mathrm{Im}\,Z)^2}\right\} \times \frac{1}{\omega} = \frac{\mathrm{Re}\,Z}{(|Z|)^2} \times \frac{1}{\omega} \tag{56}$$

In Fig. 44, four different ways of presenting the response of the same circuit are compared. The values of the components constituting the equivalent circuit were chosen as $R_F = 10$ kΩ, $R_S = 1$ kΩ and $C_{dl} = 20$ μF. Each way of presentation has its advantages and disadvantages. From the impedance plot R_F and R_S can be read directly and the double layer capacitance can be calculated, employing equation 51. The relevant time constant in this case is $\tau_C = R_F C_{dl} = 0.2$ s, hence $\omega_{max} = 5$ Rad/s. The major drawback of this representation that does not display the frequency of the measured point can be overcome by adding a third dimension of frequency in on the Y-axis of a three-dimensional plot as shown in Fig. 44 e). The complex-plane admittance plot yields the same information. One should note, however, that the relevant time constant in this type of presentation is τ_S where $R = (R_S R_F)/(R_S + R_F)$ is the parallel combination of the two resistors. In the present example $\tau_S = 0.018$ s and $\omega_{max} = 55$ Rad/s. The same information can be obtained from these two ways of presentation, but the complex-plane impedance plot is mostly preferred, because the two resistances are shown in it directly.

On the complex-plane capacitance plot the semicircle results from the series combination of R_S and C_{dl} and the intercept with the real axis yields the value of the capacitance. The vertical line is due to the parallel combination of R_F and C_{dl}.

It would seem then that the complex-plane impedance plot is the better way of presenting the data, if one is mainly interested in the value R_F and its variation with time or potential. The complex-plane capacitance plot, on the other hand, brings out more directly the value of the capacitance and its variation with the different parameters of the experiment.

Plotting the same data in the Bode-type representation, one notes two points:

1. Although the values of the two resistors are easily discerned, there is no region in which the circuit behaves as a pure capacitor.

2. The phase angle is a more sensitive test of the capacitive or resistive behaviour of the system than is the plot of log $|Z(\omega)|$ versus log (ω). The detailed shapes of these curves depend, of course, on the numerical values chosen for the various circuit elements. Having a value of $R_S = 10\ \Omega$, instead of $1000\ \Omega$, then the two horizontal lines in Fig. 44 would have been much farther apart and an (almost) pure capacitive behaviour would have been observed in the intermediate region.

The curves in Fig. 44 are all simulated using Zview Equivalent Circuit by Scribner which is based on the LEVM 6.0 programme written by Dr. J. Ross MacDonald and therefore ideal in the sense that they follow exactly the equations derived for the given equivalent circuit. In practice, the points are always scattered as a result of experimental error. Also the frequency range over which reliable data can be collected does not necessarily correspond to the time constant which one wishes to measure.
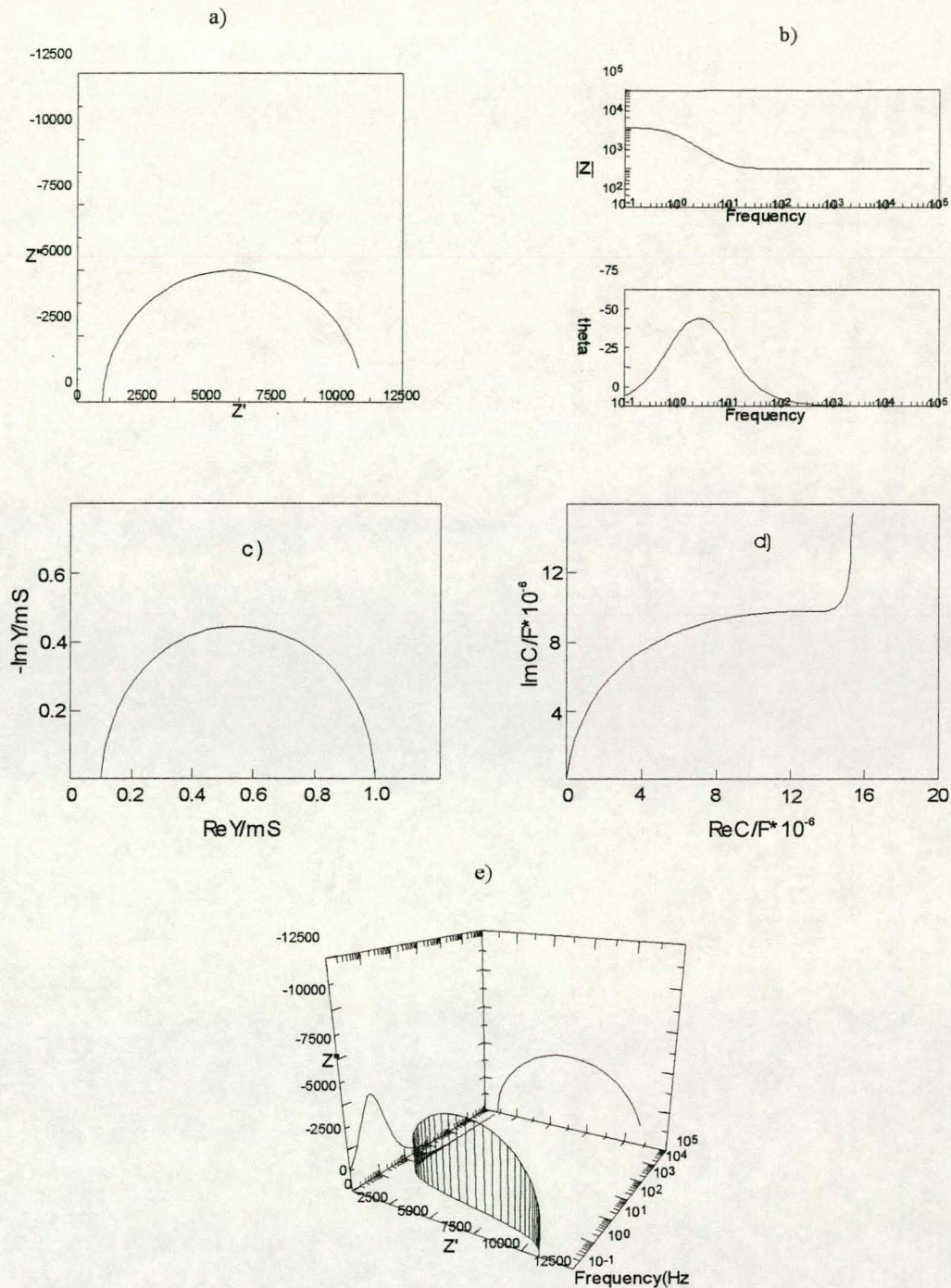
Fig. 44: Comparison of a) complex-plane impedance, b) Bode magnitude and Bode angle, c) complex-plane admittance and d) complex-plane capacitance plots for the same equivalent circuit. C_{dl} = 20 μF, R_F = 10 kΩ and R_S = 1 kΩ. e) is an attempt to overcome the drawback of the complex-plane impedance plot that does not display the frequency. In e) a three-dimensional plot of a) is shown displaying the frequency on the Y-axis.

125

6.2. Experimental

The impedance measurements were carried out at the Institute for Inorganic Chemistry at the University of Essen. A strip of Ti/SnO$_2$/Sb$_2$O$_5$, 0.3 cm wide, was cut out and exposed to the electrolyte of 1 M H$_2$SO$_4$. There the electrode material was pre-treated at 2 V versus a *R*eversible *H*ydrogen *E*lectrode (RHE) as a reference for 60 s. Impedance measurements were conducted, thereafter, over the entire frequency range of 10^5 Hz – 0.01 Hz. The potential at the working electrode (Ti/SnO$_2$/Sb$_2$O$_5$) for the different impedance measurements ranged between 0 V (RHE) and 2 V and was raised in small integrals (0 V; 0.5 V; 1.0 V; 1.3 V; 1.4 V; 1.45 V; 1.5 V; 1.55 V; 1.6 V; 1.7 V; 1.8 V; 1.9 V; 2.0 V). The steps were chosen to be particularly small around 1.5 V (RHE), because according to the results from the cyclic voltammetry the combustion reaction of phenol is expected to emerge in this potential region. In order to observe the influence of the diffusional Warburg term on the measurements, the experiments were repeatedly carried out with the electrode emerged to the electrode to different depths (3 cm, 2 cm and 1 cm). The smaller the exposed electrode area to the electrolyte, the less diffusional interference to the measurement is expected.

The entire procedure was repeated after adding 5mmol/l of phenol to the electrolyte to examine the different response due to the combustion reaction.

The experiments were conducted in an electrochemical cell equipped with a Pt-wire as a counter electrode and an RHE electrode as reference system. The Pt-wire surrounded the working electrode as a cylinder to provide an even current distribution to the working electrode. The experimental set-up can be seen in Fig. 45.

As an electrochemical interface we used an EG&G potentiostat 273 connected to a Solartron 1260 frequency response analyser.
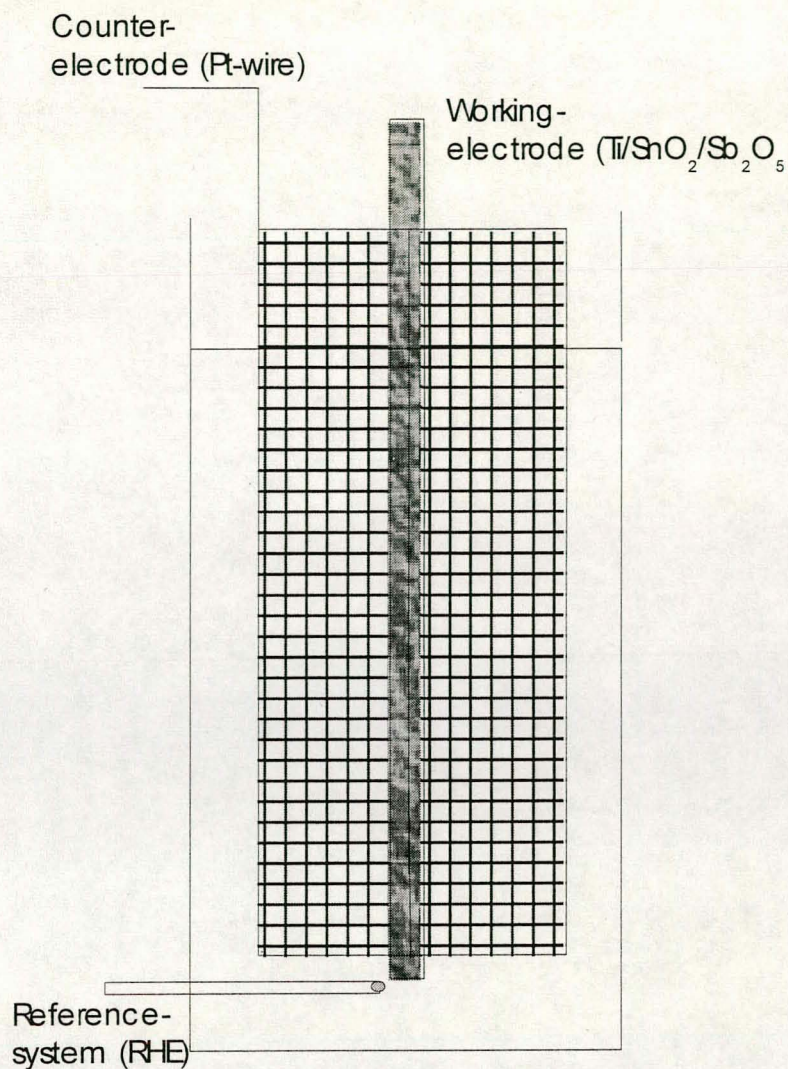
Fig. 45: Experimental set-up for the impedance measurements

6.3. Results and discussion

The impedance measurements were conducted as described in the experimental section 6.2. Two series of measurements were carried out. The first comprised frequency scans in 1M H_2SO_4, whereas for the second sequence of measurements 5mmol/l of phenol was added to the electrolyte:

127

a) 1M H₂SO₄ as electrolyte

The impedance measurements in sulphuric acid only were merely employed for the sake of general characterisation. Up to a potential of 1.6 V (RHE) diffusional Warburg terms seem to be predominant, especially at low frequencies (Fig. 46). At higher potentials Fig. 47 and Fig. 48 illustrate a change from mass transport limitation to charge transfer, as the •OH-radical production and the oxygen evolution reaction arise. The figures only displays the data of the measurements at a penetration depth of three cm of the electrode. In Fig. 46 it can already be observed that the curves become less steep with rising potential due to a decreasing effect of mass-transport limitation on the system.
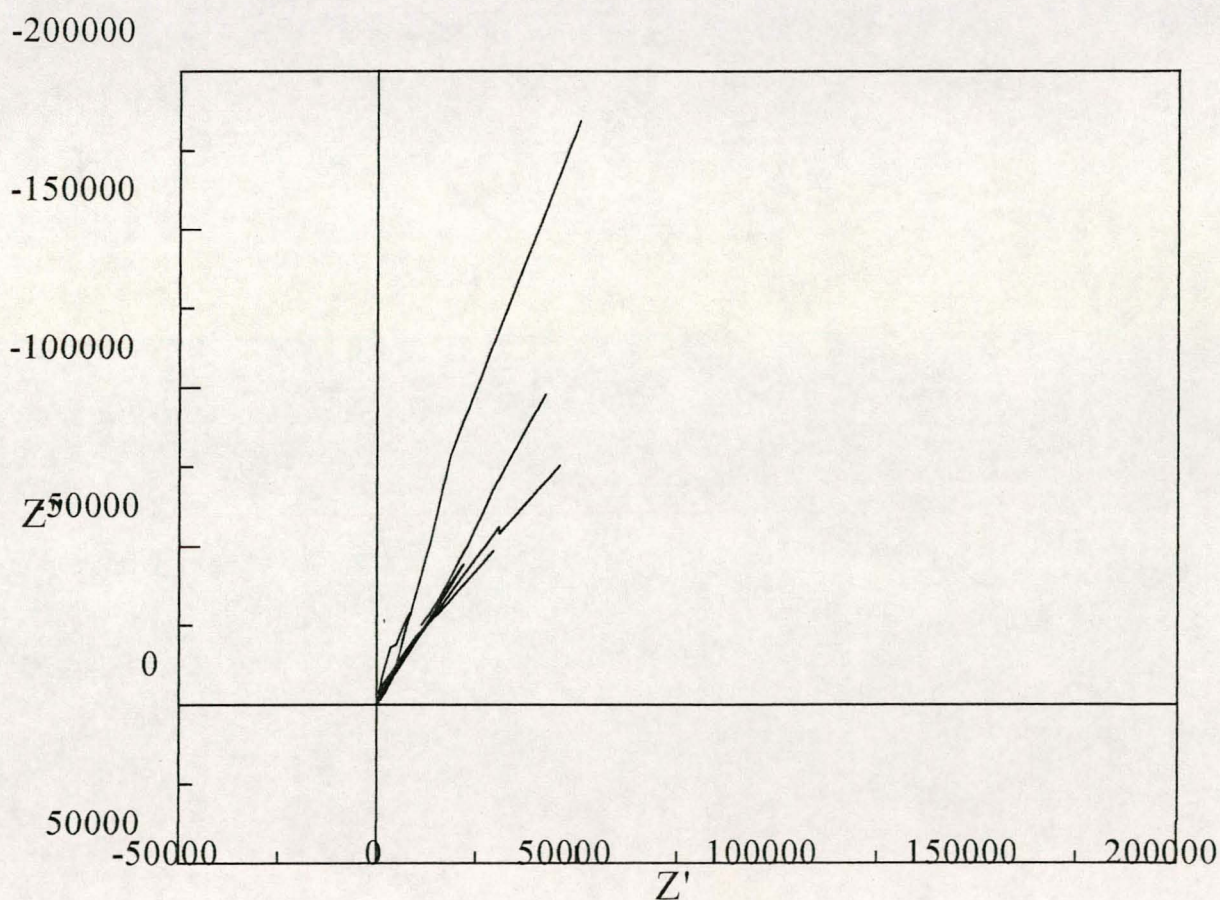
Fig. 46: Impedance measurements in 1M H₂SO₄. Penetration depth of the electrode into the electrolyte: 3 cm. Potentials: 0 V; 0.5 V; 1.4 V; 1.55 V and 1.6 V versus RHE. The curves become less steep with rising potential, due to a decreasing effect of mass-transport limitation on the system.
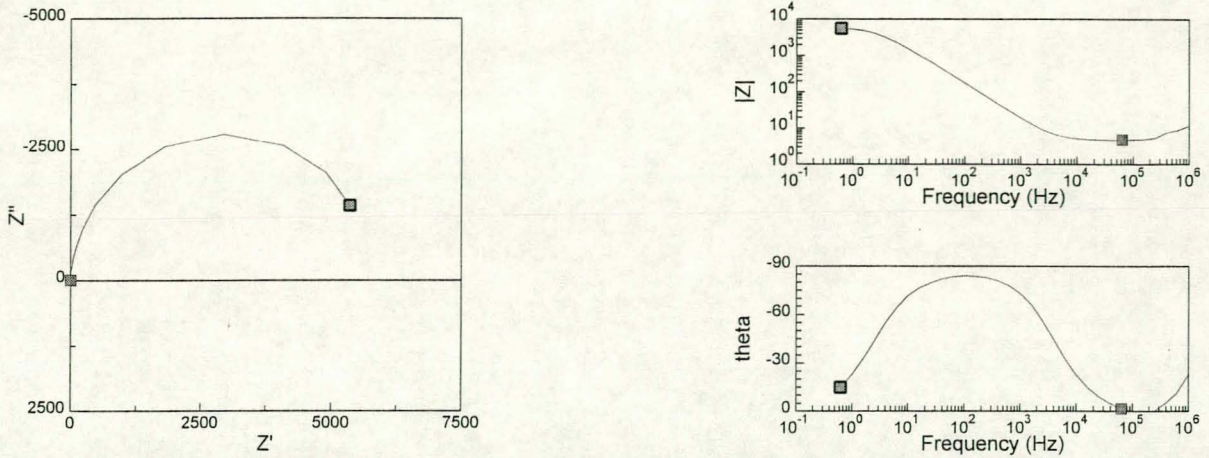
Fig. 47: Complex-plane impedance and Bode plot of the impedance measurement at 1.9 V (RHE) at a penetration depth of 3 cm into the electrolyte of 1M H_2SO_4.
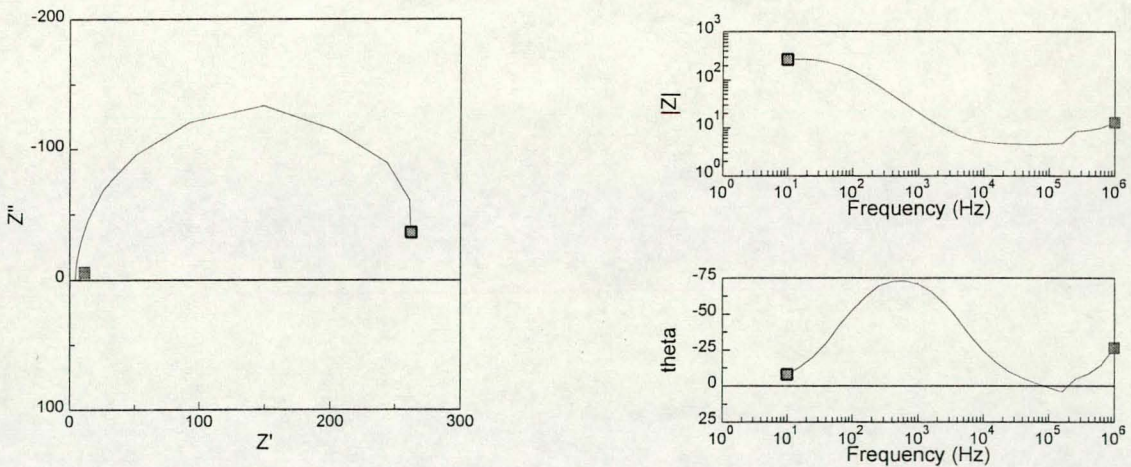
Fig. 48: Complex-plane and Bode plot of the impedance measurement at 2.0 V (RHE) at a penetration depth of 3 cm into the electrolyte of 1M H_2SO_4.

Fig. 47 and Fig. 48 display almost perfect semicircles which indicate the charge transfer reaction. As a striking feature the charge transfer resistance drops from about 6000 Ω to 270

Ω. A different reaction is thus dominating at 2 V (RHE). This phenomena can be attributed to the change from •OH-radical production to the beginning of the oxygen evolution.

b) 1M H₂SO₄ and 5mM phenol as electrolyte

Phenol (5 mmol/l) was added to the electrolyte of 1M sulphuric acid, before starting the second sequence of measurements. The kinetic studies in chapter 5 lead to the conclusion that the overall combustion reaction comprised one initial rate-determining step of the •OH-radical production, prior to the following reaction between the •OH-radical and the phenol which is second order. This reaction does not necessarily take place directly at the electrode's surface and does not indispensably involve a charge-transfer from the electrode to the electrolyte. Thus, one could expect that the addition of phenol to the electrolyte does not influence the charge-transfer step manifested in the impedance spectrum. The same trend of suppression of the diffusion term with rising potential, as observed in the previous measurements without the addition of phenol to the electrolyte, can be seen. However, an additional time constant with a value of ReZ of about 550 Ω can be seen in the low frequency domain once a potential of 1.9 V (RHE) is reached. Especially, with less penetration depth of the electrode into the electrolyte, the working electrode's behaviour approaches that of a 'large' micro-electrode, which means that once again the diffusional term fades to the background. That is why at a penetration depth of 3 cm into the electrolyte the first time constant spreads over a high range of ReZ and the second time constant is only slightly indicated at 2 V. The second time constant can most likely be referred to the beginning of the oxygen evolution. The addition of the phenol to the electrolyte does not significantly change the electrochemical response of the interphase. Consequently, the proposed mechanism from chapter 5 is confirmed and the formation of •OH-radicals is the crucial step for the combustion reaction.
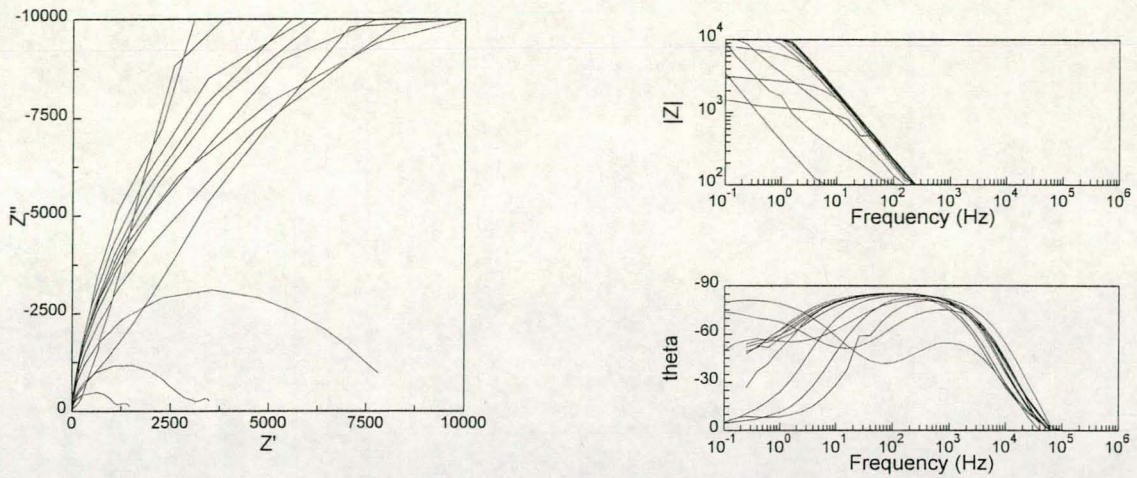
Fig. 49: Electrolyte: 1M H_2SO_4 + 5mM phenol. Potential: 0 V, 0.5 V, 1 V, 1.3 V, 1.4 V, 1.45 V, 1.5 V, 1.55 V, 1.6 V, 1.7 V, 1.8 V, 1.9 V, 2 V. Penetration depth of the electrode: 1 cm.
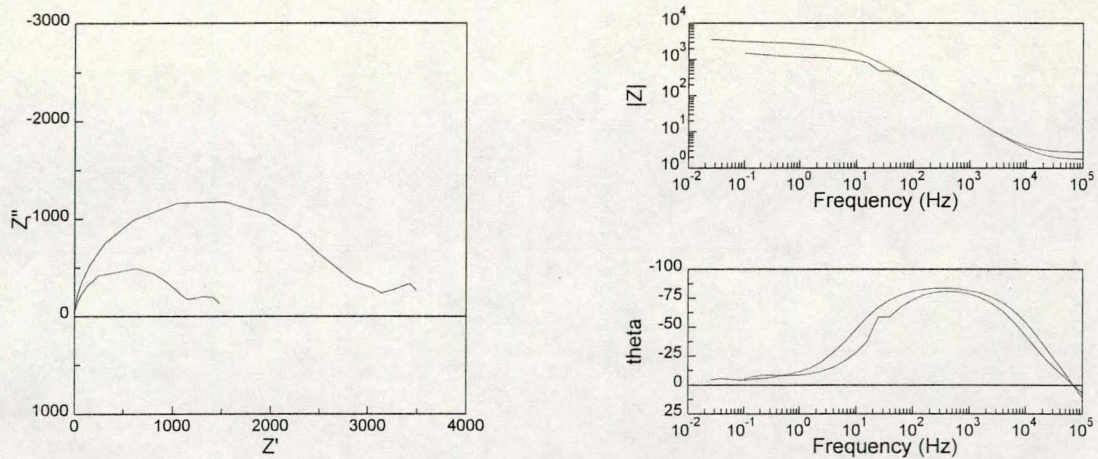
Fig. 50: Same measurement as shown in Fig. 49, displaying the results at potentials of 1.9V and 2 V only.
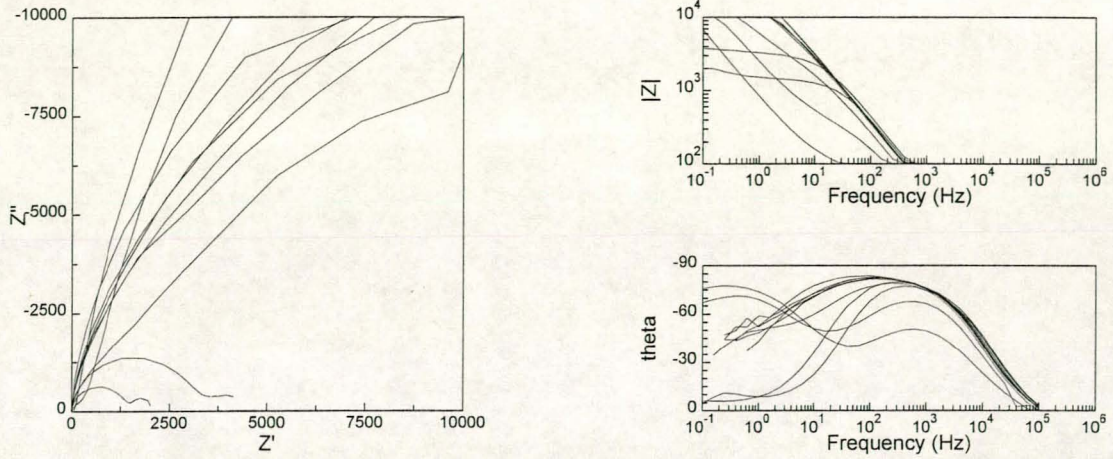
Fig. 51: Electrolyte: 1M H_2SO_4 + 5mM phenol. Potential: 0 V, 0.5 V, 1 V, 1.3 V, 1.4 V, 1.45 V, 1.5 V, 1.55 V, 1.6 V, 1.7 V, 1.8 V, 1.9 V, 2 V. Penetration depth of the electrode: 2 cm.
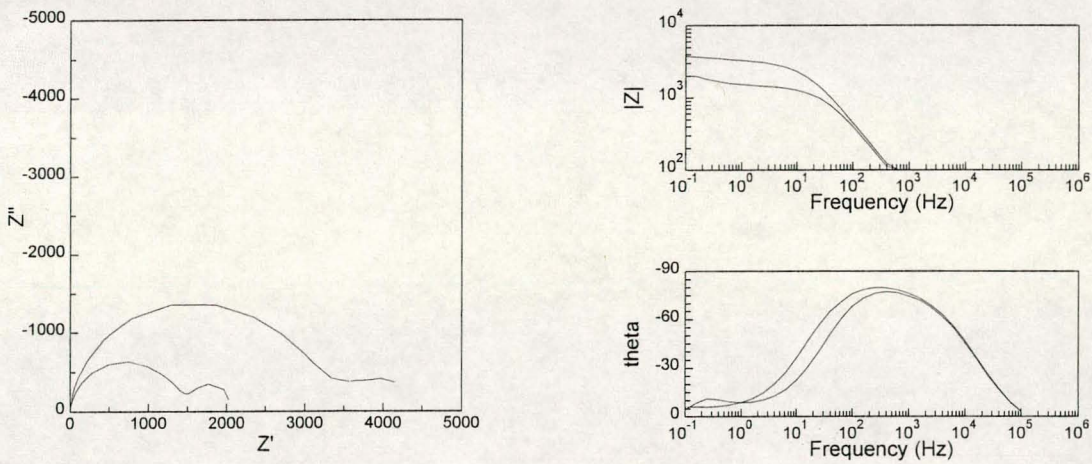
Fig. 52: Same measurement as shown in Fig. 51, displaying the results at potentials of 1.9Vand 2 V only.
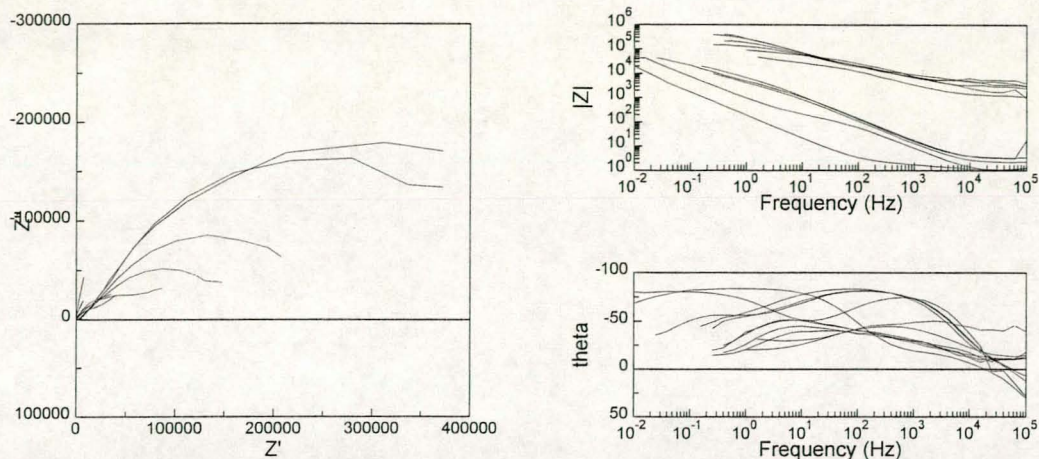
Fig. 53: Electrolyte: 1M H_2SO_4 + 5mM phenol. Potential: 0 V, 0.5 V, 1 V, 1.3 V, 1.4 V, 1.45 V, 1.5 V, 1.55 V, 1.6 V, 1.7 V, 1.8 V, 1.9 V, 2 V. Penetration depth of the electrode: 3 cm.
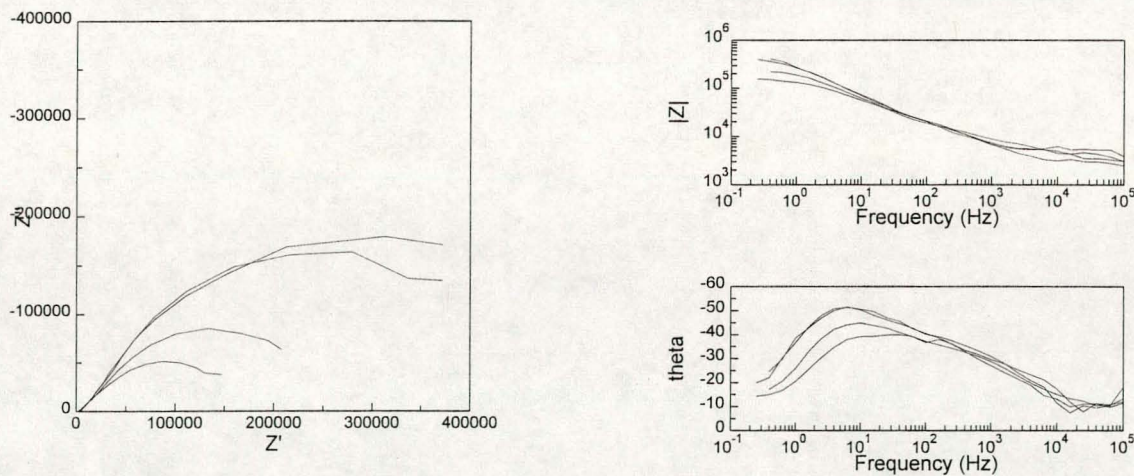
Fig. 54: Same measurement as shown in Fig. 53, displaying the results at potentials of 1.7 V, 1.8 V, 1.9 Vand 2 V only.

The impedance measurements remain somewhat vague in their results, but at least do not contradict the conclusions of the kinetic measurements in chapter 5, but can even confirm the interpretation for the proposed reaction mechanism.

Chapter 7

Application of the Sb-doped SnO_2 electrode material in a Solid Polymer Electrolyte (SPE) reactor for the electrocatalytic oxidation of phenol.

Abstract

Large scale porous titanium electrodes, up to 100 cm², have been coated with doped SnO_2 for a galvanostatic solid polymer electrolyte (SPE) application, resulting in very low voltage across the stack, even without adding supporting electrolytes to the water. Phenol was used as a standard contaminant throughout all experiments. A new method for online analysis of the phenol by fibre-optics UV/VIS spectroscopy was designed and the results compared to a well established standard colorimetric method for the determination of phenol.

7.1. Phenol as a model pollutant

Improper discharge of industrial wastewater is a major source of aromatic and phenolic compounds in water. The presence of these hazardous compounds in water represent a major threat to the enviroment. In particular, the phenolic compounds cause severe problems with respect to complete oxidation, because of their high stability due to the combination of aromatic and inductive effect.

Phenol is a strong protoplasma toxic chemical. On the skin it is highly caustic and can easily be absorbed. Swallowing or inhalation of the vapours causes respiratory paralysis, delirium and finally leads to cardiac arrest. Chronic intoxication leads to damage of the

kidneys. In case of an emergency, small areas of the skin are treated with ethanol, larger areas washed off with water. Due to its toxicity, phenol is no longer used as a disinfectant.

7.1.1. Methods for the determination of the phenol concentration

Several methods for the detection of phenol are described in the literature [Gremlin, 1997; Spiker, 1992]. Most of those include a separation step (chloroform extraction, methanol extraction or distillation) followed by analysis through UV/VIS, GS-MS, or HPLC. As only the UV/VIS instrumentation was readily available, analysis in this work focused on a colorimetric method that is standard for the determination of the so-called phenol index.

7.1.1.1. Determination of the phenol index by the German Standard Method for the examination of water, waste water and sludge [DEU, 1984]

The term phenol index as used in this specific standard only includes phenols which react with 4-aminoantipyrine under the conditions specified to give coloured compounds whose sensitivities to the reagents used in the following methods may not necessarily be the same.

The percentage composition of the various phenolic compounds in a given test sample is unpredictable. It is obvious, therefore, that a standard containing a mixture of phenolic compounds cannot be made applicable to all test samples. For this reason, phenol has been selected as a standard, and any colour produced by the reaction of other phenolic compounds is measured as phenol and reported as the phenol index.

It is not possible to use the procedures specified in this standard to differentiate between different kinds of phenols. Some phenolic compounds with substituents such as alkyl, aryl and

nitro in the para position do not produce colour with 4-aminoantipyrine. Phenolic compounds containing para substituents such as a carboxyl, halogen, hydroxyl, methoxyl or sulfonic acid, do produce colour with 4-aminoantipyrine. Hence the phenol index includes only those phenolic compounds which can be determined under specified conditions.

Two different methods are described:

Method A: Phenols and other coupling compounds form with 4-aminoantipyrine in the presence of potassiumperoxodisulfate antipyrine dyes that can be extracted with chloroform. The intensity of the colour is then determined photometrically.

Method B: Water vapour volatile phenols are separated from the rest of the dissolved substances in the water by distillation at a pH of 4. Among the volatile compounds aromatic amines can still be present. To prevent their influence on the determination the sample must be distilled under strong sulphuric acidic conditions (pH = 0.5). The phenols of the distillate form an antipyrine dye, in the presence of potassiumhexacyanoferrate (III) under alkaline conditions which is extracted with chloroform and determined by spectrometric measurement.

Interferences:

A) Oxidising substances

In case of chlorine or iodide evolution after the acidification of the sample, the oxidation agent in the sample has to be reduced by the addition of ascorbic acid.

B) Reducing substances

If the sample contains SO_2, nitrite or other reducing compounds (check the sample with potassium iodate starch), then method A is no more applicable.

C) Colouring substances

Coloured compounds or compounds that form a dye with 4-aminoantipyrine can induce a higher phenol index than actually present in the water. The absorbance has to be measured without the addition of 4-aminoantipyrine and taken as background correction.

D) Cyanides

If the sample is expected to contain cyanides in a concentration higher than 1 mg/l, method A is no more applicable. Prior to distillation 5 ml of a cobalt sulphate solution has to be added.

In this work test samples were prepared by adding defined amounts of phenol to pure water, to prove that method A would be suitable for accurate reproducible analysis.

Chemicals required

All chemicals used were of analytical grade. Water used for dilution was distilled water. The method is applicable to a concentration range of $10 - 150$ µg/l of phenol. In the case of a higher concentration the sample has to be diluted.

a) Hydrochloric acid

- HCl (ρ = 1.12 g/ml) : distilled water = 1:1

b) Caustic soda

- 40 g of NaOH in 100 ml of water

c) Ammonia solution, NH_3, ρ = 0.91 g/ml

d) Buffer solution, pH = 10

- 34 g NH_4Cl, 200 g of potassium-sodium tartrate ($KNaC_4H_4O_6 \bullet 4H_2O$) dissolved in 700 ml of water

- Add 150 ml of solution c)

- Dilution to 1 l with water.

e) Aminoantipyrine solution

- 2.0 g 4-aminoantipyrine dissolved in 100 ml of water

138

- The solution has to be prepared freshly

f) Peroxodisulphate-solution

- 0.65 g potassium peroxodisulphate, $K_2S_2O_8$ dissolved in 100 ml of water; stored in the dark, the solution can be kept for a week.

g) Ascorbic acid

h) Sodium sulphate

i) Copper sulphate

j) Chloroform

k) Potassium iodide

l) Phenol solutions of different concentrations for standardisation.

As phenolic compounds in water can be oxidised chemically as well as biologically the samples need to be examined within 4 h.

Procedure for Method A

500 ml of the sample has to be acidified to a pH of 4. Copper sulphate (0.5 g) has to be added to avoid bacteriological oxidation of the sample. The solution is then transferred to a separation funnel and 20 ml of the buffer solution (d) is added. The pH is adjusted to 10 with ammonium hydroxide if necessary. Add 3.0 ml of 4-aminoantipyrine solution (e), mix immediately, then add 3.0 ml of peroxodisulphate solution (f), and again mix immediately. The absorbing compound has to be allowed to form in the dark for 30 min (maximum 60 min). Afterwards, exactly 25 ml of chloroform has to be added for the extraction of the dye. The separation funnel has to be shaken vigorously for about 5 min to ensure extraction and further time is allowed for the phases to separate. The chloroform extract is then filtered

through Büchner funnels containing 5 g of sodium sulphate, directly into a 25 ml measuring flask. The flask is then brought to volume with chloroform.

Using the chloroform, the spectrometer is adjusted to zero absorbance at 510 nm. The absorbance must be referred to the calibration curve, obtained from measurements with defined phenol content.

7.1.2. Online-detection of phenol by means of fibre-optics spectrophotometry

For better monitoring of the process of the oxidation of phenol in an SPE-reactor a direct online-method for the phenol detection in water by fibre-optics spectrophotometry has been conceived.

The direct detection of the phenol concentration at 270 nm by means of UV/VIS spectrophotometry was interfered by the heavy noise caused by the electrolysis process itself. In order to overcome this problem, an antipyrine dye was formed with 4-aminoantipyrine in the presence of hexacyanoferrate (III) with the maximum of absorbance at 510 nm. 4-aminoantipyrine exerts an electrophilic attack upon the para-position of the phenol to form a quinone structure [Spiker, 1992].

To confirm these results the phenol index was additionally determined by the well established colorimetric method (section 7.1.1.1.).

7.2. Experimental

7.2.1. Electrode preparation for the SPE-reactor

The doped SnO_2 solutions for the dip-coating were prepared from two alkoxides obtained directly from chlorides according to the method described by Chaleton [Chaleton, 1995]. A porous, circular titanium plate with a total area of 100 cm^2 was used as a substrate for the catalyst. It was placed in a clean chamber saturated with ethanol vapour. The sol was pipetted onto the substrate through a hole in the top of the chamber, coating both sides of the electrode. The substrate was then allowed to dry for 6 h, after which it was dried in air at 100°C for 15 min. This coating procedure was carried out twice to close cracks and heal defects in the film. Calcination was then carried out in air by heating the substrate to 600°C, at a rate of 1°C/min. After the calcination process the electrode maintained its porous structure and was still permeable to water.

7.2.2. Set-up of the SPE-reactor

A porous Ti plate, coated with Pt by means of a magnetron sputtering on the surface and identical in shape to the anode, was used as a cathode. The two electrodes were mounted in the SPE reactor [Bessarabov, 1998; Sanderson, 1997], sandwiching a perfluorinated Nafion-like cation-exchange membrane in H^+-ionic form ('Plastpolymer', St. Petersburg, Russia), as shown in Fig. 55. The membrane was prepared from a blend of the copolymer of tetrafluoroethylene and perfluoro-3,6-dioxa-5-methyl-1-octene-8-sulfonyl fluoride. Thickness of the membrane was 230 μm, and equivalent mass was 1120.

The electrolyte (0.5L) was pumped through the reactor by a peristaltic pump, passing the anode- and cathode chamber in series, without separation of the two chambers, while the cation-exchange membrane ensured the ionic migration between the two electrodes. The anodic and the cathodic chamber did not have to be separated, because total oxidation was expected by •OH radicals that only exist at the electrode`s surface. Reduction at the cathode can thus not be assumed. The total area of the electrodes was 100 cm^2.
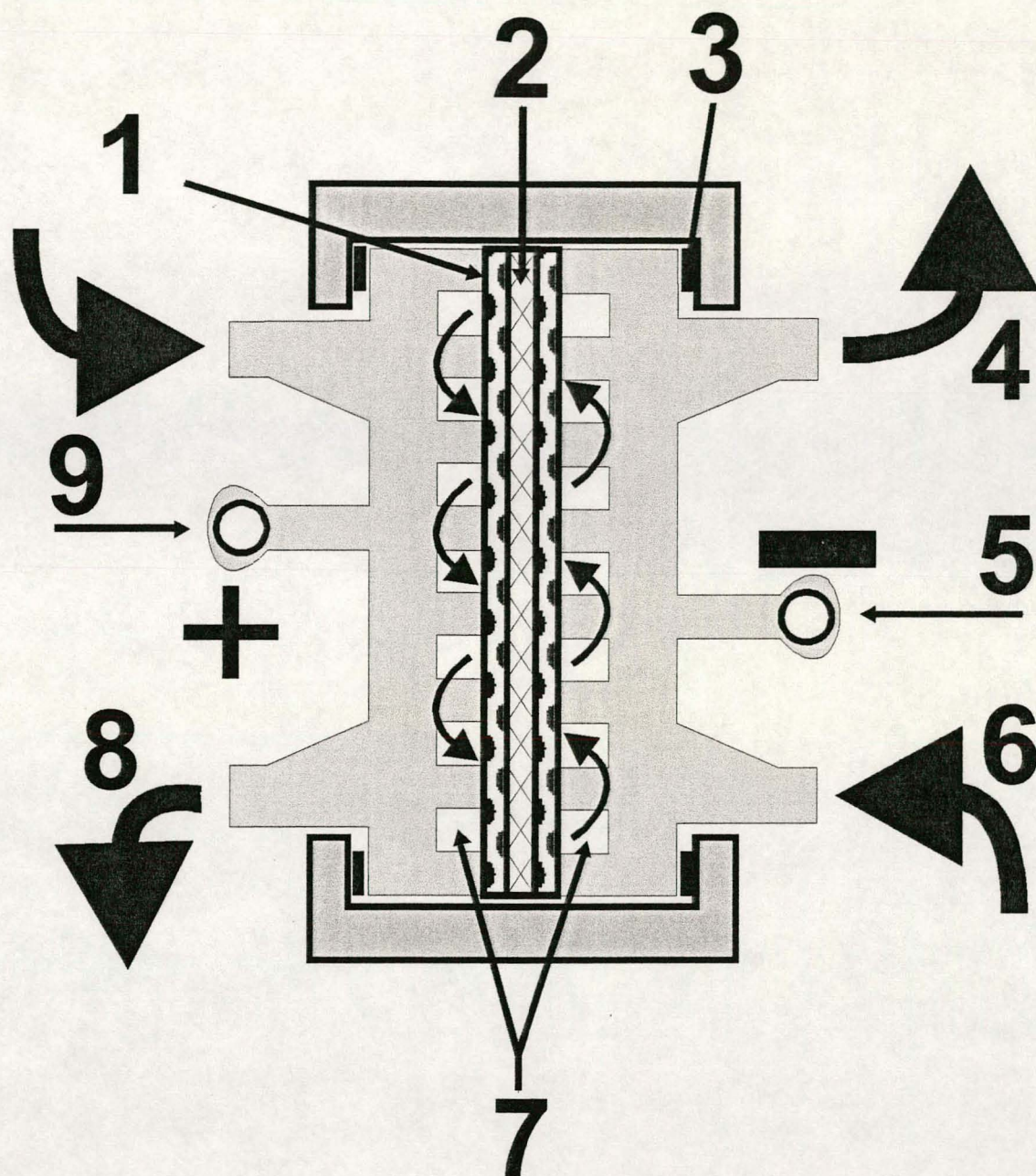
Fig. 55. SPE-reactor: (1) - porous Ti, coated with SnO_2/Sb_2O_5, (2) - Nafion membrane, (3) - isolators between electrodes and reactor, (4) - outlet for water, (5) - cathode side, (6) - cathodic inlet for water, (7) - distribution channels for cathode and anode, (8) - anodic outlet, (9) - anode.

7.2.3. Online analysis of phenol during electrolysis in the SPE reactor

The UV/VIS analysis was carried out with a Perkin Elmer Lamda 20 spectrophotometer attached to a fibre optics sensor placed inside the flow of the electrolyte (Fig. 56).

The electrolyte for the phenol determination comprised: 0.1 mol l^{-1} 4-aminoantipyrine, 2 mM $K_3[Fe(CN)_6]$, 1.3 mM NH_4Cl 0.03 mol/l NH_4OH, 1.4 mM potassium sodium tartrate tetrahydrate and 0.1 mM phenol. The red absorption band was monitored at 510 nm.
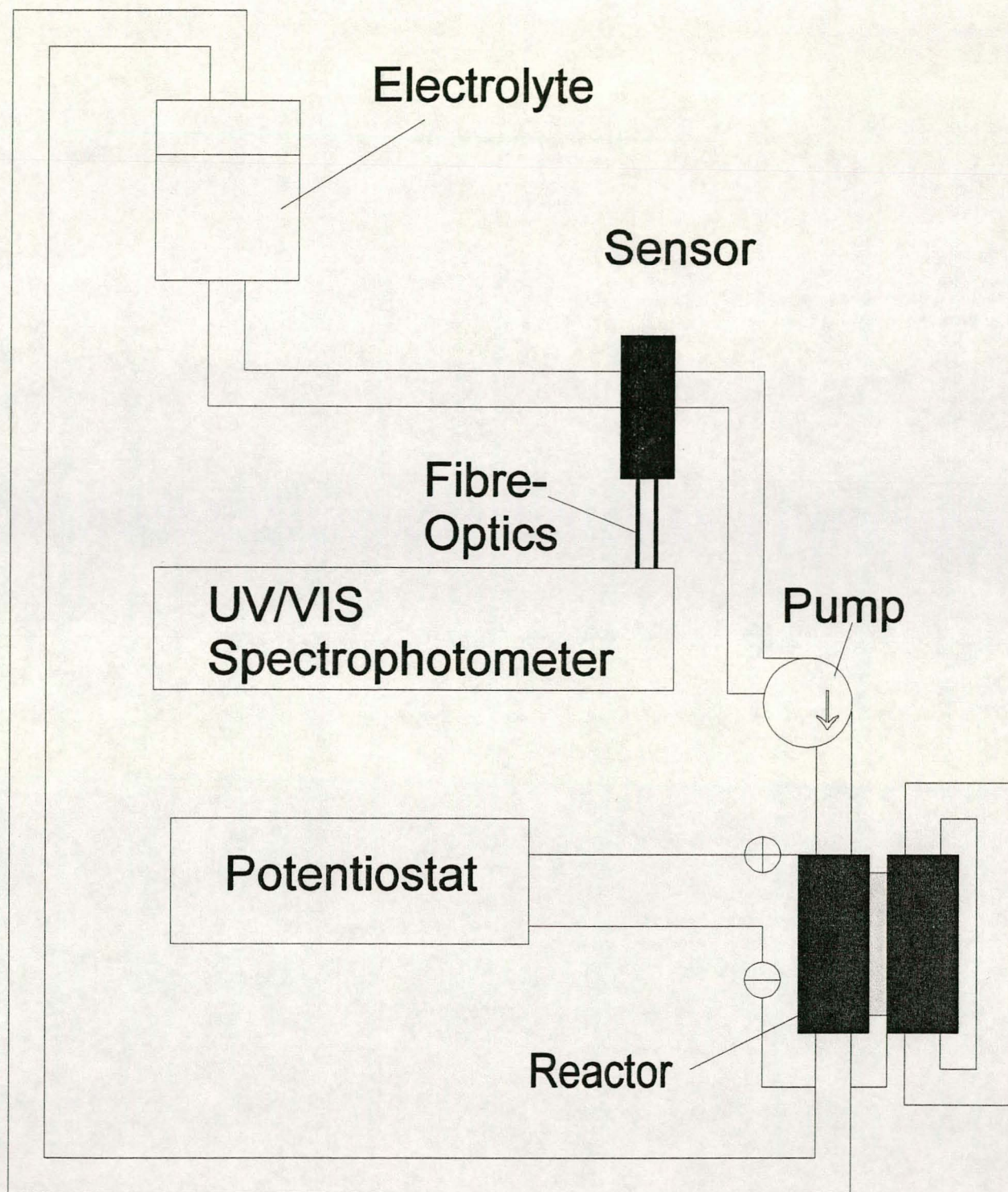
Fig. 56. Scheme for the online phenol analysis by the fibre-optics spectrophotometer.

7.2.4. Electrochemical equipment

All electrochemical measurements were carried out with a Solartron SI 1280B. Electrolysis was performed galvanostatically, with a current density of i: 20 m Acm^{-2}.

7.3. Results

7.3.1. Determination of the phenol index starting with high concentrations

Electrolyte (100 ml), containing 1g l^{-1} of phenol, was pumped through the SPE reactor during electrolysis at a current density of 20 mA cm^{-2} for 1200 min. Analysis was carried out every 15, 30, 60, 120, 240, 480, 720 and 1200 min. After a preliminary distillation and extraction with chloroform, the test samples were analysed [Murphy, 1992].

The concentration of the phenol decreased from 1 g l^{-1} to 0.22 g l^{-1} after 960 min of electrolysis. Further electrolysis could not significantly decrease that concentration. Fig. 57 shows the decrease in phenol concentration versus time.

The current efficiency was calculated under the assumption that 28 electrons are required for the complete oxidation of one molecule of phenol. With the phenol concentration decreasing, the current efficiency is also going down. After 15 min of electrolysis the current efficiency reaches 22.3 %, decreasing to 7 % after 120 min and finally achieving 2 % after 1200 min of electrolysis, as shown in Fig. 58.
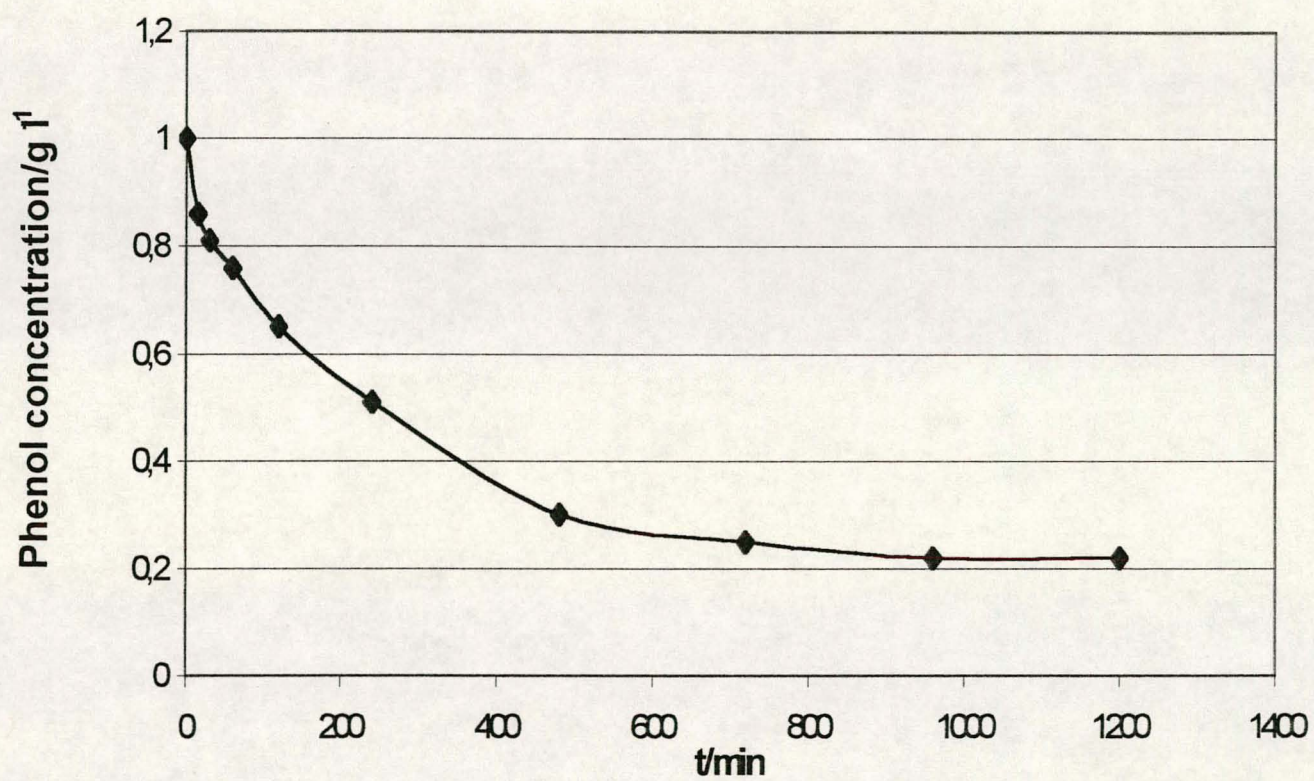
Fig.57. Phenol concentration (g l^{-1}) versus electrolysis time in the SPE-reactor, current density: 20 mA cm^{-2}
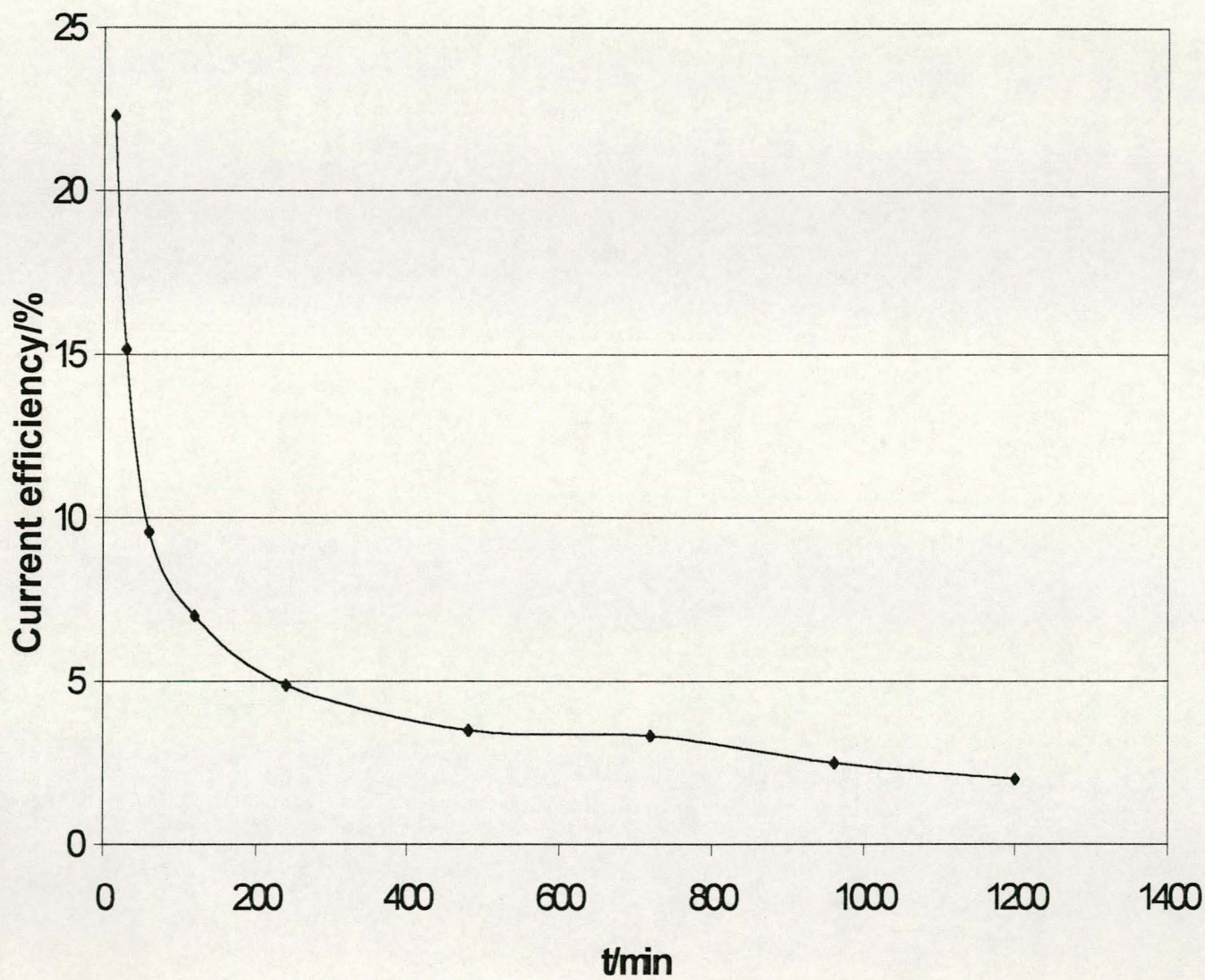
Fig. 58: Current efficiency versus time of electrolysis

The measurements are based on a calibration curve obtained from standardised measurements.

7.3.2. Determination of the phenol index starting with very low concentrations

To illustrate the effect of mass transport limitation on the current efficiency and performance of the entire process, electrolysis has been carried out with very low starting concentrations of phenol.

Electrolyte (0.5 l), containing 1mg/l of phenol, was pumped through the SPE reactor during electrolysis at a current density of 20 mA/cm^2 for 240 min. The pumping rate was 70 ml/mon. Analysis was carried out every 30 min. After a preliminary distillation, the test samples were analysed [Murphy, 1992].

The concentration of the phenol decreased from 1 mg/l to 0.02 mg/l after 240 min of electrolysis. Fig. 59 shows the decrease in phenol concentration versus time.

The entire process consumed 2.98×10^{-3} moles of electrodes, while only 5.19×10^{-6} moles of phenol were converted.
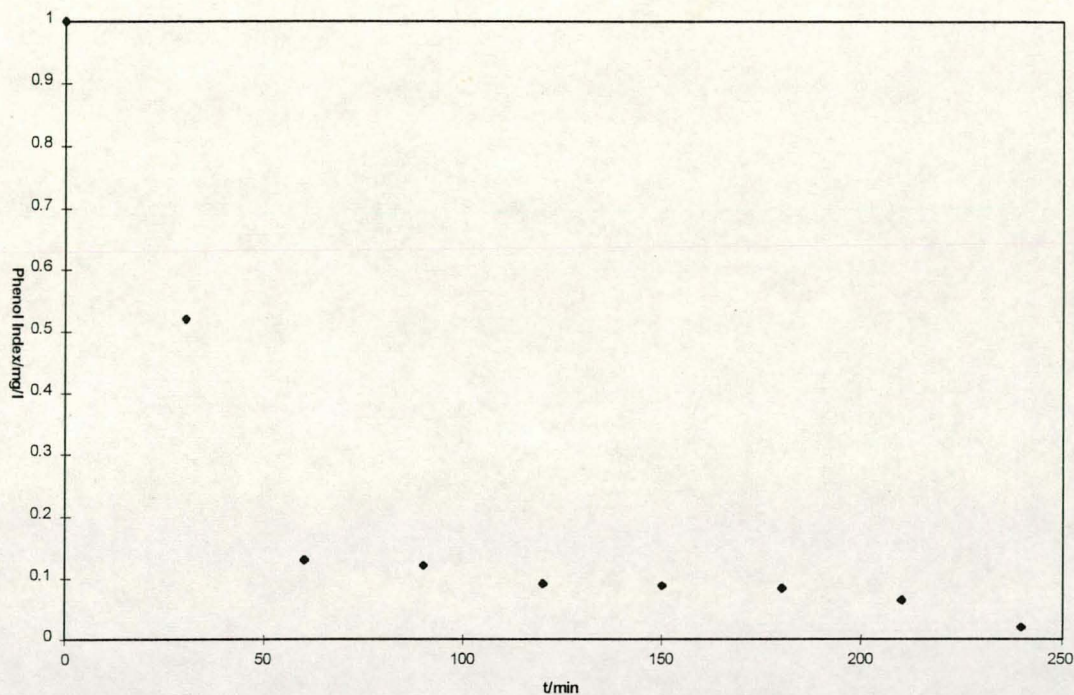
Fig. 59. Phenol index (mg/l) versus time during electrolysis in the SPE-reactor, current density: 20 mA/cm^2.

The determination of the phenol index was executed at the Private Institut für Umweltanalytik in Flöha, Germany.

7.3.3. Voltage across the reactor using the proton exchange membrane compared to a simple separator

By using the cation exchange membrane inside the reactor the voltage drops from 25V, using a simple separator between cathode and anode, to ca. 3.4 V as shown in Fig. 60. The application of the proton exchange membrane thus overcomes the necessity of adding supporting electrolytes.
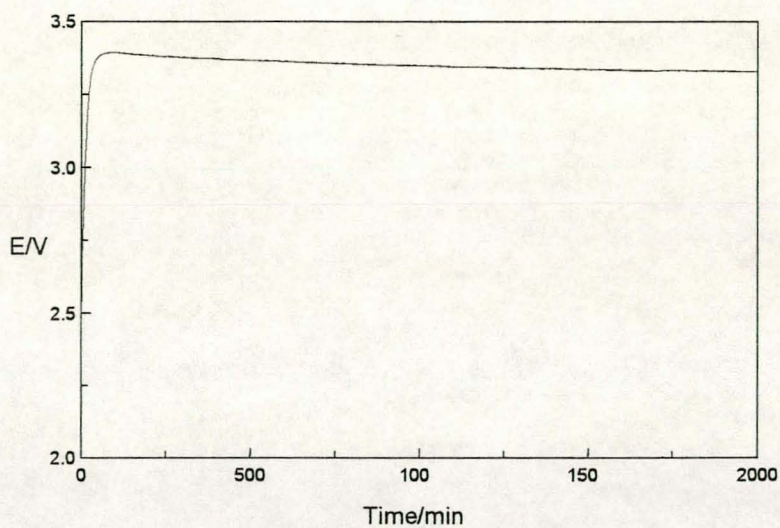
Fig. 60. Voltage across the stack versus time during electrolysis with Nafion as membrane between cathode and anode.

7.3.4. Online phenol analysis with 4-aminoantipyrine by fibre-optics

For the online determination of phenol, 0.1 mM of phenol was mixed with 0.1 mol l^{-1} 4-aminoantipyrine, 2 mM $K_3[Fe(CN)_6]$, 1.3 mM NH_4Cl 0.03 mol l^{-1} NH_4OH and 1.4 mM potassium sodium tartrate tetrahydrate to form 0.5 l of the coloured antipyrine dye which was pumped through the reactor at a current density of 20 mA cm^{-2}. The concentration of the phenol was determined by the fibre-optics spectrophotometer at a wavelength of 510 nm. Fig. 61. illustrates the decrease of the phenol concentration, versus time, during electrolysis.

The concentration drop was not as rapid as shown for the accurate determination in Section 7.3.1., but seems to resemble the situation described there quite well. This indicated that the quinone structure formed between phenol and 4-aminoantipyrine, was much more stable than the phenol itself, and that more accurate direct assessment of the phenol combustion process was not possible. Part of the inaccuracy can also be attributed to mass transport limitation to the fibre-optic sensor.
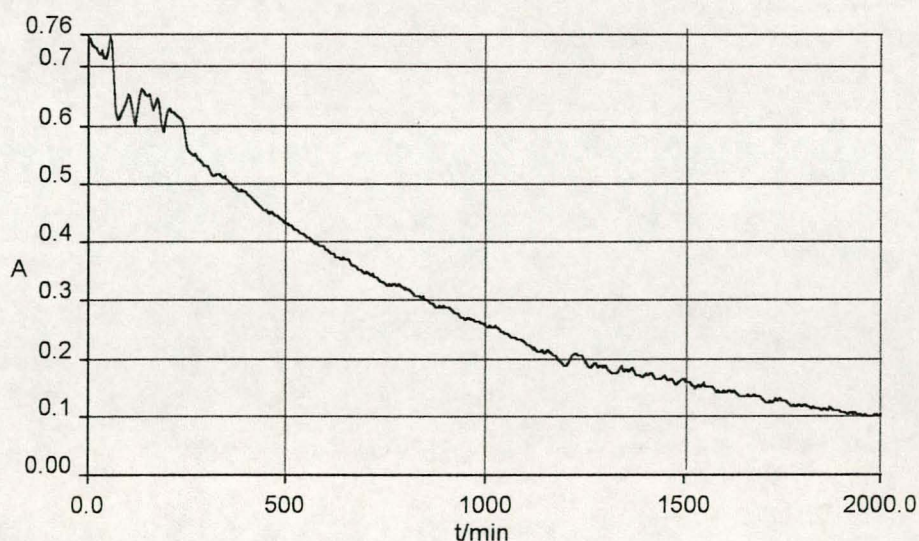
Fig. 61. Phenol concentration with 0.01g l^{-1} as initial concentration. Complexing agent: 4-aminoantipyrine, Online-detection at 510 nm, electrolysis in SPE-reactor, i = 20 mA cm^{-2}

152

7.4. Discussion

The reactor design, facilitating the Nafion membrane to separate anode and cathode, proved to be very effective, delivering very low voltage.

Direct phenol determination by fibre-optics was possible only with loss of accuracy, because the quinone structure formed between the 4-aminoantipyrine and the phenol, seems to be more stable to electrocatalytic attack than the phenol alone was. Furthermore, mass transportation limits to the fibre-optics sensor must be considered.

In an SPE-application sol-gel SnO_2 -based electrodes were a very powerful electrochemical tool for the electrochemical water purification of organic pollutants.

Upgrading of the system is easy to conceive, as any number of stacks of the described reactor design can be mounted together as required. The losses in current efficiency can be explained through side reactions such as oxygen evolution. The cyclic voltammograms (chapter 4), however, show a clearly separated, sharp phenol peak. Thus further study will focus on finding the suitable current density for a variety of phenol concentrations, so that at any point, side reactions can be suppressed to a minimum.

As a future perspective the use of an HPLC should be mentioned to find intermediates of the oxidation process which could also give further information on the reaction pathway.

Chapter 8

Anodic oxidation of chlorate ion to perchlorate on antimony-doped tin dioxide electrodes

Abstract

The previous chapter focused on the electrocatalytic oxidation of hazardous organics in water for water purification. Perchlorate is produced on an industrial scale electrochemically at a very high anodic potential. The electrode material of choice has so far been PbO_2. Since PbO_2, as electrocatalytic material, has many characteristics in common with SnO_2, it is a logical approach to test our novel sol-gel $Ti/SnO_2/Sb_2O_5$ electrode material for the anodic oxidation of chlorate to perchlorate

8.1. Background

8.1.1. The chemistry of the perchlorate ion and its industrial application

By heating potassium chlorate to elevated temperatures it disproportionates forming chloride and perchlorate:

$$4\ KClO_3 \rightarrow KCl + 3KClO_4 \qquad (57)$$
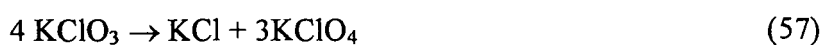
Increased heating causes the perchlorate to disintegrate into chloride and oxygen:

$$ClO_4^- \rightarrow Cl^- + 2O_2 \qquad (58)$$

The addition of concentrated sulphuric or hydrochloric acid results in the formation of perchloric acid:

$$KClO_4 + H_2SO_4 \rightarrow KHSO_4 + HClO_4 \qquad (59)$$

which can be distilled carefully under vacuum.

Industrially, perchlorates are obtained by anodic oxidation:

$$ClO_3^- + H_2O \rightarrow ClO_4^- + 2\,H^+ + 2\,e^- \quad (\varepsilon_0 = +1.19\ V) \qquad (60)$$
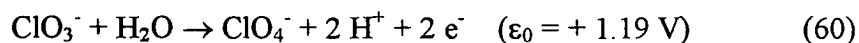
(Anode: PbO_2, Cathode: Fe, current density: 3000 A/m^2).

The salts of the perchloric acid are the most stable oxygen salts of chlorine and practically well characterised with all metals. Most of them are very soluble in cold water, except for potassium, rubidium and caesium perchlorate. NH_4ClO_4 is a fundamental ingredient of solid rocket propellants (75% NH_4ClO_4 and 25% high molecular organic substances).

8.1.2. Hypochlorite, chlorate and perchlorate, the electrochemical behaviour and industrial production

Electrolysis of a NaCl-solution in an undivided cell results in disproportion of the anodically evolved chlorine by consuming the cathodically built hydroxide ions into chloride and hypochlorite ClO^-.

$$6Cl^- \rightarrow 3\ Cl_2 + 6\ e^- \qquad (61)$$

$$3Cl_2 + 6\ OH^- \rightarrow 3\ ClO^- + 3Cl^- + 3H_2O \qquad (62)$$
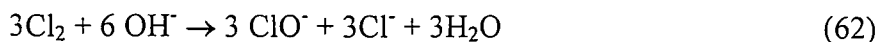
The hypochlorite can anodically be further oxidised:

$$3ClO^- + 3/2\ H_2O \rightarrow ClO_3^- + 2\ Cl^- + 3\ H^+ + ¾\ O_2 + 3\ e^- \qquad (63)$$
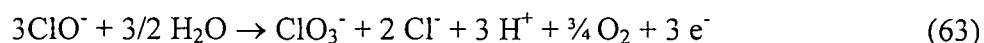
Accordingly, per mole of obtained chorate – without consideration of the yield – 9 faraday are consumed. Only 6 faraday as a whole for the production of chorate are needed by making use of a chemical reaction step following equation (62).

$$2\ ClO^- + 2H_2O \rightarrow 2\ HClO + 2\ OH^- \qquad (64)$$

$$2\ HClO + ClO^- \rightarrow ClO_3^- + 2\ Cl^- + 2\ H^+ \qquad (65)$$
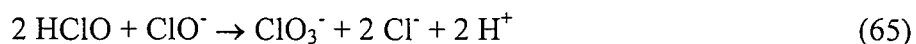
Hypochlorite as well as chlorate can be produced in undivided cells.

a) *Hypochlorite.*

Electrolysis is industrially carried out in bipolar cells between two graphite electrodes. The undesired formation of chlorate according to equation (63) can be suppressed by high chloride concentrations in the electrolyte. Additionally, high current density (the current – potential curve is less steep for the chlorine evolution than for the chlorate production) favour the hypochlorite formation. The chemical reaction of equations (64) and (65) can be avoided by working at low temperatures.

The produced alkaline chloride-ions and chlorine containing hypochlorite solution can directly be applied for bleaching or disinfection. An interesting variation of the process is

156

described by the use of sea water instead of NaCl as raw material, especially for the purification and disinfection of swimming pools and effluents at coastal areas. To keep heat exchangers or condensers that are run with sea water free from bio-material, part of the cooling water just has to be run through an electrolysis cell.

b) Chlorate.

For the production of chlorate the chemical formation of chlorate (equations (64) and (65)) has to be promoted to suppress the energetically less efficient electrochemical production (equation (62)). This can be done by:

- Raising the working temperature to ca. 80° C.

- Using cells providing a large volume for the solution above the bipolar plates, because reaction (63) is heterogeneous, whereas reaction (64/65) is homogeneous.

Stainless steel serves as cathode material; the anode is of graphite or Pt-coated titanium.

c) *Perchlorate*

Chlorate can anodically be oxidised to perchlorate:

$$ClO_3^- + H_2O \rightarrow ClO_4^- + 2\,H^+ + 2\,e^- \qquad (66)$$
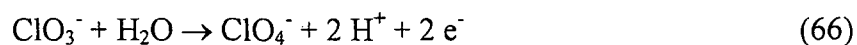
Anodes are platinum or lead-dioxide. Graphite is not stable under the reaction conditions. The direct production of perchlorate from NaCl in a single, undivided cell by successively running the reactions (61) – (66) only leads to very low yields with regard to perchlorate. Therefore, a pure sodium chlorate solution is electrolysed.

8.1.3. Mechanism of the different anodic reactions

The most common industrial way of producing perchlorate is the electrochemical oxidation of aqueous chlorate solution [Ibl, 1981]. The anodic material is crucial to obtain a high current efficiency for the perchlorate formation. Only two materials, viz. smooth platinum and lead dioxide are used industrially [Ibl, 1981].

The anodic oxidation of chlorate ion to perchlorate ion is not only of considerable importance technologically, but also from a scientific point of view. The scientific importance stems from the unique conditions under which the reaction takes place, for example, the oxidation occurring at high positive potentials (1.5 – 2.5 V versus SCE) in spite of the possibility of anodic oxygen evolution, the oxidation occurring on an oxide covered (or oxide coated) surface and the oxidation probably passing through several intermediate steps since it involves a transfer of two electrons and two reactant species. It has been demonstrated that the ionic strength of the solution has a marked effect on the rate of perchlorate formation, whereas the pH of the solution does not influence the reaction rate.

Mechanisms for the anodic oxidation on platinum or lead dioxide have been proposed in the literature [Munichandraiah, 1987]. Most of the mechanisms suggested in previous literature are based on indirect or inadequate experimental support. Munichandraiah and Sathyanarayana (1987) have shown that the most probable mechanism involves the oxidation of a water molecule in a one-electron transfer step to give an adsorbed hydroxyl radical as the rate determining step of the overall reaction.

$$H_2O \rightarrow \bullet OH_{ad} + H^+ + e^- \qquad\qquad (67)$$

8.1.4. Perchlorate analysis

There are various methods described in the literature for the quantitative analysis of perchlorate, the most common known is probably the gravimetric precipitation with potassium ions which, however, lacks accuracy.

The use of large organic cations as precipitants for certain anions such as perchlorate, perrhenate, tetrafluoroborate, iodide, etc. has been well documented [Kodama, 1963; Boltz, 1973; Welcher, 1948]. 1,2,4,6-Tetraphenylpyridinium acetate replaced the potassium ion as a gravimetric reactant [Chadwick, 1975] and, especially, tetraphenylarsonium chloride has received widespread attention for the determination of perchlorate ion as a new precipitant for large ions such as perrhenate and perchlorate [Chadwick, 1975]. Thereafter, several methods using tetraphenylarsonium chloride have been applied such as potentiometric titration [Baczuk, 1968] and conductometric titration [Baczuk, 1967]. Furthermore, spectrophotometric method makes use of a dye that is formed after the extraction of perchlorate as protritylinium perchlorate [Burns, 1997]. The different methods employed are now briefly described:

- *The gravimetric method using 1,2,4,6-tetraphenylpyridinium acetate*

1,2,4,6-Tetraphenylpyridinium acetate is prepared in > 95 % yield by reacting 1,3,5-triphenyl-2-penten-1,5-dione with aniline in glacial acid. The compound quantitatively precipitates ClO_4^- from aqueous solution. At each concentration for the ClO_4^- determination, the relative error of the mean is < 0.1 % and the relative standard deviation is < 0.3 %.

- *Potentiometric titration using tetraphenylarsonium chloride*

A potentiometric precipitation method with tetraphenylarsonium chloride has been described by Baczuk and DuBois [Baczuk, 1968]. The titration is followed with a perchlorate

ion specific electrode and a double-junction calomel electrode. The method is based on the availability of a perchlorate sensitive electrode which is provided by the Orion model 92-81. The Orion perchlorate ion specific electrode operates in a manner, somewhat similar to the conventional glass pH electrode. Both electrodes develop a potential across a thin layer of conductive material. However, with the perchlorate electrode a water immiscible liquid ion exchanger, held in place by an inert semipermeable polymer disk, is substituted for glass. According to the manufacturer (Orion Research, Inc., Instruction Manual, Perchlorate Ion Electrode, Model 9-81), this electrode exhibits a high specificity for the perchlorate ion and responds in Nerstian fashion to this ion between concentrations of 10^{-1} M and 10^{-5} M. The only serious interference reported, is for the hydroxide ion which has a selectivity constant equivalent to that of perchlorate. The electrode is recommended for use from a pH of 4 to 10. Best results are obtained with solutions between pH 4 and 7. The method is simple, rapid and free from common interference. However, extremely large amounts of some simple anions distort curve shapes. Overall 95 % confidence limits were $\pm$ 0.16 %. In addition, the perchlorate electrode was found to respond linearly to permanganate, dichromate and periodate ions over an appreciable concentration range.

- *Conductometric titration perchlorate with tetraphenylarsonium chloride*

Another approach for the use of tetraphenylarsonium chloride for perchlorate determination, incorporates the use of conductance for the titration of perchlorate. Conductance titration performed in acidic solutions resulted in titration curves that, however were found to be nonlinear, making it difficult to readily determine the end point. Curves were also of decreasing conductance in this area, which was not expected. Both, the decrease in conductance and curvature were attributed to a dilution effect [Baczuk, 1967]. Titration at a neutral pH gave curves that were linear with a slight increase in conductance prior to the end point, and thus were satisfactory for quantitative work.

- *Spectrophotometric determination of perchlorate after extraction as protriptylinium perchlorate*

Relatively few spectrophotometric methods have been reported for the determination of perchlorate ions [Snell, 1981; Williams, 1979; Boltz, 1978; Marczenko, 1986; Nemcove, 1996]. Most utilise extraction with basic dye cations such as those of the monoethyl analogue of Malachite Green [Akiyama, 1983], Methylene blue [Iwasaki, 1963], Crystal violet [Uchinkawa, 1967]and Brilliant Green [Fogg, 1971]. These reagents suffer from temporal effects after dilution of its concentrated solutions and by adsorption on cuvette walls.

A novel quantitative extraction of the perchlorate ion with the protriptylinium cation is described by Burns [Burns, 1997]. The absorbance of the extract is measured in a 1 cm cuvette at 292 nm.

In this work the conductivity measurement during titration with tetraphenylarsonium chloride has been applied for the perchlorate determination. Preliminary experiments, however, revealed that not only perchlorate, but also chlorate precipitates considerably with tetraphenylarsonium chloride. As notable amounts of chlorate were present in the analysed samples, the chlorate had to be separated from the solutions prior to determination. A means to selectively destroy the chlorate is the addition of hydrochloric acid at elevated temperatures:

$$HClO_3 + 5\,HCl \rightarrow 3\,Cl_2 + 3\,H_2O \tag{67}$$
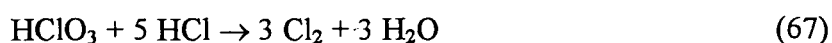
The perchlorate is more stable for steric reasons.

8.2. Experimental

8.2.1. Experimental set-up for electrolysis

The experimental set-up with two separate solution circuits is shown in Fig. 62. The electrolysis cell has been described previously (chapter 7.2.2.). The anodic and cathodic compartment of the cell were separated by a cation exchange membrane ('Plastpolymer', St. Petersburg, Russia). The working electrode was a $Ti/SnO_2/Sb_2O_5$ porous electrode prepared by sol-gel. The counter electrode was porous Pt-coated titanium.

The electrolyses were carried out for 15 min galvanostatically, using a power supply (Amptron) at 50° C. The potential between cathode and anode was measured by a voltmeter.

thermostated cathodic vessel

thermostated anodic vessel

Pumps

SPE-Reactor
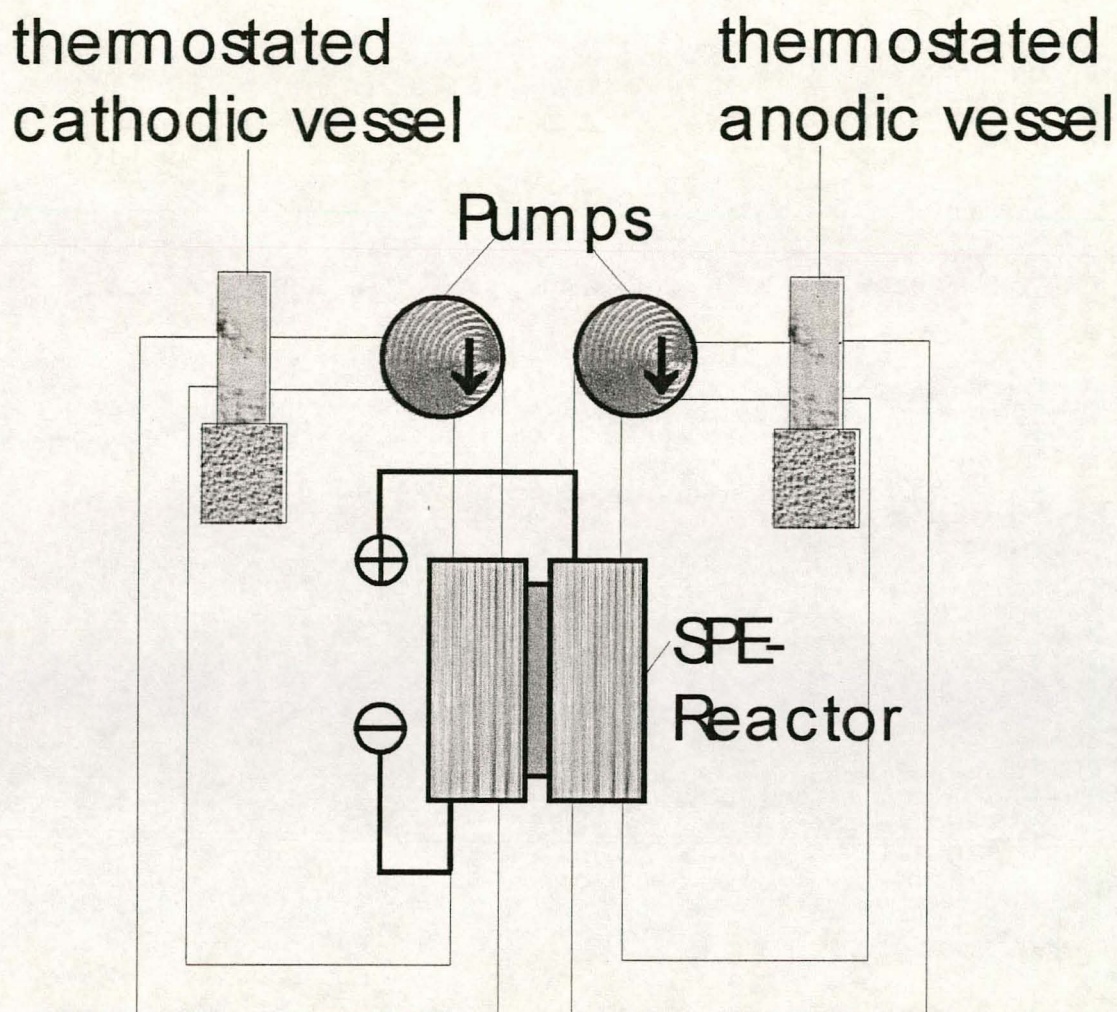
Fig. 62: Experimental set-up

The concentration of the 100 ml perchlorate solution per batch was varied from 0.5 M to 3.5 M. Electrolysis was implemented at different current densities (0.2 A/cm^2, 0.22 A/cm^2, 0.25 A/cm^2, 0.28 A/cm^2 and 0.30 A/cm^2).

8.2.2. Perchlorate analysis

10 ml of the electrolysed sample was accurately withdrawn from the solution and placed in an evaporating dish. 200 ml of concentrated hydrochloric acid was added. The sample was

evaporated to dryness on a hot plate to selectively destroy the chlorate. Sputtering must be avoided carefully in the final stages of the evaporation. Three further additions of 40 ml of water and complete evaporation were necessary in order to remove all the acid. The residue was dissolved in water and diluted to approximately 500 ml. The conductivity of the sample should be close to 675 µS after the dilution step. Thereafter, the solution was titrated with tetraphenylarsonium chloride. The concentration of the titrant was 0.1 M.

8.3. Results and conclusions

8.3.1. Yield of perchlorate ion after electrolysis and current efficiency

Conductance titrations were performed in neutral pH solutions. The titration curves were found to be linear, making it easy to readily determine an end point, as can be seen in the example of Fig 63., where the decrease in conductance and its increase after the end point are illustrated. The tetraphenylarsonium chloride precipitates perchlorate ion reducing the number of ions present in the electrolyte which causes the conductivity to go down. Once the end point is reached, the solution contains no more dissolved perchlorate ions. The dissolving titrant itself, added to the solution, hence contributes to the increase of conductivity. Electrolysis for the perchlorate production was carried out for 15 min for all experiments, whereas the current and concentration were varied. The volume of the solution was kept constant at 100 ml. Fig. 63 derives from an initial chlorate concentration of 0.5 M. The current was 28 A. 10 ml of the sample were withdrawn for analysis.
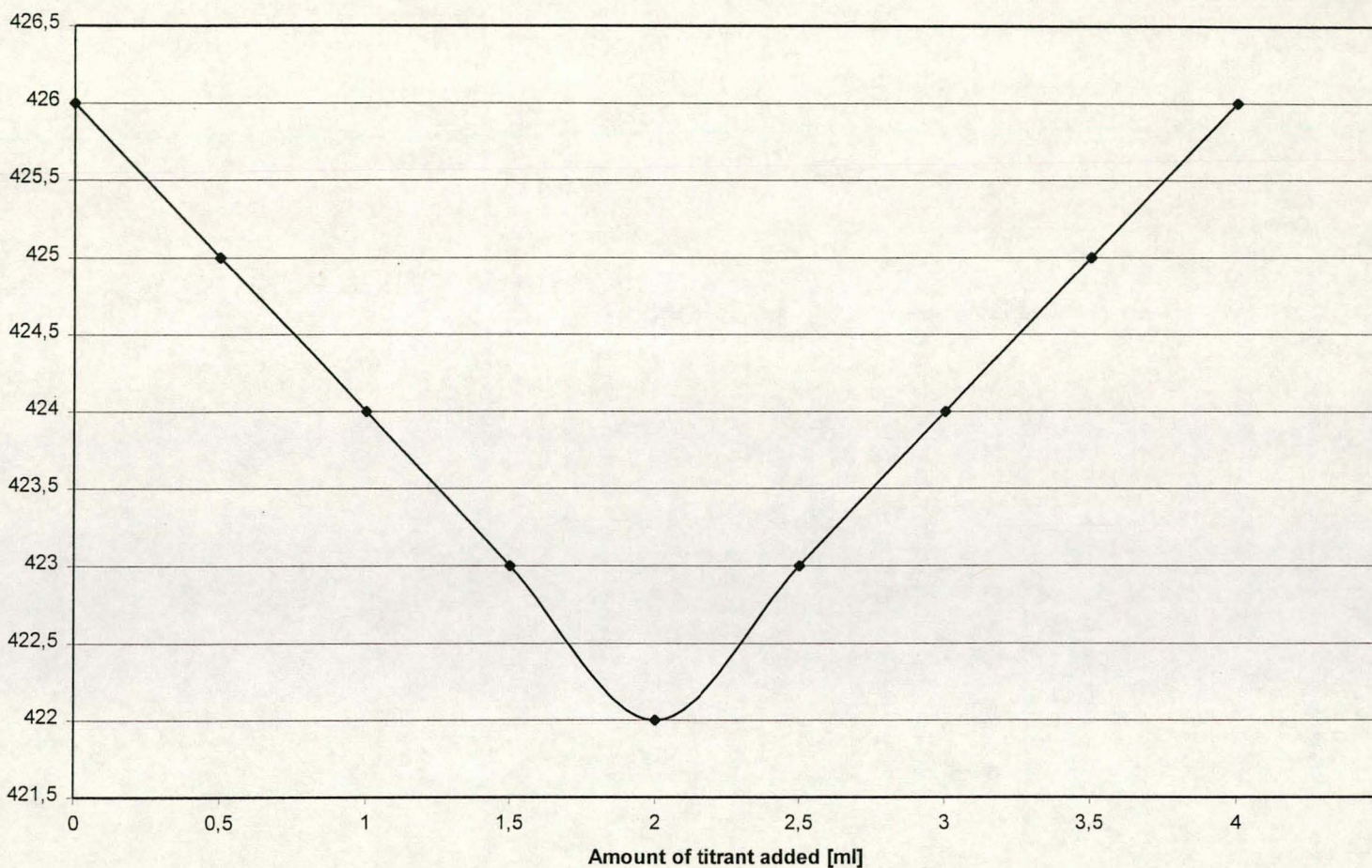
Fig. 63: Titration of perchlorate ion after 15 min of electrolysis. Titrant: 0.1 M solution of tetraphenylaronium chloride; initial chlorate concentration: 0.5 M; current: 28 A.

The perchlorate concentration is plotted against the applied current on the X-axis and against the initial chlorate concentration on the Y-axis. Fig 64 shows those results.

In accordance with previous reports in the literature [Munichandraiah, 1987; Janssen, 1995] the perchlorate production could be enhanced by either increasing the current or the initial chlorate concentration.

The same assumptions are valid for the yield of perchlorate against current and initial chlorate concentration. That relation is given in Fig. 65.

Fig. 66 shows the current efficiency of perchlorate production dependant on initial chlorate concentration and current. Once more increasing the initial chlorate concentration gives a higher current efficiency. Raising the current, however, does not improve the current efficiency.

The Tables 3 - 5 summarise the above results:

	20 A	23 A	25 A	28 A	30 A
0.5 M Chlorate	0,017 M	0,015 M	0,015 M	0,02 M	0,023 M
1 M Chlorate	0,03 M	0,037 M	0,0375 M	0,045 M	0,045 M
1.5 M Chlorate	0,105 M	0,125 M	0,15 M	0,17 M	0,175 M
2 M Chlorate	0,12 M	0,13 M	0,155 M	0,175 M	0,178 M

Table 3: The concentration of perchlorate after 15 min of electrolysis, dependent on the initial chlorate concentration and current applied. The initial solution contained 100 ml of electrolyte.

	20 A	23 A	25 A	28 A	30 A
0.5 M Chlorate	0,034	0,03	0,03	0,04	0,046
1 M Chlorate	0,03	0,037	0,0375	0,045	0,045
1.5 M Chlorate	0,07	0,083	0,1	0,113	0,117
2 M Chlorate	0,06	0,065	0,0775	0,0875	0,089

Table 4: Yield of perchlorate concentration ($[ClO_4/ClO_3]$) after 15 min of electrolysis dependant on the initial chlorate and the current applied. The initial solution contained 100 ml of electrolyte.

	20 A	23 A	25 A	28 A	30 A
0.5 M Chlorate	0,91	0,699	0,643	0,766	0,822
1 M Chlorate	1,608	1,725	1,608	1,723	1,608
1.5 M Chlorate	5,629	5,826	6,432	6,509	6,254
2 M Chlorate	6,433	6,059	6,647	6,700	6,361

Table 5: Current efficiency in % concentration after 15 min of electrolysis, dependant on the initial chlorate concentration and the applied current. The initial solution contained 100 ml of electrolyte.

The perchlorate yield was calculated by dividing the final perchlorate concentration by the initial chlorate concentration, which gives a data range from 0 – 1.

Accordingly, the current efficiency was obtained by dividing the moles of perchlorate produced by the moles of electrodes consumed during the oxidation process.

The most striking feature from all the figures and tables is that raising the initial chlorate concentration from 1.0 M to 1.5 M results in a far better output in concentration, yield and current efficiency. The reason for this phenomena can once more be seen in mass transport limitations to the electrode surface. Possibly, a sufficiently high concentration of the reacting ions in the pores of the electrode material for reasonable conversion can only be achieved by having an initial chlorate concentration of at least 1.5 M. The problem with mass transfer limitations related to the electrode configuration in our SPE reactor system has already occurred and been discussed in chapter 7. Overall it has to be conceded that the current efficiency and yield of the perchlorate production was rather low compared to results obtained with PbO_2 as electrode material [Janssen, 1995].

Perchlorate Concentration
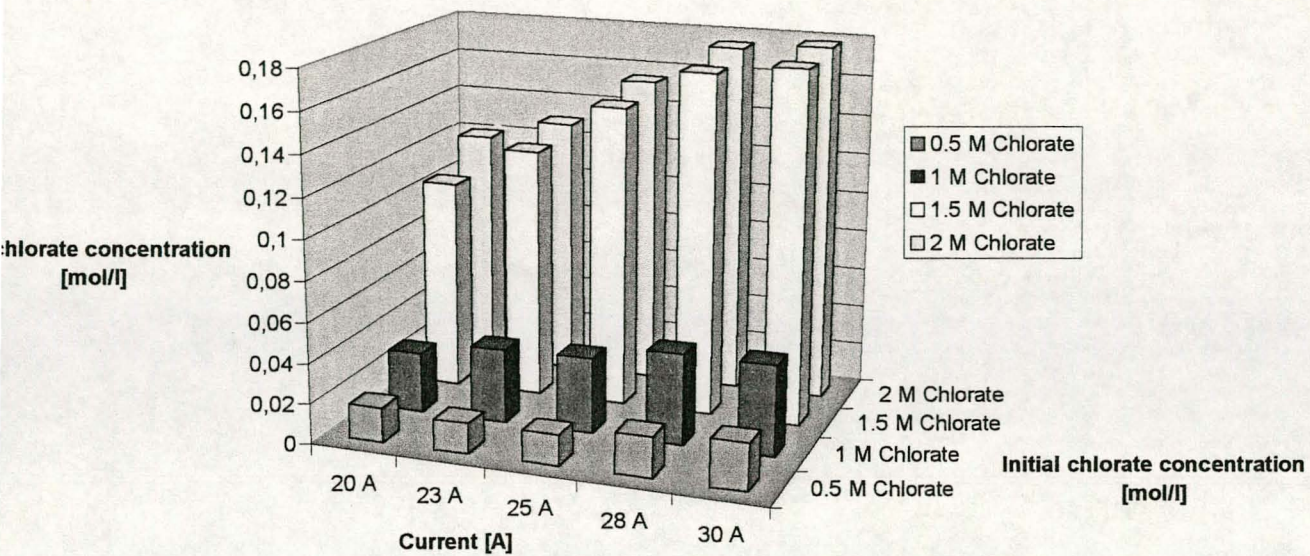

Fig. 64: Perchlorate concentration after 15 min of electrolysis versus applied current and initial chlorate concentration.
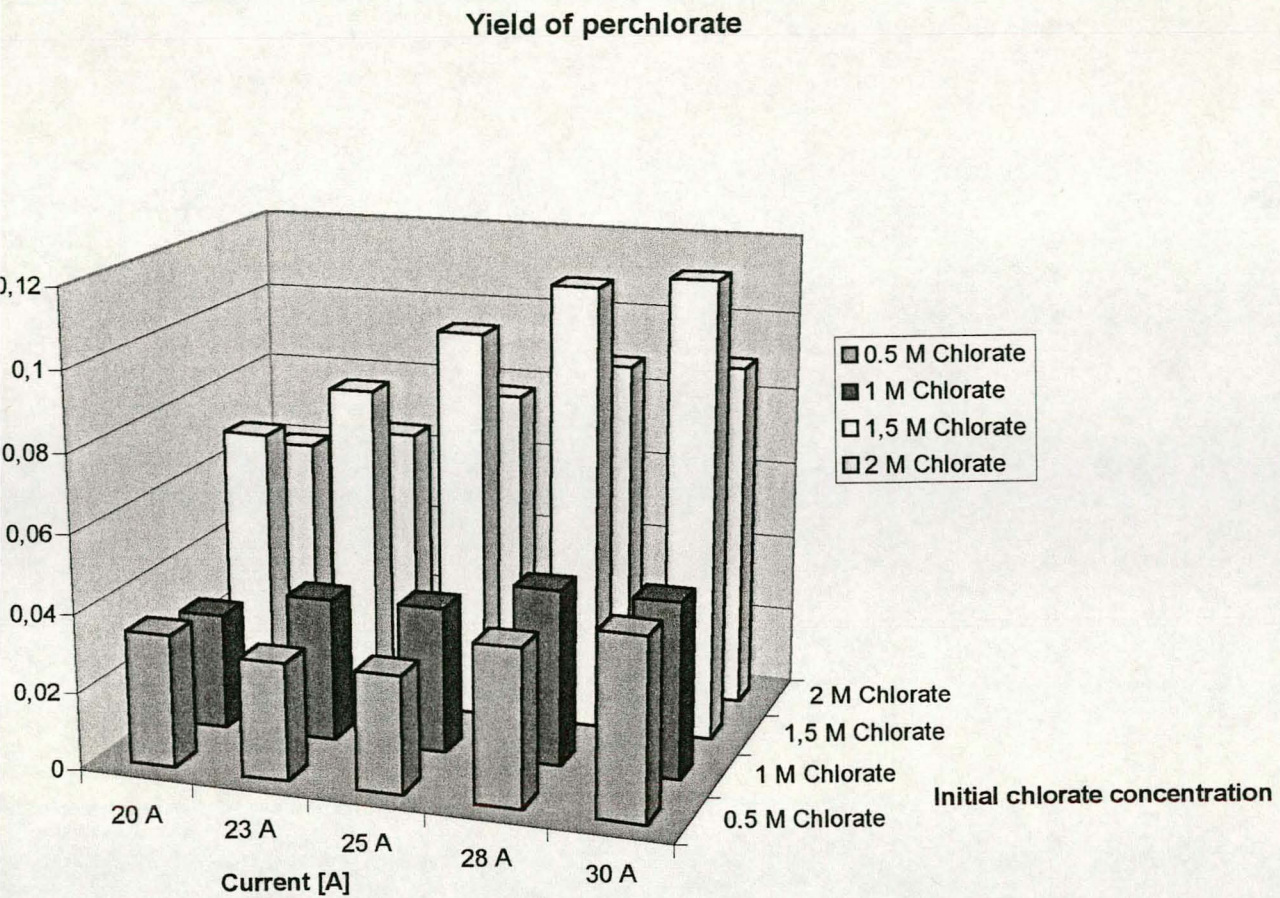
Fig. 65: Perchlorate yield after 15 min of electrolysis versus applied current and initial chlorate concentration.
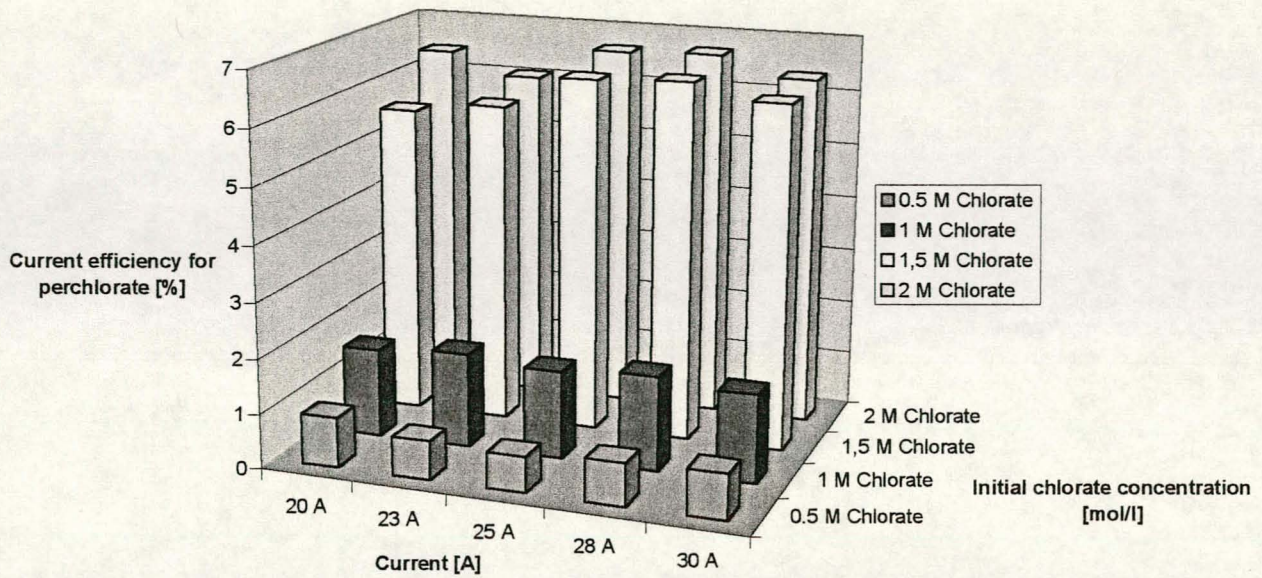
Fig. 66: Current efficiency for the perchlorate ion production after 15 min of electrolysis versus applied current and initial chlorate concentration.

Chapter 9:

Conclusions and suggestions for continuation of the project

A novel electrode material ($Ti/SnO_2/Sb_2O_5$) for the combustion reaction of hazardous organic compounds in water has been successfully designed by a sol-gel dip-coating technique.

Electronic conductivity of the doped films was achieved and cyclic voltammetry proved the specific catalytic activity of the electrodes towards the oxidation of phenol in water. In comparison to traditional electrode material (PbO_2) the SnO_2-based material surpassed its competitors.

The deposition of the doped film on the substrate could be confirmed by XPS-spectroscopy and microprobe analysis.

Kinetic measurements followed by means of fibre-optics UV/VIS-spectroscopy revealed a rate determining step of the second order for the crucial formation of the •OH-radicals as an intermediate for the combustion of phenol.

These kinetics could be confirmed by impedance spectroscopy.

An SPE-reactor for the combustion of phenol was designed and tested with good results. However, mass-transport limitation seem to decrease the efficiency of the reactor. In addition, a novel online technique for the evaluation of the reactor performance was developed to improve analysis.

The electrode material proved to also be active for the electrochemical perchlorate production, although the yield was not satisfactory which can also attribute to the mass-transport limitation caused by the reactor designed.

Further work on the project should focus on the improvement of the reactor design to understand and finally control the mass-transport limitations in the reactor. A different approach for the reactor design such as a fluidised bed reactor could also be visualised.

References

S. Akiyama, K. Nakashima, S. Naketsuji, M. Hamada and Y. Izaki, Bull. Soc. Chim. Japan **56** (1983) 947

A.C. Almon, Small Scale Electrolytic Destruction of Spent Tributylphosphate Extractant. WSRC-RP-89-1229, Savannah River Site, Aiken, SC, 1986

A.C. Almon and B.R. Buchanan, Electrochemical oxidation of organic waste. Electrochemistry for a cleaner environment, The Electrosynthesis, Co. Inc., Buffalo, 1992

M. Andelman (1996) US 5,547,581, patent

N.J. Arfsten, J. Non-Cryst. Solids, **63** (1984) 243

J.R. Backhurst, M. Fleischmann, F. Goodridge and R.E. Plinley, J. Electrochem. Soc. **116** (1969) 1600

R.J. Baczuk and W.T. Bolleter, Anal. Chem. **39** (1968) 93

R.J. Baczuk and R.J. DuBois, Anal. Chem. **40** (4) (1968) 685

J.B. Bard and L.R. Faulkner (1980) Electrochemical Methods, John Wiley & Sonc, Inc.

D. Batthacharai, S. Freshour and S. Mawhinney, Nat. Res. **30** (9) (1995) 1949

D.G. Bessarabov, J.Grimm, Papers of the Water Institute of South Africa-Biennial conference, v. 1, P 4, Cape Town, 4-7, May, 1998

D.F. Boltz, , CRC-Critical Reviews in Analytical Chemistry, L. Mel and B.M. Cambell, Eds., CRC Press, Cleveland, Ohio, 1973, p.147

D.F. Boltz, J.A. Howell (Eds.), Colorimetric Determination of Non Metals, Wiley, New York, 1978

W. Bors, M. Savan, E. Lengfelder, C. Michel, C. Fuchs and C. Frenzel, Photochem. Photobiol. **28** (1978) 629

M. Boudeulle, Colloquium on Basic Properties of Binery Oxides, Sevilla, September, 1983

D.T. Burns, M.D. Dunford and P. Sutthivaiyakit, Analytica Chimica Acta **356** (1997) 141

C.J. Brinker, A.J. Hurd, G.C. Frye, K.J. Ward and C.S. Ashley, J. Noncrystal. Solids **121** (1990) 294

T.C. Chadwick, Anal. Chem. **47** (1975) 433

J.P. Chaleton, C. Terrier, E. Bernstein, R. Berjoan and J.A. Roger, Thin Solid Films, **247** (1994) 37

J.P. Chaleton, C. Terrier, E. Bernstein, R. Berjoan and J.A. Roger, Thin Solid Films, **263** (1995) 37

U.R. Chaudhuri, K. Ramkumar and M. Satyan, J. Phys. D: Appl. Phys., **23** (1990) 994

Y.-L. Chen and T.-C. Chou, J. electroanal. Chem. **360** (1993) 247

C. Comninellis, Electrochim. Acta **39** (11/12) (1993) 1857

C. Comninellis, Electrochimica Acta, **39** (1994) 1857

C. Comninellis, B. Correa-Lozano and De Battisti, J. Appl. Electrochem. **26** (1996) 689

A. Czapla, E. Kusior and M. Bucko, Thin Solid Films, **182** (1989) 15

J.T. Davis, E.K. Rideal, Interfacial phenomena, Academic Press, New York, 1963

Deutsche Norm, Deutsche Einheitsverfahren zur Wasser-, Abwasser- und Schlammuntersuchung, DIN 38 409 Teil 16, Bestimmung des Phenol-Index (H16)

M. Fleischmann and M. Liler, Trans. Faraday Soc. **54** (1958) 1370

P.J. Flory, Principles of Polymer Chemistry; Cornell University Press: Ithaka, NY, 1953, Chapter 9

J. Fricke, Ultrastructure Processing of Advanced Ceramics, Wiley, New York, 1988

M. Ebelmen, Ann. Chimie Phys. **16** (1846)129

M. Ebelmen, C.R. Acad. Sci. **25** (1847) 854

B.E. Erschler, Discuss. Faraday Soc. **1** (1947) 269

R.A. Floyd, R. Henderson, J.J. Watson, P.K. Wong, Free Radic. Bio. Med. **2** (1986) 13

A.G. Fogg, C. Burgess and D.T. Burns, Analyst **96** (1971) 854

L. Friberg, Cadmium in the Environment, 2nd edition, Chap. 2 CRC Press. Cleveland, Ohio, 1974.

J. Fricke, J. Ed. Aerogels; Springer Proceedings in Physics; Springer Verlag: Heidelberg, 1986, Vol. 6

C. Gabrielli, 'Identification of Electrochemical Processes by Frequency Response Analysis', Solartron-Schlumberger, Ref. No. 004/83, 1980

R.M. Galvin, Water SA **22** (1) (1996) 7

H. Gerischer, Z. physik. Chem. **198** (1951) 286

R. Glöckler, J. Weitkamp, 5. German Workshop on Zeolites, Universität Leipzig, 14.-16. März, 1992

W.O.K. Grabow, Water SA **22** (2) (1996) 193

T. Graham, J. Chem. Soc. **17** (1864) 318

C.G. Granqvist, Thin Solid Films **193/194** (1990) 730

J.E. Graves, D. Pletcher, R.L. Clarke, F.C. Walsh, J. Appl. Electrochem. **22** (1992) 200

V.A. Grinberg, N. Zhuravleva, J.B. Vasil'ev and V.E. Kazarinov, Elektrokkimiya **19** (1983) 1447, (Sovjet Electrochemistry **19** (1983) 1299

B. Halliwell, M. Grootveld, J.M.C. Gutteridge, Meth. Biochem. Anal. **33** (1989) 59

B. Halliwell and K. Harparkash, Free Rad. Bio. Med. **10** (1991) 439

H.K. Heinisch, Crystal Growth in Gels; Pennsylvania State University Press, State College, PA, 1970

H.S. Hamed and R.M. Hudson, J. Amer. Chem. Soc. 73 (1951) 650

L.L. Hench and D.R. Ulrich, Ultrastructure Processing of Ceramics, Glasses and Composites, Wiley, 1984, p. 15

H.N. Holmes, In Colloid Chemistry, Chemical Catalog Co, New York, 1926, p 796

N. Ibl and H. Vogt, in 'Comprehensive Treatise of Electrochemistry', vol. 2 (edited by J. O'M Bockris, B.E Conway, E. Yeager and R.E. White), Plenum Press, New York and London (1981) p. 208

I. Iwasaki, S. Utsumi and C. Kang, Bull. Soc. Chim. Jpan **36** (1963) 325

L.J.J. Janssen and P.D.L. Van der Heyden, J. Appl. Electrochem. **25** (1995) 126

M.R. Kadam, N. Vittal, R.N. Karekar and R.C. Aiyer, Thin Solid Films, **187** (1990) 1990

T. Karlsson, A. Smith and J.F. Baumard, Thin Solid Films, **208** (1992)

T. Kawahara, Desalination **96** (2-3) (1994) 341

D.W. Kirk, H. Sharifan and F.R. Foulkes, J. Appl. Electrochem. **15** (1985) 285

S.S. Kistler, Nature **127** (1931) 742

S. Klein, W.F. Maier, Angew. Chem., 108 (1996) 2376; Int. Ed. 35 (1996) 2330; S. Klein, PhD-Thesis, University of Essen 1996

K. Kodama, 'Methods of Quantitative Inorganic Analysis', Interscience Publisher. New York, N.Y., 1963

G. Kreysa, Metalloberfläche **35** (6) (1981) 211

G. Kreysa and E. Heitz, (1986) Principles of Electrochemical Engineering. Weinheim; New York: VCH.

I. Kvaljic and C.M. Trumbore, J. Am. Chem. Soc. **20** (1965) 2547

C. Lange, B. Tesche, S. Storck, W.F. Maier, J. Catal., **175** (1998) 280

A. Lehmani, P. Turq and J.P. Simonin, J. Electrochem. Soc. **143** (6) (1996)1860

R.E. Liesegang, Photogr. Archiv. (1896) 1896
R. Liu and P.S. Fedkiw, J. Electrochem. Soc. **139** (1992) 3514

D.J. Lloyd, In Colloid Chemistry, Chemical Catalog Co, New York, 1926, p 767

L. Lundberg, C.L.Milanes, N. Pernalete and J.R. Weisinger, Am. J. Physiol. **253** (1987) F401

J.R. MacDonald, Impedance Spectroscopy, J. Wiley and Sons, New York, 1986

W.F. Maier, I.C. Tilgner, M. Wiedorn, H.C. Ko, A. Ziehfreund, R. Sell, Advanced Materials, **10** (1993) 730

W.F. Maier, C.H. Ko, Catalysis Today, **25** (1995) 429

Z. Marczenko, Separation and Spectrophotometric Determination of Elements, 2nd edn., Ellis Horwood, Chichester, 1986

M. Mayr, W. Blatt, B. Busse and H. Heinke "Electrolytic Systems for Applications in Fluoride-Containing Electrolytes," presented at The Fourth International Forum On Electrolysis in The Chemical Industry, Florida, 1990

K.S. Mazdiyasni, Ceram. Int. **8 (2)** (1982) 42

R.C. Mehrotra, J. Noncrystat. Solids **121** (1990) 1

L.P. Mc Cafferey, J.P. Willis and R.T. Watkins, (1995) Distribution and cause of high-fluoride groundwater, Western Bushveld, South Africa. Ground Water 95, Ground Water Recharge and Rural Water Supply, organised by the Ground Water Division of the Geological Society of South Africa and the Borehole Water Association of Southern Africa

G.J. McCarthy, R. Roy, J.M. McKay, J. Am. Ceram. Soc. **54** (1969) 344

N. Munichandraiah and S. Sathyanarayana, J. Appl. Electrochem. **17** (1987) 22

O.J. Murphy et al., Wat. Res. **26 (4)** (1992) 443

I. Nemcove, Spectrophotometric reactions, Marcel Dekker, New York, 1996

Z. Ogumi, K. Nishio and S. Yoshizawa, Electrochim Acta **26** (1981) 1779

Y. Oren and A. Soffer, Electrochim. Acta **28** (1983) 1649

S.Y. Park, S.I. Mho, E.O. Chi, Y.U. Kwon and H.L. Park, Thin Solid Films **258** (1995) 5

M.J. Pieterse, Water SA **15** (3) (1989) 169

L.I. Popova, M.G. Michailov, V.K. Gueorguiev and A. Shopov, Thin Solid Films, **186** (1990) 107

T.H. Randle and A.T. Kuhn, in A.T. Kuhn (Ed.), The electrochemistry of lead, Academic Press, London, 1979, p217

J.E. Randles, Discuss. Faraday Soc. **1** (1947) 11

D.M. Roy and R. Roy, Am. Mineral. **39** (1954) 957

R. Roy, J. Am. Ceram. Soc. **39** (1956) 145

R. Roy, J. Am. Ceram. Soc. **52** (1969) 344

R.D. Sanderson, D.G. Bessarabov, Y.M. Popkov, V.V. Valuev, S.F. Timashev, Ind.   Eng. Chem. Res., 36 (1997) 2487

J. Sarrazin and A. Tallec, J. Electroanal. Chem. Interfacial Electrochem. **137** (1982) 183

H. Sharifan and D.W. Kirk, J. Electrochem. Soc.: Electrochemical Science and Technology **113** (1986) 921

O. Simond, V. Schaller and C. Comninellis, Electrochim. Acta **42** (1997) 2009

M. Sluyter-Rehbach, J.H. Sluyters, ,AC Techiques', Comprehensive Treatise of Electrochemistry, Vol. 9, ed. E. Yeager et al., Plenum Press, New York, 1984

F.D. Snell, Photometric and Fluorometric Methods of Analysis, Non Metals, Wiley, New York, 1981

K.H. Stern, Bibliography of Liesegang Rings; National Bureau of Standards Miscellaneous Publication No. 292, 1967

J.K. Spiker, D.L.Crawford and E.C. Thiel, Appl, Microbiol. Biotechnol., **37** (1992) 518

Sun Li-Cheng, Wat. Supply **3** (1985) 177

S. Trasatti, Elsevier Scientific Publishing Company; Amsterdam, Oxford, New York, 1980, p. 214

F.M. Turner, (1957) S Harwell, U.K. (Ref. Med/M17)

S. Uchinkawa, Bull. Soc. Chim. Japan **40** (1967) 798

USEPA (US Environmental Protection Agency) (1977) Toxicology of Metals, Vol. II. Washington DC (USA)

B.L. Vallee, D.D. Ulmer, Ann. Rev. Biochem. **41** (1972) 91

P.M.Verbost, G. Flik, P.K.T. Pang, J. Biol. Chem. **264** (1989) 5613

D.W. Wabner andR. Huss, Metalloberfläche Angew. Elektrochem. **28** (1974) 305

D. Wabner and C. Grambow, J. Electroanal. Chem., **195** (1985) 95

E. Warburg, Ann. Phys. Chem. **67** (1899) 493

J. Weitkamp, P. Kleinschmit, A. Kiss, C.H. Berke, Proc. 9th Intern. Zeolite Conference,
    Montreal, 5.-10. July 1992

F.J. Welcher, 'Organic Analytical Reagents', Nostrand Company, New York, N.Y., 1947,

G.B.R. Wesenberg, Scand. J. Dent. Res. **90** (1982) 95

WHO (World Health Organisation) (1986) Directives de Qualite pour l'eau du Boisson, Vol.
    I, II and III. Geneve (Switzerland)

M. Wien, Wiedemann Ann. **58** (1896) 27

W.J. Williams, Handbook of Anion Determination, Butterworths, London, 1979

B.E. Yoldas, Bull. Am. Ceram. Soc. **54** (1975) 286

S.Y.T. Yoshiki, M.O. Kimura and S.M.T. Suzuki, Arch. Environ. Health **30** (1975) 559

List of publications based on the thesis

- J. Grimm, D. Bessarabov and R. Sanderson, Desalination **115** (1998) 285-294, Review of electro-assisted methods for water purification.

- J. Grimm et al., Desalination **115** (1998) 295-302, Sol-gel film preparation of novel electrodes for the electrocatalytic oxidation of organic pollutants in water.

- J. Grimm et al., J. Appl. Electrochem., in press, Characterisation of doped tin dioxide anodes prepared by a sol-gel technique and their application in an SPE-reactor.

Oral presentations

- Water purification by electro-assisted membrane systems, 2nd WISA-MTD-Workshop on membrane technology: New Developments in Membrane Process, Badplaas, South Africa. 21 – 24 October 1998

- SPE-membrane –application of doped tin dioxide anodes prepared by a sol-gel techique. ICOM 99, Toronto, Canada, 12 – 18 June 1999.

Poster presentations

- Electrochemical ozone generator based on solid polyelectrolyte (SPE) membrane technology for water disinfection, WISA 98, Cape Town, South Africa, 4 – 7 May, 1998.

- Preparation and characterisation of novel thin film electrode material for anodic oxidation of organics in water, WISA 98, Cape Town, South Africa, 4 – 7 May, 1998.

- Sol-gel film preparation of novel electrodes for the electrochemical oxidation of organic pollutants in water, First International Conference on Inorganic Materials, Palais de Congres de Versailles, France, 16 – 19 September, 1998.

- Preparation of inorganic electrode material, Inorganic 99, Stellenbosch, South Africa 1998.